The Role of Instantaneous Forces on Particle Movement

Krista Greer

Thesis submitted to the faculty of the Virginia Polytechnic Institute and State University
in partial fulfillment of the requirements for the degree of

Master of Science

In

Civil Engineering

P. Diplas, Chair
C. L. Dancey, Co-Chair
J. C. Little

August 31, 2006
Blacksburg, Virginia

Keywords: sediment transport, incipient motion, impulse, electromagnet

The Role of Instantaneous Forces in Particle Movement

Krista Greer

ABSTRACT

Many methods and equations have been developed to predict bed load transport rates, most of which use some comparison between shear stress and critical shear stress. The critical shear stress is determined by the point of incipient motion. Researchers have attempted to predict bed load transport both deterministically with mean parameters and stochastically attempting to take into account the fluctuations of velocity at points near threshold. This work attempts to show that more than simple force balances are needed to determine the point at which a particle will move. Turbulent fluctuations in velocity seem to have an effect of particle entrainment. The fluctuations in velocity can be several times greater than their time averaged counterparts. These short durations of high velocity often result in particle movement even though the mean flow may be less than or very near critical conditions. Through experiments of a single spherical particle on a simple bed geometry in air without the effects of water, it is shown that time duration of force has an effect on entrainment. This shows that there may be a constant force-time combination, or impulse, required to entrain sediment.

Acknowledgements

There are many people a number of people who I would like to thank for their help during my course of time at Virginia Tech. I especially thank my advisors, Dr. Diplas and Dr. Dancey for their immense help and advice as well as their patience and constant encouragement throughout.

I would like to thank the other member of my committee, Dr. Little for his assistance and advice. Additionally, the other members of our research group, Dr. Tanju Akar, Ozan Celik, and Manos Valyrakis for their assistance, encouragement, advice and suggestions throughout the course of this study.

There were many additional faculty members and graduate students who helped me learn and understand more about electronics, data acquisition, and electromagnetics over the past several months. I would like to thank Dr. Wicks, Dr. Kasarda, Dr. Robertshaw and Dr. Vlachos for their assistance and also for their generosity in loaning equipment essential for these experiments. I would like to thank Jesse Hurdus for his help with the LabView programming and I especially would like to thank Ph.D. candidate John Bird of the mechanical engineering department for the many hours he spent with me designing, building, testing, re-designing, re-building, and re-testing the circuitry and electronics for these experiments.

Last, but certainly not least, I would like to thank my friends and family who encouraged me and their patience through my gripes and frustrations as well as my joys and elations.

I appreciate all the help and support you all have given me and especially the understanding and encouragement that my family bestows upon me even though they have no idea what I am doing.

This work was supported by the National Science Foundation and is gratefully acknowledged.

Table of Contents

List of Figures

List of Tables

Nomenclature

The following is a list of abbreviations and symbols used frequently in this work.

a	Acceleration
A	Cross-sectional area
B	Magnetic flux density
C_D	Coefficient of drag
C_L	Coefficient of lift
d	Particle diameter
Dur	Pulse duration
F	Force
F_D	Drag Force
F_G	Gravitational Force
F_L	Lift force
h	Air gap between magnet face and object
I	Current
m	Mass
N	Number of turns of wire in electromagnet
R	Electrical resistance
S	Data samples
s	Seconds
t	Time
T	Time duration of pulse
U_*	Friction velocity
u	Instantaneous streamwise velocity
V	Nominal voltage (same as magnet voltage)
Vs	Voltage input to pulse generation program
Vm	Amplified voltage received by electromagnet
w	instantaneous vertical velocity

W	Particle submerged weight
w_m	Density of energy
W_m	Total energy

Greek Symbols

β	Pivot angle
γ	Specific weight of water
γ_s	Specific weight of sediment
μ	Permeability of substance
μ_o	Permeability of free space
ν	Kinematic viscosity
ρ	Density of water
τ_o	Shear stress
τ_c	Critical shear stress
ω	Signal frequency
Φ	Magnetic flux

Abbreviations

LDV	Laser doppler velocimetry
DAQ	Data acquisition
TTL	Transistor-transistor logic

Chapter I

Introduction and Literature Review

I.1 Sediment Transport in Nature

Forces acting on solid bodies are an extremely natural occurrence. One of the most elemental uses of force is to make an object move. There are examples of this everyday in our lives as well as in nature. Fingers apply a force to press the keys on a keyboard or a foot provides a force to kick a soccer ball. The current work concerns the force issued by river flow to move a particle of sediment.

The study of sediment movement has implications in many aspects of engineering and science. Sediment fluxes of rivers at impoundments as well as water quality and stream degradation are not the only problems associated with sediment transport; many others are affected by this problem as well. During heavy rain events, farmers can lose significant portions of their top soil to erosion which can lead to reduced crop yields and economic hardships. In areas where the people's food source is the land they work, an unsuccessful crop season can not only be extremely detrimental to their livelihood, but also their health and the health of those that depend on them for food. In rivers where fish require certain depths and velocities of water for spawning, areas where sediment is

not being moved, areas of aggradation and sandbar development, reduce the number of areas where these fish can live and propagate.

The scour caused by flowing water can cause a great deal of harm. In addition to crops and fish, scour can lead to destruction of bridges and piers. One of the leading causes of bridge failure comes from scour at piers and abutments. Today there are many projects that involve stream bank stabilization in order to protect channels from erosion. In each of these instances however, the most critical question to be answered, is when the sediment will move. This incipient motion condition is the driving force behind finding solutions for some of the problems that sediment transport or the lack there of, can cause.

I.2 Traditional Sediment Transport

Over the past several decades, a number of methods for determining sediment transport have been derived both theoretically and empirically based on field and laboratory data. Most of these equations give some sort of relationship between the shear stress applied by the flowing fluid compared to the critical shear stress required to move a particle at its incipient point. The determination of this incipient point of motion has been the most difficult and most critical notion to understanding sediment transport.

Traditionally the threshold of motion is thought of as the point where the streamwise drag force and/or the lift force overcomes the resistive forces of a particle lying on the stream bottom. Several researchers (Middleton 1984) have tried to evaluate the required force through a balance of forces or moments. The lift force, which acts normal to the fluid

flow, is a difficult value to determine; it is, however directly related to the drag force. The determination of the drag force itself usually relies on an experimentally determined coefficient to compensate for the various parameters affecting the movement such as particle shape, direction of flow, and bed geometry. It is also commonly accepted that the effects of the lift force can be included in the drag force coefficient.

The drag force can be expressed by

$$F_d = c\ \tau_o\ d^2 \qquad \textbf{(I.1)}$$

where c is a constant, τ_o is the bed shear stress, and d is the particle diameter. The resistive force, the submerged weight can be expressed by

$$W = c_2\ (\gamma_s - \gamma)\ d^3 \qquad \textbf{(I.2)}$$

where c_2 is a constant, γ_s is the specific weight for sediment and γ is the specific weight for water. The constants used in these equations are site and situation specific and need to be determined experimentally. In order to develop a more generalized system, non dimensionalized methods of shear stress measurement were developed.

The most commonly used of these is the Shields parameter (Shields 1936). The Shields parameter is derived from a dimensional analysis of the major variables affecting incipient motion. These variables include τ_o, d, $\gamma_s - \gamma$, ρ, the density of water, and ν, the kinematic viscosity. Together these can be grouped as

$$\frac{\tau_o}{(\gamma_s - \gamma)d} = F\left(\frac{U_* d}{\nu}\right) \qquad \textbf{(I.3)}$$

where U_* is defined as $(\tau_o / \rho)^{1/2}$. The left side of the equation is known as the Shields stress and the right the boundary Reynolds number.

Shields (1936) conducted many flume experiments during which sediment transport was measured at various states of flow, monitoring the various boundary Reynolds numbers and Shields stresses. Shields made the assumption that the point at which sediment transport ceased would equal the point of threshold motion and in many cases extrapolated data to this zero sediment transport point. Through these experiments Shields was able to develop the curve in Figure 1.1 identifying the point of critical stress for a varying range of $\frac{U_* d}{\nu}$, particle Reynolds values. Points above this line imply sediment movement, while points below do not. Shields original diagram actually showed a shaded region for areas representing the beginning of sediment movement. Researchers over the years beginning with Rouse in 1939 have changed the shaded zone to a line. The graph has been updated by many researchers and has come to be known as the Shields diagram.

Shields concluded that his critical parameter $\tau_c / (\gamma_s - \gamma) d$, where τ_c is the shear stress at initial movement, or the critical shear stress, remained constant in the turbulent flow region. Turbulent flow, where boundary Reynolds values exceed 400, have a hydraulically rough boundary. The graph shows that for particle Reynolds values of about 500 and greater, the critical Shields stress parameter attains a value of 0.06; meaning that the Shields stress at the threshold of motion would be 0.06. This value was obtained, however, through the extrapolation of his previous data. Shields linearly extrapolated his data to find the point of no motion. Other researchers including Paintal

(Paintal 1971), have conducted more experiments at lower flow and transport conditions finding that a Shields parameter of 0.06 might be an upper limit, values as low as 0.03 have been suggested. Paintal conducted additional research focusing on areas where Shields stresses were below 0.06 and found a non-linear curve to the data rather than a straight line extrapolation. This area of the research has given data with high levels of scatter causing debate. One such cause for this scatter might be the use of mean flow velocities or shear stresses in turbulent flow.

I.3 Turbulent Flow and its Effect on Sediment Transport

Most flows in nature are turbulent with high fluctuations in velocity. These fluctuations can generate instantaneous local velocities reaching values several times the average velocity. Some researchers (Einstein 1937; Balakrishnan 1997; Papanicolaou 1997; Kleinhans 2002) have begun pursuing a stochastic method of determining sediment transport rates based on fluid mechanics and probability. These researchers have observed that a particle's point of incipient motion appears to occur rather randomly leading to the notion that the stochastic nature of turbulent velocities could be at play. Supporting this notion is the fact that in many studies, flows that should be below traditional threshold levels do indeed transport sediment. These observations led to the idea that chance turbulent fluctuations in velocity might be responsible for moving these particles.

Turbulent flow is a complicated process of seemingly random bursts of flow in varying magnitudes and directions. Early on, turbulent flow was modeled as adding random

velocity components to that of the time-averaged counterparts. This method has been determined inadequate as researchers have shown that turbulence may not be as random as previously thought. Kline (Kline 1967) was able to show that two types of turbulent events occur more often near the boundary. These are, "ejections" with high lifting forces and "sweeps" with high streamwise forces that form the phenomenon known as the turbulent burst. These bursts occur in a somewhat repeatable fashion in both time and space but not in any periodical sense. These bursts are thought to be the increased velocities and hydrodynamic forces and Reynolds stresses associated with sediment movement.

In order to better visually represent the characteristics of turbulent velocities, Willmarth and Lu (Willmarth 1972) developed a quadrant method of depiction. The velocities are plotted in a graph of w, instantaneous vertical velocity component, and u, instantaneous streamwise velocity component. Each velocity measurement obtained during experimentation has a positive or negative value for each ordinate. Plotted, these values fall into four quadrants. The first quadrant, $u > 0$ and $w > 0$, is known as outward interactions, the third quadrant, $u < 0$ and $w < 0$, the inward interactions. The two most commonly occurring pairs are in the second quadrant, $u < 0$ and $w > 0$, known as ejections, and the fourth quadrant, $u > 0$ and $w < 0$, known as sweeps.

I.4 The Stochastic Method

The development of these stochastic transport methods, first begun by Kalinske (1947) and Einstein(1950) consider the stability of the particle that is subjected to the rapidly

changing hydrodynamic forces of turbulent flow. These models often use the assumption that the normal and shear stress components can be represented by a normal distribution. However more recent models assume that these components fit better to other distributions such as the gamma distribution. Papanicolaou (1999) conducted a comparison between several probability entrainment methods. The wide range of values and probabilities led to the research around the need to develop a stochastic incipient motion model based on physical aspects.

The development of the stochastic transport model is dependent on the flow criteria at which the sediment randomly begins its motion. These flow conditions however, are dependent also on the shape, size, bed features, etc. of the sediment. Moore (Moore 1994) gives a detailed description of the variety of parameters affecting the point of incipient motion just in terms of sediment characteristics; the random nature of turbulence only adds to these factors. In an attempt to develop a physically based stochastic model, Balakrishnan (1997) and Papanicolaou (1997) investigated the effects of bed geometry and bed packing density along with that of turbulent fluctuations. Several experiments were completed with varying packing densities around mobile particles. The varying nature of turbulent flow would cause different levels of lift and drag forces depending on the location of surrounding particles and therefore causing some of the probabilistic features of sediment transport. These experiments were done with single sized spherical particles in a flume on a bed of densely packed equal sized spheres. The incipient criteria for the varying packing densities were also compared to

that of a single exposed ball on a densely packed flat bed. Even in this simple set up it was still difficult to determine when the ball would entrain.

The objective of their experiments was to determine the probability of sediment movement during varying turbulent flows using a stochastic method. 2-Dimensional velocities were taken with a Laser Doppler Velocimeter (LDV) at a point just upstream of the particle. In addition, video images were taken of the particle to determine the point of incipient motion. An example of some of the data taken is shown in Figure I.2.

As the figure shows, there is an extreme fluctuation in streamwise velocity with peaks several times greater than that of the time-averaged velocity. The arrows located on the graph show the corresponding points of sediment movement as observed by the video imagery. One can see that these points of movement usually correspond with peaks in the streamwise velocity; however, they do not occur for every peak. If the magnitude of the velocity fluctuation was the sole reason for particle entrainment, then the ball should have moved at each sufficient peak, however this was not so, leading to the question of what else could be causing the particle entrainment.

Another effect that can also be seen through the data taken by the LDV during the Papanicolaou and Balikrishnan experiments was the relative duration of the fluctuating peaks in the streamwise velocity. It can be seen that some peaks appear to have longer duration than others. The question arises; does the time duration affect the force felt by

the particle? If so, is there a standard force-time relation that results in a better predictor of incipient motion?

I.5 Study Objectives

The overall objective of the present study is to determine if varying forces with varied durations has an effect on particle dislodgement. In order to complete this in a setting where the researcher can control most aspects and reduce the unknown factors to as few as possible, the experiments were not conducted in running water. The randomness of turbulent flow is apparent and in an effort to control this, the turbulent forces in these experiments are simulated by a more controllable medium, electromagnetics.

The use of electromagnetics allows the researcher to apply a specific "force" (see the Analysis and Results section for how force is controlled) to the particles representing sediment. In addition, the particles are spherical and sitting on a bed of other spherical particles. The force is also applied so that the particle is in optimum position for rolling from the pocket. These simplifications allow for easier comparison to the previously discussed forces on a sediment particle calculations. In addition, the experiments are carried out in air, thus removing the complication of fluid movement around the particle as is necessary to consider in flume and field experiments.

The objective of these experiments is to show that, for the case of very short lived forces, the time duration of a force applied to a particle in a pocket has an effect on whether the

particle will be entrained or not; and if so, how do these force-time combinations vary and what are they. These questions are addressed by the following:

1) Using electromagnetics, apply controlled force-time combinations to varying sized particles in varied sized bed pockets. Plotting these combinations to show groupings that move the particle and those that do not.
2) Use high speed imagery, to record the movement of the particle. From its position track, determine the acceleration of the particle which will lead to the force applied during this movement.

These experiments show the elementary effects of a force on a spherical particle. These results will then be used to show the relationship to similar effects of fluid forces on submerged particles in flume studies.

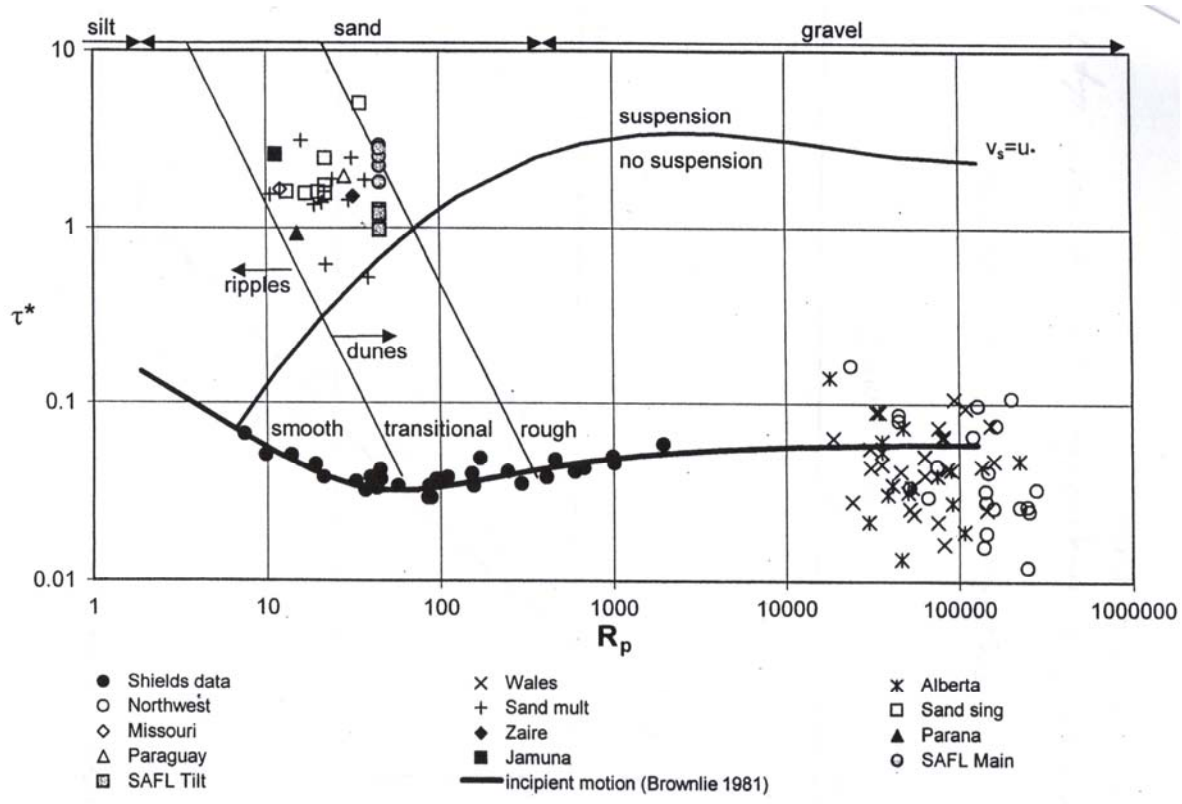

Figure I.1: Updated Shields Diagram showing line of critical Shields stress (Parker).

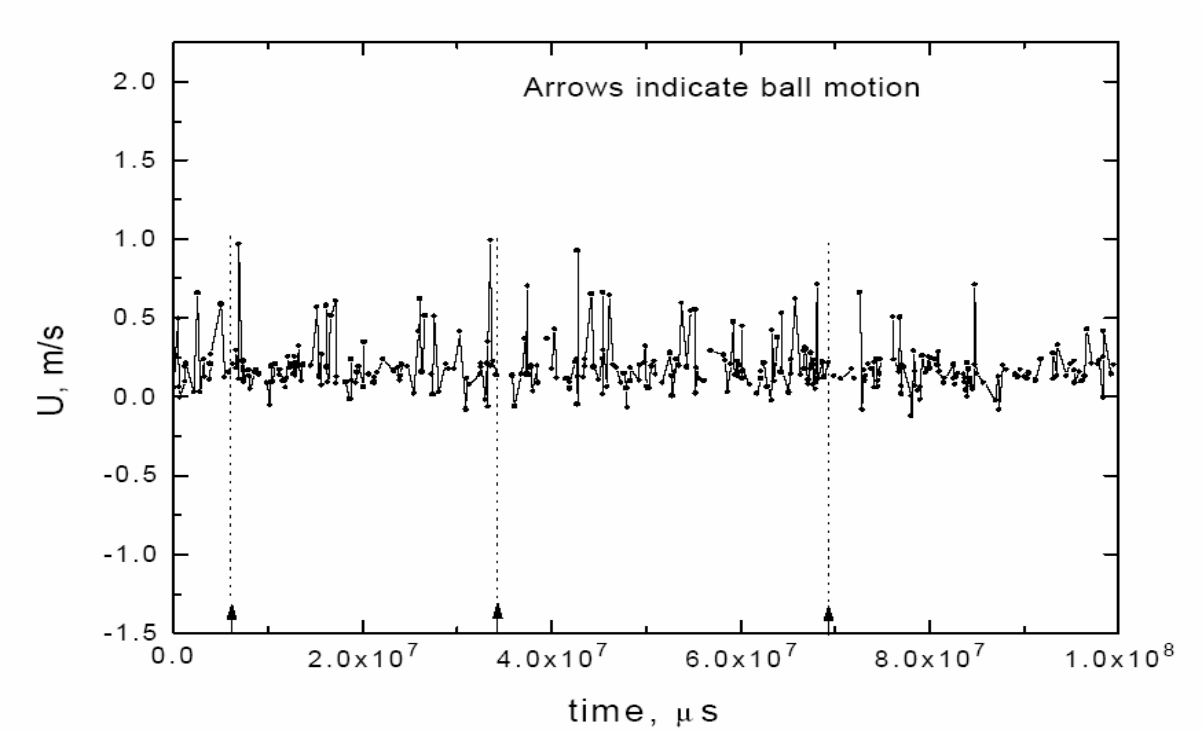

Figure I.2: Sample LDV data from single ball flume experiments. The arrows indicate ball motion. (Balakrishnan 1997)

Chapter II
Experimental Facilities

All of the experiments were completed at the Kelso S. Baker Environmental Hydraulics Laboratory located at Virginia Polytechnic Institute and State University, Blacksburg, Virginia. Some of the preparatory work and testing was completed at the Unmanned Research Laboratory run by the Mechanical Engineering Department also at Virginia Tech.

II.1 Experiment Components and Setup

There are five main components to the experiments discussed in this document: (1) the electromagnet and particles, (2) the data acquisition system and signal generator, (3) the amplification circuit, (4) the stabilization structure, and (5) the camera. Each will be described in the following sections and further under Preparatory Work.

II.2 Electromagnet and Particles

The electromagnet used in these experiments is commercially available from McMaster-Carr. It is a 32 lb max pull, 1 inch diameter round surface electromagnet. The energized

electromagnet's outer edge will produce a magnetic field surrounding the center pole. Several different size and shape magnets were tried. During testing, the 1 inch diameter round electromagnet was able to move a test particle at a given distance from the face. In addition, it was thought that with the small, even distribution of the magnetic field around a central point (the cylindrical iron core) would produce a more accurate force to be directed at the particle rather than a larger or rectangular face which would create wider fields.

The balls that are used in the experiments to represent the sediment particles were obtained from Bal-Tec™ a division of Micro Surface Engineering, Inc. The experiments were originally designed to be tested on 8 mm diameter particles however it was later decided to include particles of different sizes; 6 mm and 4 mm diameter particles were added. The choice of diameter was originally set to match the existing particles from previous flume experiments which were completed with 8 mm diameter particles. The moveable particles are Grade 25 chrome steel-51200 chrome alloy balls which are highly magnetic. Additional properties of the particles can be found in Table II.1. The base balls were obtained from the same company. These balls are the same diameters and made of Teflon as not to interfere with the magnetic field.

II.3 Data Acquisition System and Pulse Generator

The computer programs used in the experiments were created in National Instruments LabVIEW 7.1. LabVIEW is an icon based programming language that allows for simplified programming to control instruments and read and record data. Two separate

programs were created for these experiments, the pulse generation program, and the data read in program. These programs and their development are discussed further in the Preparatory Work chapter.

The data acquisition system (DAQ) that was used for these experiments included a data acquisition board and a signal processor both on loan from the Virginia Tech Mechanical Engineering Department. The signal processor used was an SC-2345 Signal Conditioner with configurable connectors from National Instruments. The only processing units used were feed through modules. The DAQ board was the NI DAQPad-6015 also from National Instruments. The DAQ board was a USB connected system with plug-and-play features for portability as the experiments were run through the researcher's laptop computer. The DAQ board was one of the more limiting features during the experiments. The DAQ had 16 bit resolution in both analog input and output and could obtain up to 200 kS/s input sampling rates. However, the maximum hardware timed analog output rate was 50 S/s (allowing for a minimum pulse duration of 20 ms) and a maximum software timed analog output rate of 300 S/s (allowing for a minimum pulse duration of 3 ms). The researchers were hoping to achieve small pulse durations (on the order of 1 ms), however due to the limitations of the system, the best results would be obtained from using the software timed program as addressed in the next chapter, and only being able to achieve pulse durations in multiples of 3 ms with 3 ms being the smallest obtainable. The NI DAQPad-6015 maintains a 16-bit accuracy with a ±10 V range. This provides a 0.000305 V resolution and ±0.0001525 V quantization error. Other product information for the NI DAQPad-6015 can be found in Table II.2.

II.4 Amplification Circuit

An interface was needed to properly control and measure the voltage input to the electromagnet. The DAQ system was limited to an input and output range of ±10 V. This range was not large enough to capture all of the voltage values that would be needed to remove the particles from their pockets. In order to obtain higher values an amplification circuit was designed and built for the interface. This circuit amplifies the signal sent by the DAQ system to the magnet, reads the voltage drop across the electromagnet as well as the current and then de-amplifies these signals to an appropriate range to be read back in by the DAQ. The circuit and its development are discussed further in the Preparatory Work chapter.

II.5 Stabilization Structure

It was important during these experiments that the center of each moveable ball be inline with the center of the core of the electromagnet. The distance from the electromagnet can cause variations in the amount of force applied to a particle. A structure was developed that would allow the researcher to properly align the moveable particle. This structure, as can be seen in Figure II.1, mounts the electromagnet to an optical stage with vertical mobility. The electromagnet also has a needle attached to its top which is inline with the center of the electromagnet's mounting hole. This needle is used to assist with proper alignment; it is also aluminum and will not affect the electromagnetic field.

The base particles are situated on another two-dimensionally adjustable setting. The base particles are made of Teflon and glued in groups of four to an aluminum plate. This plate is then attached to an optical stage with lateral mobility. This lateral stage aligns the base particles with the center of the magnet core. This stage is also attached to a second optical stage that allows for control of the distance the base lies from the electromagnet face. Figure II.2 shows this arrangement. All of the stages are aluminum as to not affect the magnetic field, the only magnetic pieces of the structure are the turning knobs of the stages; however, these are only slightly magnetic and far enough away from the electromagnet to warrant little effect on the field surrounding the balls.

II.6 High Speed Camera

A high speed digital camera was used during the end of the experimentation phase to capture images of the ball movement. The camera was a Phantom v4.2 from Vision Research, Inc with a 2048 megabyte on board storage capacity. The camera has the capability of running at up to 2,100 pps at full sensor of 512x512 resolution or up to 30,000 pps at lowest resolutions. The camera also comes with its own Phantom 6.0.4 image analysis software. This program allows for trimming of video to only selected frames and play back at lower speeds. The software also has a point tracking function where the user can select points in a series of frames and a text file is generated with the x and y coordinates of the points as well as their frame number. This software allows for the user to change the scale from pixels to millimeters and other measurements of distance. The accuracy of the program is dependent on the pixel size and the zoom of the image as well as the accuracy of the users point selections.

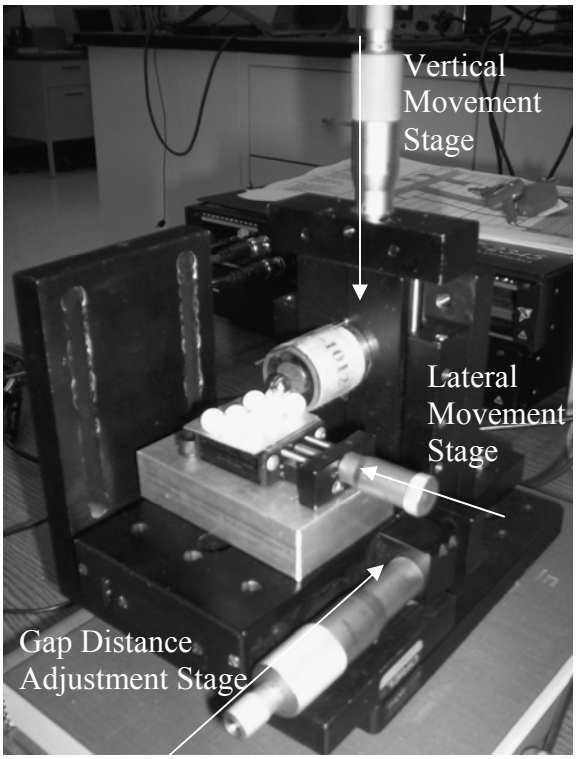

Figure II.1: Stabilization structure

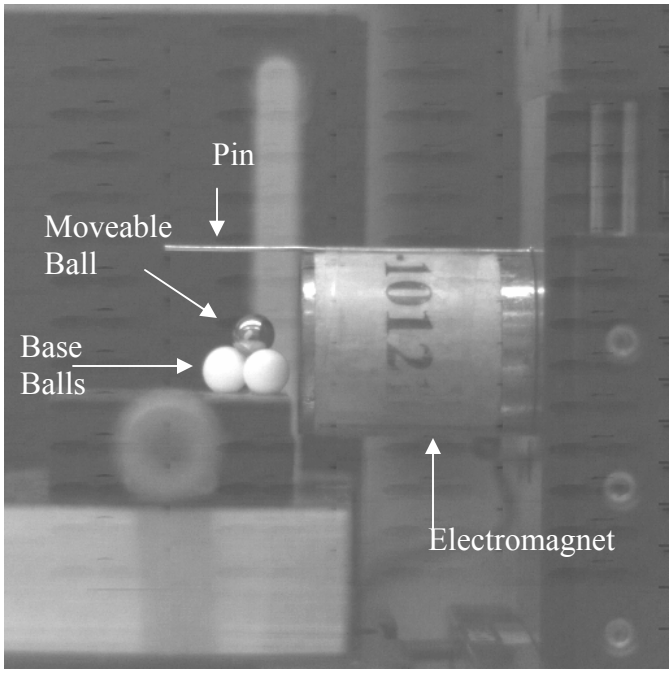

Figure II.2: Side view of magnet attached to vertical stage with horizontal pin. Base arrangement attached to lateral stage.

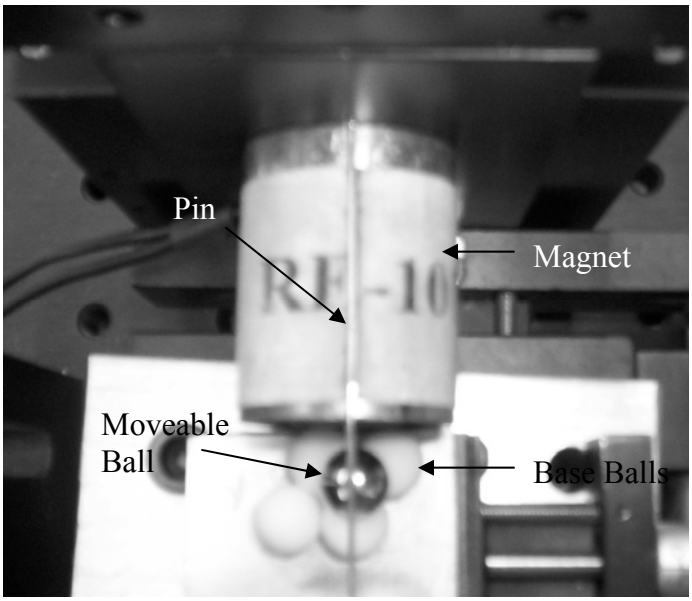

Figure II.3: Top view of particle set up.

Table II.1: Properties of moveable particles

Diameter	Material	Grade	Sphericity	Diameter Tolerance	Avg. Weight	Density
8mm	Chrome Steel	25	0.000025	±0.0001 in	2.0870 g	7831 kg/m^3
6mm	Chrome Steel	25	0.000025	±0.0001 in	0.8807 g	7831 kg/m^3
4mm	Chrome Steel	25	0.000025	±0.0001 in	0.2603 g	7831 kg/m^3

Table II.2: Properties of NI DAQPad-6015

Bus	USB	**Analog Outputs**	2
Input Resolution	16 bit	**Output Resolution**	16 bit
Max Sampling Rate	200 kS/s	**Max Hardware Output Rate**	50 S/s
Input Range	±10 V	**Max Software Output Rate**	300 S/s
Resolution	0.000305 V	**Output Range**	±10 V

Chapter III

Preparatory Work

Most experimental work is preceded by a large amount of preparations. This chapter discusses the development and alterations made to many aspects of these experiments and the equipment involved.

III.1 Electromagnet

A simple electromagnet is a coil of wire around a solid core. When electrical energy is applied to the coil, current flows through the coil creating an electromagnetic field with force flowing perpendicular to the current; cut the current off, the magnetic field collapses and the force dies. Electromagnets are easily made, however to produce significant levels of force, a commercially made electromagnet is needed.

The amount of force produced by an electromagnet is dependent on not only the amount of current, but also the physical properties of the magnet such as number of turns of wire, the core material and the distance the magnet is from the object it is attracting. (Electromagnetic force will be discussed further in the Analysis section). The amount of

electromagnetic force decreases significantly with any size air gap between the magnet and the object it is attracting, which is why most electromagnets are sold as surface mount electromagnets and their force abilities are listed for that use. In addition, at the start of the preparation, it was not known what type of forces the researchers would be looking for in the resulting experiments. These two complications made selection of an appropriate electromagnet a trial and error situation.

The magnetic flux of an electromagnet is highly affected by the medium through which that flux must travel. As mentioned earlier, magnetic flux density decreases significantly while passing through air. Plonus (1978) gives the expression

$$B = \frac{\mu_0 N I}{h} \qquad \textbf{(III.1)}$$

where B is the magnetic flux density in teslas, μ_0 is the permeability of free space, N is the number of turns of wire, I is the current in amperes, and h is the air gap distance in centimeters. This expression describes how the flux density will significantly decrease as the face of the electromagnet is moved further from the object which it is trying to attract. During preliminary testing of electromagnets, it was found that surface electromagnets with capabilities less than the currently used 32 pull-lbs had difficulty moving the test particle from a distance of 1 cm.

Another aspect of the electromagnet to consider was the shape. It was felt that a circular faced electromagnet would allow for easier estimation of the center of the magnetic force. Also, to be able to try and point the electromagnetic force towards the center of the particle as best as possible, a large faced electromagnet would not work; higher pull-force

rated electromagnets tend to have larger core diameters resulting in wider magnetic fields. The 1 inch diameter round electromagnet with ½ inch diameter iron core seemed to have the best characteristics for use in these experiments.

III.2 Signal Programming

The key to these experiments is controlling the force amplitude and duration (pulse) felt by the particle. To do this, a computerized pulse generation program was created that could send signals out through a data acquisition (DAQ) system and the pulse felt by the electromagnet read back into the program through the DAQ system.

The pulse generation program is user defined. The program is designed to take the inputs from the user for pulse parameters, such as amplitude and duration, and insert these parameters into an array. This array is then sent to the DAQ system at a user specified rate. The program will repeat until stopped by the user. The user can choose the pulse to repeat in a variety of different means: (1) repeat same pulse, (2) repeat with increasing amplitude and constant duration, (3) repeat with increasing duration and constant amplitude, (4) repeat with random values for duration and constant amplitude, (5) repeat with random values for amplitude and constant duration, (6) repeat with random values for both amplitude and duration. These experiments make use of program options (1), (2), and (3). The other options were designed with simulation of a random turbulent event in mind, although no experiments have been done using these options.

There are several limitations involved with the pulse generation program. Due to constraints from the DAQ system, the program is specified to run under software timing. There are two methods by which a program can run, hardware timed and software timed. Hardware timed programs are controlled by the clock within the DAQ system. The user may specify a particular sample rate and the pulses are generated in a highly accurate manner. Software timed programs are controlled by the timing of the software. This method cannot be used with a specified sample rate. The user may decide the length of the array (number of samples to send out) and the wait time between samples which can be used to calculate an average sample rate. However, because this type of program is run by the software clock, it is not as accurate as the hardware clock and can have faster or slower wait times depending on the computer and other programs running, etc. As mentioned earlier, it would be ideal to be able to adjust the pulses at the smallest rate possible to more accurately determine the pulse required for initial movement. The DAQ system used in the experiments however was limited to a 300 S/s analog output rate which correlates to a minimum pulse duration of 3ms. For example, an array of 400 points is created where 399 points have a value of 0 and 1 has a non-zero value. This is the pulse. The duration is one point, however the DAQ must wait 3 ms before sending out the next point, so that non-zero pulse will last for 3 ms before changed to a zero value. Adding another point to the non-zero pulse lengthens the pulse duration to 6ms before changing back to a zero value. Therefore, each pulse that is sent out increases by 3 ms interval; the true pulse duration needed to create initial movement however, could be less than the recorded pulse duration. For example, if the particle was not removed at 9 ms, but was removed at 12 ms, it is possible that a duration of 11, 10, even 9.5 ms

would have been able to remove the particle. It is impossible to determine with this current system which duration is the minimum required to dislodge the particle. This determines the maximum error or uncertainty in these calculations.

One way to bypass this source of error was to use the increasing voltage program. This program allows the user to choose a constant pulse duration and apply that pulse with increasing amplitudes. However, the accuracy of the pulse parameters can vary. For instance, when using option (2), holding the duration constant, the amplitude increments can vary. For most of the experiments, the amplitude increase was set at 0.1 system volts, Vs, 0.25 magnetic volts Vm (as result of the magnification as discussed later). That is, as each pulse is sent the amplitude is magnified by 2.5, resulting in minimum increments of 0.25 V. It is possible to program smaller increments, however doing so causes increased inaccuracy in the pulse durations. Also while using option (3), holding the amplitude constant with increasing durations, the pulse durations can fluctuate significantly in a non-predictable pattern. A balance is needed between amplitude increments and timing increments that will produce accurate and repeatable results. It is not really understood why this happens. This is compensated for by repeating each run several times until 3 like results are achieved. This helps to ensure that there were no fluctuations that caused greater values in either time or amplitude to cause the particle to dislodge.

The second program used is a simple read in program. The voltage across the electromagnet is measured using the circuit described later and then reported back to the

computer. This data is sampled using hardware timing (highly accurate as discussed earlier) at a rate of 2000 S/s. This data is graphed for visual comparison and also saved in a LabVIEW measurement file, a tab delimited text file. This file contains the relative time of the sample taken and the value of the voltage at that time. This allows a record of pulse durations accurate to the 0.0005 second. It is possible to read in data at faster rates, however, this affects the software timed program and reduces accuracy. After testing several different sampling rates, 2000 S/s was determined to be the fastest rate not causing loss of accuracy in the pulse generation program. As described previously, the NI-DAQ Pad 6015 has an accuracy of ±0.000305 V and each reading will give a value down to the microvolt.

III.3 Amplification Circuit

The most time consuming aspect of the preliminary work and experiment development was the design and fabrication of the amplification circuit that connects the data acquisition system and the electromagnet. The DAQ system is only capable of sending signals between ±10 V. At the beginning of the experiment design it was not known what range of voltages would be needed to dislodge the particle from its pocket at very short durations, but an assumption was made that it could be more than 10 V. A system was needed that would amplify the analog signal to an appropriate range to move the particle, measure the change in voltage across the electromagnet and then de-amplify the readings to an appropriate range that could be read by the DAQ system.

The first step in choosing amplifiers for the circuit was to determine some basic characteristics that would be ideal for the amplifiers. In electronics, an electromagnet is modeled as a resistor and inductor in series. A digital multimeter was used to determine both the resistance and inductance of the electromagnet, which were determined to be 41.5 Ohms and 0.054 Henrys respectively.

A second point was determining the maximum voltage rise time needed for the circuit. The voltage rise time is just as it sounds, the time needed for the voltage to rise to a certain amplitude. As this is just a rough value to be used in amplifier selection, exact values were not needed and maximum desired values were used. To simplify matters, the signal was also assumed to by sinusoidal. With this, the signal can be expressed as

$$V(t) = A \sin \omega t \qquad \textbf{(III.2)}$$

where V(t) is voltage at time t, A is the amplitude of the signal in volts, ω is the frequency of the signal in rad/s and t is time in seconds. In order to minimize the voltage rise time, greater than maximum values were used. An assumption of 50 V as the amplitude and a signal frequency of 5000 /s were used. This results in

$$V(t) = 50 \sin (2\pi 5000)t \qquad \textbf{(III.3)}$$

Voltage rise time can be determined by taking the derivative of this equation. The maximum voltage rise time would be where that derivative is at its maximum or when the second derivative is equal to zero.

$$dV/dt = (50)(2\pi 5000)\cos(2\pi 5000t) \quad \textbf{(III.4)}$$

where dV/dt is at its maximum when cos (2π5000t) = 1; when t = 0, therefore maximum rise time = (50) (2π5000) = 1.5 V/μs.

Up to this point in the design, the circuit was merely considered to be a black box type of connector between the DAQ system and the electromagnet; at this point it was necessary to decide exactly what the circuit needed to accomplish and how. Figure III.1 is a schematic of the finalized circuit which includes three amplifiers. The triangles symbolize the amplifiers. The first amplifier increases the voltage from the DAQ, the second amplifies the voltage differential across a small resistor which returns the current felt by the electromagnet, and the third follows a voltage divider which returns the an amplified voltage felt by the electromagnet. With this information, a line driver was chosen to run the circuit.

The line driver, chip, that was recommended for this circuit was the AD8392 from Analog Devices, Inc. This chip was chosen for its very high slew rate, also known as voltage rise time, and its ability to produce high currents while using low power levels. Another significant feature of this chip was its inclusion of 4 amplifiers; all of the amplification could be routed through one chip. The chip operated with either single or dual power supply and was capable of a peak linear output current of 400 mA.

The next step in the development process was the design and construction of the circuit board. The design was completed using an electronic circuit board layout design program, Eagle version 4.15. Eagle is a CadSoft USA product which allows the user to create a schematic of the circuit board as seen in Figure III.2 and then converts that into the necessary CAD files needed for construction. The program also checks for electronic errors and design rule errors. Figure III.3 shows the board layout design developed by Eagle. Once the final board CAD file is created the program then generates CAM files from the board design. These CAM files are standard files used in board construction that include information on design, layout, soldering, layers, copper, drill hole locations, etc. These files were then sent to Advanced Circuits, a company who constructs the actual circuit board. The files are then checked again by Advanced Circuits, once the files are approved, the board is constructed.

The last steps in production of the circuit board were done at the Unmanned Research Laboratory at Virginia Tech. All of the circuit's pieces are surface mountable and must be soldered on. This allows for changes to be made to the circuit if certain parts of the design prove ineffective and require replacing. At this point, resistor values were chosen that would provide a 2.5 gain to the input voltage and then sufficient reductions to be sent back to the DAQ; meaning that a 1 V signal from the DAQ would produce 2.5 V signal to send to the electromagnet. Once all the resistors, the line driver, and connecting wires were soldered into place, the board was then tested with simulated signals and oscilloscopes to test for correct measurements.

One of the largest problems with these experiments was that without having any previous experiments for comparison, it was impossible to tell whether the circuit would be capable of producing the results needed; when testing using the electromagnet and sample balls began, it was decidedly incapable. Many problems arose with the first circuit design which evolved into many weeks of trial and error changing settings to achieve the desired results. The most frequent problem was overheating of the chip. As described earlier, the peak output current of the line driver was 400 mA. It was expected that the electromagnet would require approximately 350 mA, running the chip near its peak for long periods of time seemed to cause the chip to overheat frequently. The chip often burned out completely or shorted requiring a change in chip.

A second problem with the design resulted from the power supply. The circuit was being run with a single power supply, meaning it could provide only positive voltages. The chip, when run on a single power supply is able to produce voltages between 0 and 24 V with an actual max voltage swing of 23.0 V meaning the chip would never actually be able to reach its rails. During testing it was found that the lower rail of 0 V was much higher than anticipated, nearly 1 V, which when magnified was sometimes enough to remove the particle, thereby defeating the purpose of the experiments. It was necessary to have the resting voltage as close to 0 V as possible. The solution to this problem was adding a DC-DC converter to the circuit. This piece, the PT5062, a ±15 V DC-DC converter from Texas Instruments takes in the power from a single power supply and converts it to a dual power system. The dual power system now has rails of ±15 V (the chip actually has rails of ±12 V for dual power operation) and allows for absolute zero

values, however it does reduce the upper rail from 24 V to 12 V which corresponds to a reduction in the amount of electromagnetic force able to be created.

The DC-DC converter circuit was then added to the original circuit, however many of the original problems with overheating and burning of the line driver still remained; the solution to this problem was more involved, requiring a completely new circuit with different line drivers. It was decided to use two separate line drivers to accomplish the amplification. The voltage amplification of the input signal required the most power and produced the most heat and so a second chip was added to handle this. The THS6182 from Texas Instruments is a low-power dissipation ADSL line driver. Not only significantly larger in size allowing for more heat dissipation, but the THS6182 also has a higher peak output current of 600 mA and a larger voltage output swing of 44 Vpp. The voltages from the voltage drop and voltage divider were then handled by a separate operation amplifier, the OPA2251 also from Texas Instruments. The OPA2251 is also larger in size than the original line driver and has a dual supply range of ±18 V. The switch to these two new op-amps required the design and construction of a new circuit board using Eagle; the DC-DC converter was also included on the new board. Figures III.4 and III.5 show the schematic and board layout for the final amplification circuit.

Once all the components of the final circuit board were soldered, tests were conducted at the Unmanned Research Laboratory with simulated signals. The new circuit was able to handle the heat and high power levels much better than the previous board. The limiting device was now the DC-DC converter with rails of ±15 V. During testing it was found

that voltages in the 12.5-15 V range were often not resulting in the correct gains. Additionally applying power to the circuit without sending a signal causes high currents and high power levels that can damage the chip if run for significant portions of time. Also, the electromagnet should only be connected to the circuit after the power is turned on.

The second circuit that was designed was the final circuit used in these experiments. As noted earlier, conducting these experiments with no prior knowledge as to the desired outputs, much of the design was trial and error. The final circuit produces nearly the highest amount of power capable from a non-professionally design circuit. Voltage and current peaks higher than the ones available from this circuit will require a greater power supply and circuitry only available from a circuit board manufacturer. This circuit is suitable for these first experiments, however, if ever completed again; a professionally designed and constructed board would be a recommendation. Figure III.6 is a photograph of the entire experiment system setup.

III.4 Circuit Parameters and Testing

The previous section described in detail the elements comprising the electronic circuit controlling the electromagnet. This section will give some detail as to the parameters set for these experiments and their bearings on the results.

A frequency response test was done to help determine the degree of accuracy that will be achieved for measuring the time durations of each pulse. The DAQ system has the

capability of reading in voltages at a rate of 10 kS/s. Three sample tests were run at this rate, to show how voltage rise time varied with different amplitudes, this helps to determine the accuracy of the durations. Three different amplitudes were used 2.5 V, 6.25 V, and 12 V covering the range of amplitudes used during the experiments. Each pulse was sent for a duration of 6 ms. Figures III.7 – III.9 show the data taken for a single pulse. For both 2.5 V and 6.25 V the frequency response is approximately 0.2 ms, for the 12 V case, the response time increased to nearly 0.4 ms. Each of these however, is less than the error due to the chosen sampling rate of 2000 S/s.

III.5 Ball Placement

As electromagnetic fields cannot be seen, it was important that for each experiment, the location of the moveable particle be known and at the same location in repeated experiments. The moveable balls are each spherical with diameters of 4 mm, 6 mm, and 8 mm. The base balls are the same, only Teflon. In order to maintain consistency for the experiments, the location of the center of the moveable ball was kept track of and used for alignment.

Three separate bases were created to be used for these experiments. The bases consist of four equal diameter balls in a tetrahedral arrangement. These balls are then affixed to an aluminum plate. This plate is then affixed to the top most stage in the stabilization structure. From this point, the moveable particle is aligned to the center of the core of the electromagnet. An aluminum pin is affixed to the top of the electromagnet parallel to the center of the core. This pin is used to find the center of the pocket of the base balls

through which the moveable ball will roll. The base is laterally adjustable for this alignment. Additionally, to align the center of the moveable ball to the center of the magnet core, the ball is placed in the pocket and vertical stage measurements are taken at the top and the bottom of the ball using the pin. The distance from the pin to the center of the core is known and a vertical alignment can be made. The third and final alignment is the distance from the face of the magnet. As mentioned earlier, the air gap between the attractable object and the electromagnet is very important. The greater the air gap, the less force produced. With this variation in force, it would be nearly impossible to compare the result of these experiments. Seven different sets of experiments were conducted; five of these sets were completed with the center of the moveable ball being at the same distance from the face of the electromagnet. The first basic experiments were done with the moveable ball and the base balls of equal diameter. The base balls were located such that the fronts of the base balls were touching the face of the electromagnet. Additionally, four more experiments were run with different combinations of ball and base diameters. Each of these experiments was run at an equal distance from the front of the electromagnet for better comparison.

Although great care was taken to insure the location of the center of the moveable ball was consistent for each experiment, a check was done to see what might occur if the moveable ball were off center. Measurements of a "steady state" condition were taken while the ball was at center and at varying distances off center until the ball was over half a ball diameter off center. The voltages required to move the ball remained the same. It

was then determined that the location of the ball laterally was not as important as the distance of the ball from the face of the magnet.

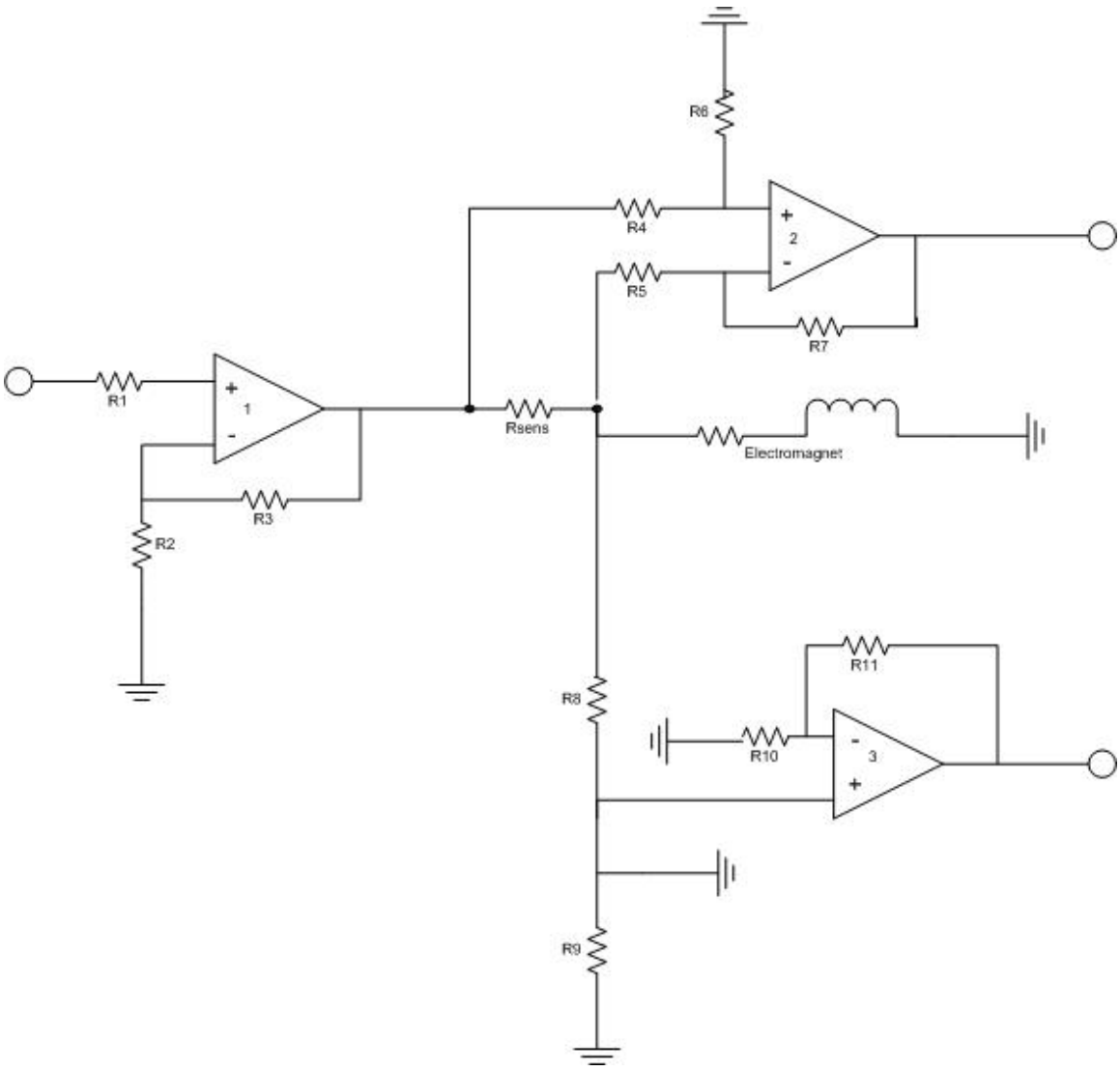

Figure III.1: Schematic of electronic circuit

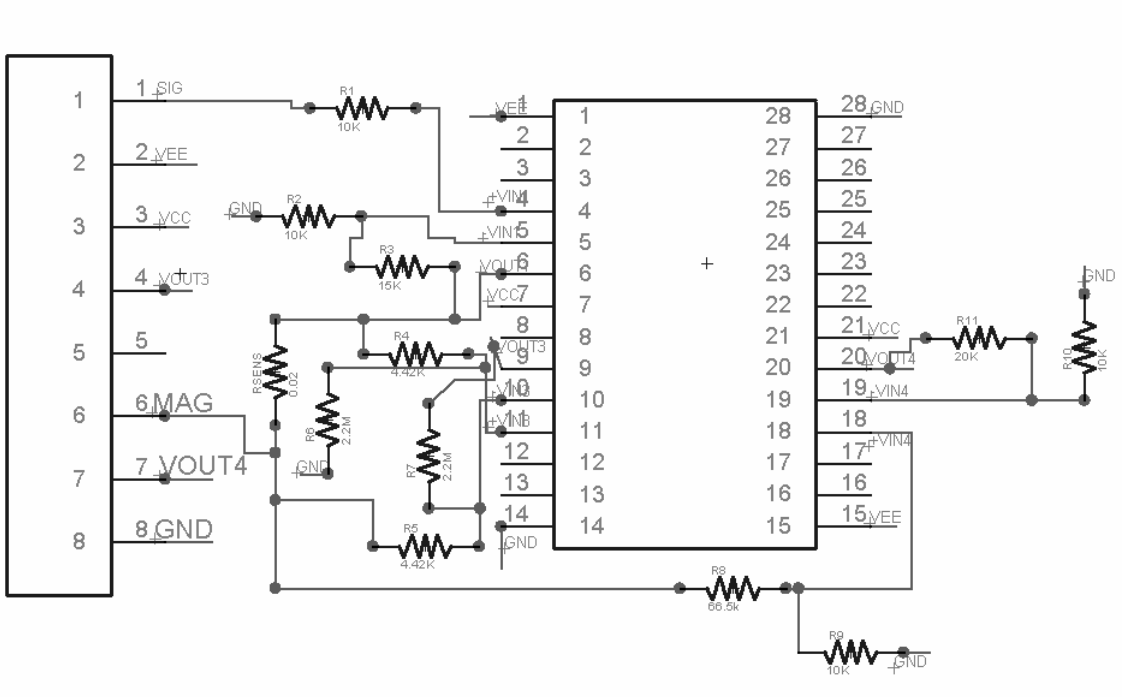

Figure III.2: Schematic drawing of first electronic circuit with AD8392 line driver.

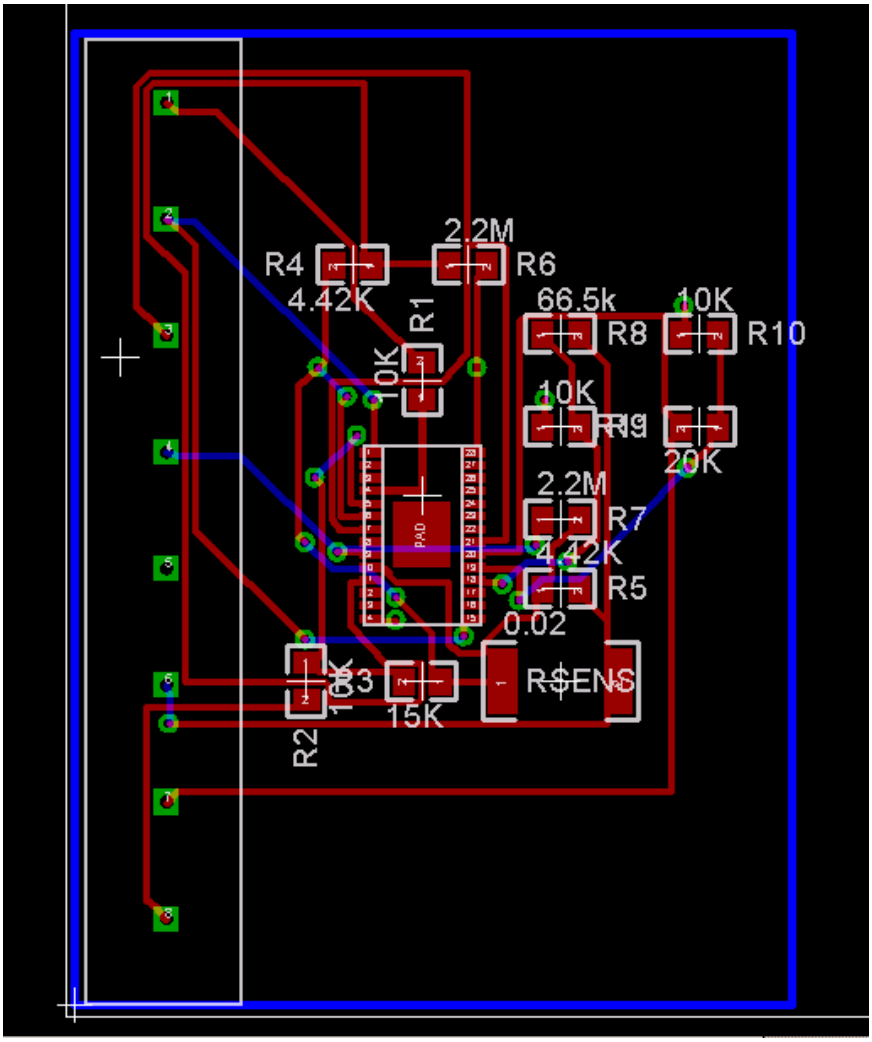

Figure III.3: First electronic circuit board layout design developed using Eagle

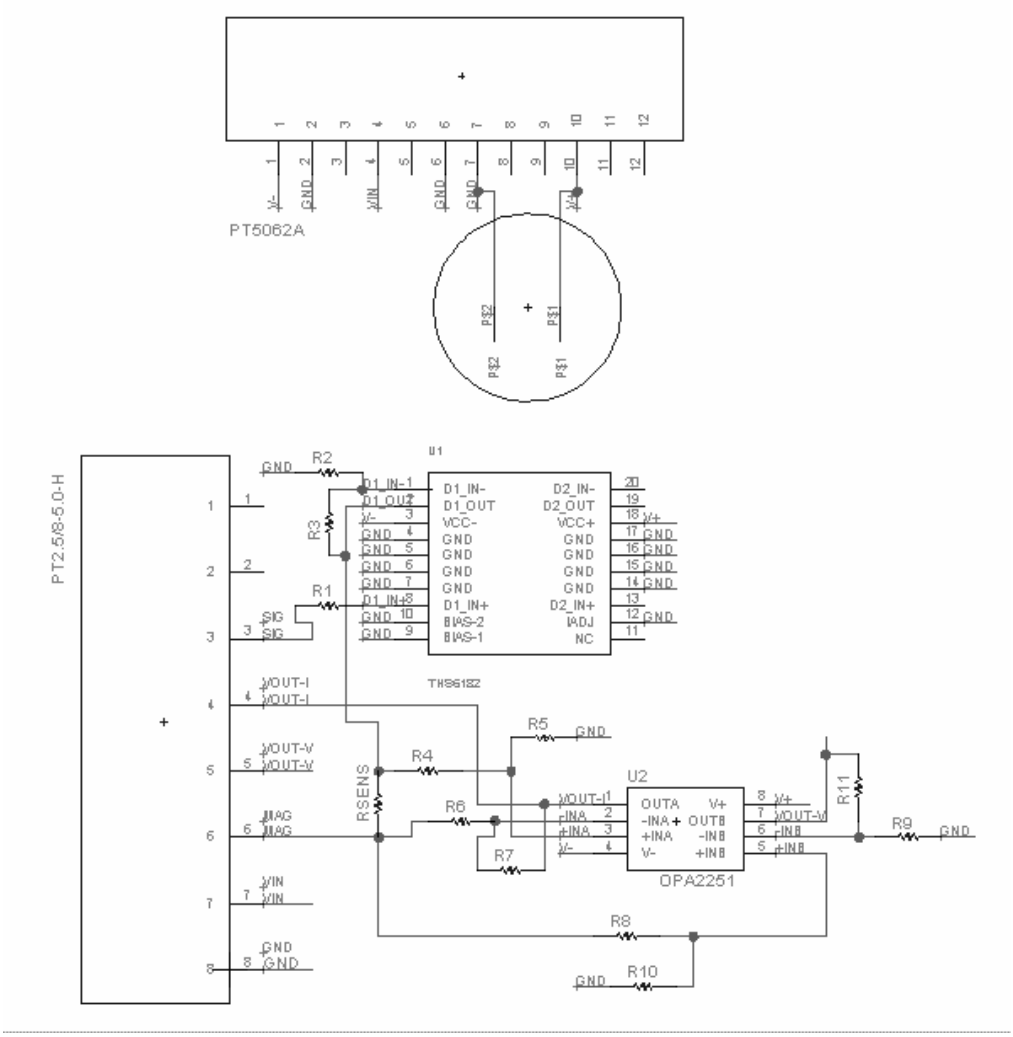

Figure III.4: Schematic of final electronic circuit using THS6182 and OPA2251 line drivers.

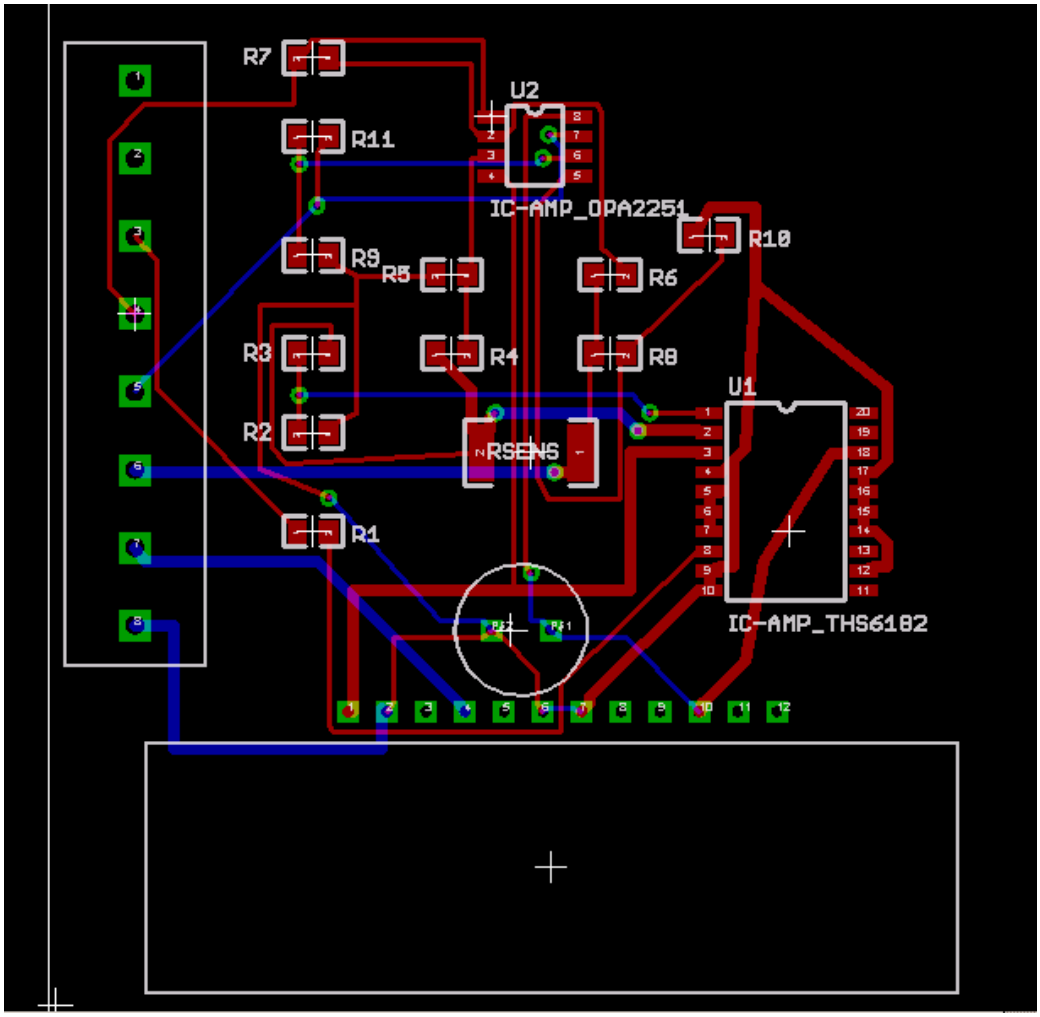

Figure III.5: Final electronic circuit board layout design created using Eagle.

Figure III.6: Photograph of complete experiment system set up.

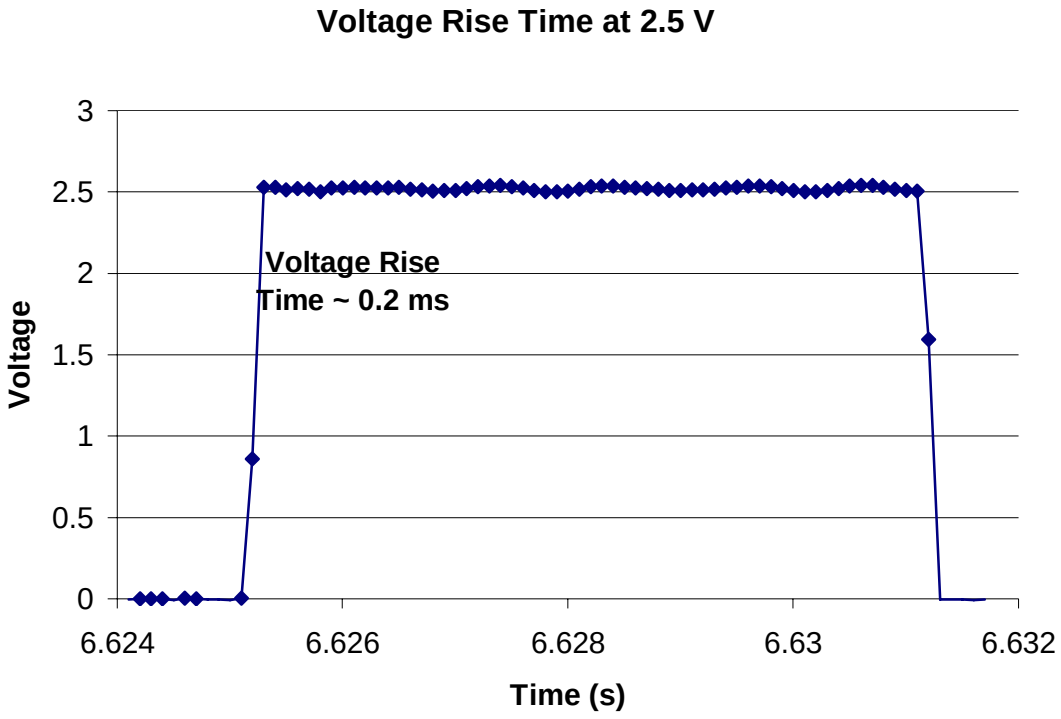

Figure III.7: Voltage rise time for a 2.5 V pulse sampled at 1000 S/s

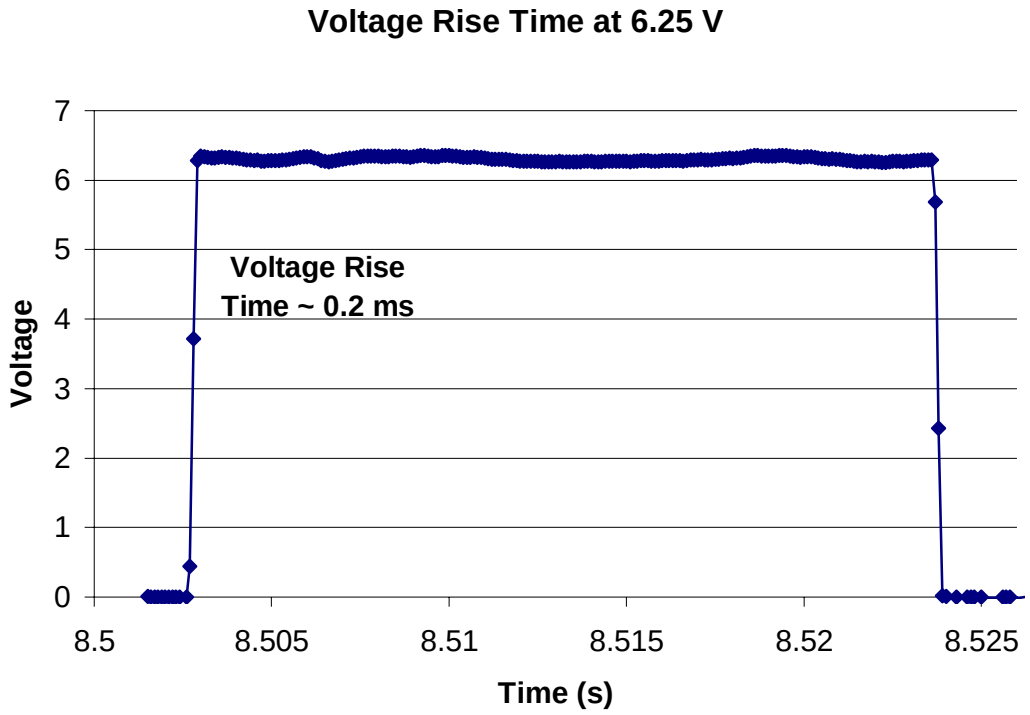

Figure III.8: Voltage rise time for 6.25 V pulse sampled at 1000 S/s.

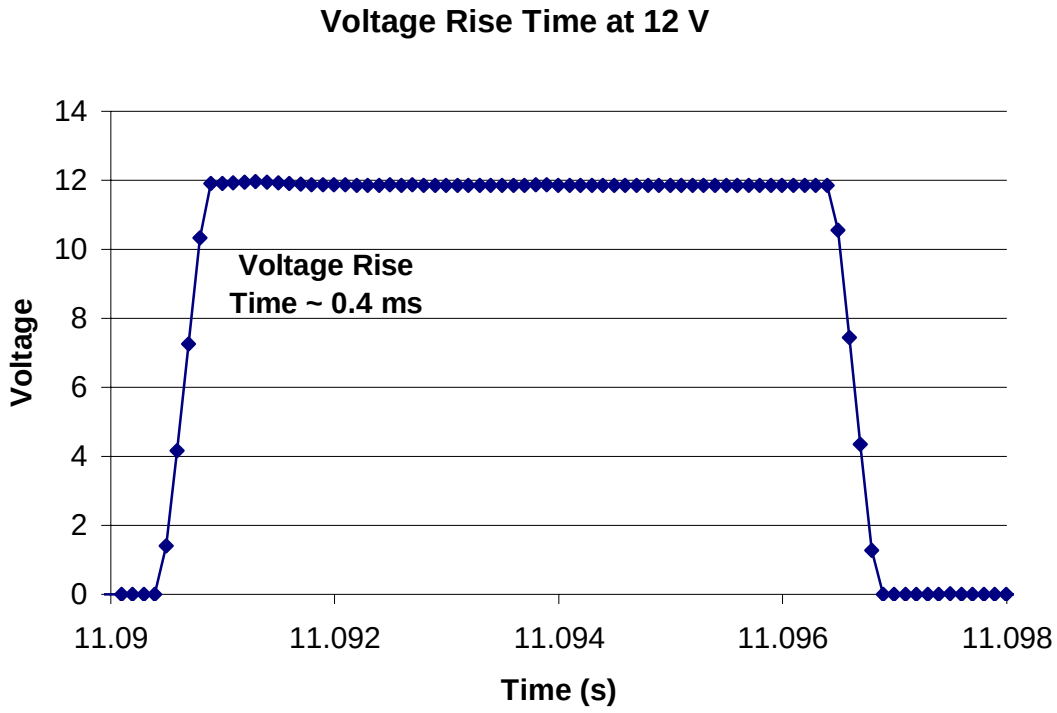

Figure III.9: Voltage rise time for 12 V pulse sampled at 1000 S/s.

Chapter IV
Analysis and Results

IV.1 Introduction

This chapter discusses the results of the final electromagnetic motion experiments. First, the equations of particle motion are described as well as the simplified equations that are used for these experiments. These experiments are a simulation and simplified version of what might happen in a natural stream or even an experimental flume setting with electromagnetic forces acting as the fluid drag force. These forces are not easily directly correlated; however a discussion of how the electromagnetic forces work and a discussion of their overall relation also follow.

IV.2 Particle Motion

Determining the forces required to move a single particle from a bed of particles is a problem that has been evaluated by many researchers (Coleman 1967; Middleton 1984; Moore 1994; Chien 1999). There are many aspects that can alter the particle movement scenario such as particle shape and bed packing density; overall however, the same mechanical principles apply. Of the three main forces acting on a sediment particle, two are fluid forces. The drag force is typically more predominant because it acts parallel to

the flow over the entire exposed face of the particle while the lift force is often less and dependent on pressure differences between the top and the bottom of the particle. The final dominating force is the submerged weight of the particle.

In order to determine particle movement for the particle arrangement used here, a balance of moments is needed. To determine these moments, the following expressions are often used to determine the dominant forces.

1. The submerged weight of the particle, F_G

$$F_G = \frac{\pi}{6} d^3 (\gamma_s - \gamma) \qquad \textbf{(IV.1)}$$

where d is the diameter of the particle and $\gamma_s - \gamma$ is the particle submerged specific weight.

2. The instantaneous drag force, F_D, exerted on a particle is

$$F_D = \frac{1}{2} C_D \frac{\pi}{4} d^2 \rho u^2 \qquad \textbf{(IV.2)}$$

where C_D is the drag coefficient, ρ, the fluid density, and u is the instantaneous fluid velocity at the center of the particle. The equation uses the diameter of the particle to determine the frontal area as the surface over which the drag force acts, many equations however alter this and use only the frontal exposed area if the particle is not overly exposed.

3. The instantaneous fluid lift force, F_L exerted on a particle

$$F_L = \frac{1}{2} C_L \frac{\pi}{4} d^2 \rho w^2 \qquad \textbf{(IV.3)}$$

where C_L is the lift coefficient and w is the instantaneous normal velocity.

Figure IV.1 is a typical representation of these forces and their locations on an exposed particle. The figure does not assume that the drag force acts through the center of gravity of the particle. As stated previously, some researchers prefer to used an exposed area in determination of the drag force; this would alter the location through which the drag force would act.

Assuming that the fluid lift force is negligible compared to the other forces acting on the particle, movement of the particle is determined when the moment created by the drag force is greater than the moment of the gravitational force. The moments are taken about the pivot point, a, in Figure IV.1. The moment balance shows that movement occurs when

$$F_G \sin\beta \cdot x_1 < F_D \cos\beta \cdot x_2 \qquad \textbf{(IV.4)}$$

The purpose of these experiments was to see if force-time combinations had any effect on the determination of when a particle would move. As mentioned earlier, the above equations make certain assumptions and there are many natural factors such as particle shape, bed geometry, particle location and exposure that can alter how and when a particle moves. In order to focus on just the aspect of force-time combinations, it was necessary to remove or reduce as many of these natural factors as possible. The particles used in these experiments were all spherical particles in beds of same geometry of various sizes. The particles sat high on the bed and the pivot angles were determinable. The experiments were also conducted in air so submerged weights were not taken into account. Although it is difficult to determine, it was assumed that the electromagnetic

forces acted over the entire frontal area of the particle and were directed at the center of mass of the ball. These simplifications can be seen in Figure IV.2. No lift forces were used in these experiments and the electromagnetic force was used to simulate the drag force. Using these simplifications and performing a moment balance, it can be said that movement in this situation will occur when

$$F_G \tan\beta < F_D \qquad \textbf{(IV.5)}$$

IV.3 Electromagnetics

Creating an experiment to study incipient motion without having outside forces or other complications affecting the motion was very difficult. Another difficult aspect was measuring those forces in a non-intrusive manner. Using electromagnetic forces gave a way to apply varying forces to the particle in a way that would act similar to that of a surrounding fluid. Instead of pushing the particle out of the pocket however, the electromagnetic force would work in the opposite direction and pull the particle out of the pocket.

For this project, electromagnets were the best way for producing a controllable force in a non-intrusive manner. An electromagnet is simply wire coiled around an iron core. The electromagnet used in these experiments was manufactured to create high levels of force. The ½ inch iron core was tightly wrapped with coil. As a voltage is supplied to the electromagnet, current runs through the coils. As the current runs through the wire, a magnetic field is developed that is perpendicular and circular around the wire. Figure IV.3 gives a good representation of the magnetic field about the wire. The magnetic field

is highest nearest the wire and lessens as it travels away from the wire. An easy way to magnify this field is to coil the wire as is done in electromagnets. The coiling of the wire increases the magnetic field and wrapping the coil around an iron core creates a magnet similar to a natural bar magnet. Figure IV.4 shows how the field changes as the wire is turned. The magnetism increases near the core where the field is dense. This magnetic field is controlled by the amount of current, and thereby the amount of voltage running through the coil, which makes this magnet an electromagnet. The magnet is naturally attractive; reversing the current still causes the field to be created perpendicular and circular around the wire, so the magnet is still attractive. The field is created instantaneously as the current runs through the coil and falls off completely as the current is cut.

Electromagnets are commonly used in industry. The controllability of the magnet is the main draw. Often these magnets are created with enormous attractive forces and are used to lift and transport cars and storage containers as the force can be turned on an off at will. In order to make these high force magnets, higher voltages and currents can be run and greater number of coils can be turned. The main feature with these magnets however is that they are all designed for surface use. Electromagnetism is a force that is greatest when actually touching at metallic surface. All materials on Earth have a known value called magnetic permeability. Magnetic metals have a high value, air has an extremely low value, it is known and the permeability of free space. Electromagnetic forces have an extremely difficult time traveling through air. Imagining a normal bar magnet that might be used on a refrigerator, one can see that the attractive force isn't felt until the

magnet is placed very close to the refrigerator surface; an electromagnet has even less straying power. To give some reference, the electromagnet used in these experiments at full voltage is designed to lift 32 lbs, however, at full voltage this magnet cannot attract a 2 g ball at a distance of 1 cm.

To explain this idea in a more precise manner, the following manipulation of the equations for electromagnetism from Plonus (1978), can show the effects of an air gap.

The magnetic field, also known as the magnetic flux density, B

$$B = \Phi/A = N\ I\ \mu / h \quad \text{weber/m}^2 \qquad \textbf{(IV.6)}$$

where Φ is the magnetic flux, A is the surface area, N is the number of turns of wire, I is the current, μ is the permeability of the medium and h is the air gap.

As the magnetic field works to exert forces to close the air gap, energy is stored in the gap. The density of energy stored, w_m, in a field is

$$w_m = B^2 / 2\mu \quad \text{joules/ m}^2 \qquad \textbf{(IV.7)}$$

If the gap is small, a uniform field may be assumed for the gap, then the total energy, W_m, in the gap will be

$$W_m = w_m\ Ah = B^2Ah / 2\mu_0 \quad \text{joules} \qquad \textbf{(IV.8)}$$

where μ_0 is the permeability of free space and A is the surface area of the gap.

Energy can also be written as force times a distance, using this manipulation and those from the previous steps, it can be shown that

$$F = B^2A / 2\mu_0 = N^2\ I^2\ \mu\ A / 2\ h^2 \quad \text{Newtons} \qquad \textbf{(IV.9)}$$

From equation (IV.9) one can see that the force created by an electromagnet is inversely proportional to the square of the distance of the air gap meaning that as a particle moves further from the face of the electromagnet, the more force is needed to attract that particle.

IV.4 Voltage and Force Correlation

Using electromagnetics to cause a particle to roll from its pocket was a completely non-intrusive method of applying a force. In keeping with that idea, a non-intrusive method was needed to measure that force. Traditional methods of measuring force such as strain gauges would have physically altered the ball and would have been difficult to implement in these experiments. In order to find a way to explain the electromagnetic force and connect it with the force needed to remove the particle, other methods of measurement were looked into.

The first step in understanding electromagnetic force was understanding in a general sense how the various characteristics of an electromagnet correlated with the resulting force. Turning to the equations for electromagnetics helps to generalize this. Looking back at equation (IV.9) from Plonus (1978), the electromagnetic force can be determined by

$$F = N^2 I^2 \mu A / 2 h^2 \quad \text{Newtons} \qquad \textbf{(IV.9)}$$

Assuming that for each experiment the same electromagnet is used, the values of N, A and μ will remain constant. These values are often known if the electromagnet is home made. Most manufacturers also keep this information on file; however, the manufacturer

of the electromagnet used in these experiments was unable to provide this information. Additionally, if for each set of experiments the air gap between the face of the electromagnet and the particle being attracted remains the same, h can also be represented by a constant. Those working in the field of electromagnetics are still uncertain as to how a magnetic field decreases through an air gap, especially on of the relatively large distance needed in these experiments. Also, modeling of magnetic fields around a spherical particle is something still being researched. All this leads to an additional uncertainty factor that plays into the assumed h constant. However, with this uncertainty constant, the equation can simplify to

$$F = c\, I^2 \qquad \text{Newtons} \qquad \textbf{(IV.10)}$$

where c is the constant parameter representing N, A, μ, and h. Current is not the parameter that is controllable in these experiments; voltage is. However, Ohm's Law states that

$$V = I\, R \qquad \textbf{(IV.11)}$$

and the resistance value of the electromagnet is also a constant for all of the experiments. Rearranging this again and combining with equation (IV.10), it can be shown that

$$F \propto V^2 \qquad \textbf{(IV.12)}$$

Knowing that electromagnetic force is proportional to voltage squared allows for a general comparison to be made during the experiments. Finding a way to determine exactly how force varies with voltage for these experiments was much trickier, so much so that the actual correlation was not determined. As mentioned previously, there are many uncertainty factors that will play a role in this proportionality, however, if all the

above constants are kept the same for a particular set of experiments, it is reasonable to believe that with direct measurement of applied voltage and either direct or indirect measurement of applied force, that the proportionality could be determined. A method of using high speed imagery was formulated as a possible way of indirectly determining the applied force and the results of the preliminary experiments can be found in the following chapter. It is proposed that these experiments will continue and the high speed imagery will be able to show the direct relationship between force and voltage and better understand the forces causing these particles to move.

IV.5 Incipient Motion Experiments

The purpose of these experiments was to better determine what causes incipient motion of a particle lying on a simulated idealized river bed. As discussed earlier there are many different variables that play into what force will cause a particle to move, i.e. particle shape, weight, position on bed, packing density, direction of flow, force of flow and many others. Traditionally, critical shear stress, τ_c, is used to describe the river conditions that will cause a particle to move. Recall that traditionally mean flow characteristics and extrapolated data were used to determine the point of incipient motion (Shields 1936). With most equations for bed load transport based on the amount of shear stress over that of the critical shear stress, it is important to truly understand and accurately determine the point of incipient motion.

IV.5.1 Same Geometry Experiments

The main consideration with these experiments has been to try to reduce variability as much as possible to clearly identify the mechanism responsible for particle movement. There are seven different sets of experiments overall. The first three are referred to as the same geometry experiments because of their set ups. Three different sized steel particles were used. These are the moveable particles that are attracted by the electromagnet. Each particle is made of the same material and theoretically equally as attractive to the magnet and assumed spherical.

The particles are all placed on a densely packed bed of particle of the same diameter. These bed particles are made of Teflon which is a completely non-magnetic material. The bed particles are glued together in a 4 ball tetrahedron where the metallic ball sits on top of three base balls. When attached to the stabilization structure as described earlier, the front two base particles align with the magnet. This allows for the easiest path of motion (a roll between the center of these two front balls) to be inline with the electromagnetic force. Figure IV.5 shows the particles path as it leaves the pocket. With all of these precautions, limiting friction, complete sphericity, easiest path of motion, it is assumed that the resulting force required to remove the particle from its bed is the least force possible, equating with true incipient motion.

These three experiments are referred to as the same geometry experiments because in each experiment the metallic ball is placed on a bed of equal diameter and place so that the center of the metallic ball is 0.788 times its diameter away from the face of the

magnet (equating to the front of the base balls touching the magnet face). These set ups can be seen in Figure IV.6. As Figure IV.6 also shows, the center of the moveable particle aligns with the center of the electromagnet both vertically and horizontally.

The hypothesis being tested in these experiments is that the amount of force applied on the ball is not the only factor in determining whether a particle will move or not, but that the time duration of that force also plays a roll. To test this, with each different set up, multiple voltage pulses with varying amplitudes and durations were applied to the particle. As described earlier, the pulse generation program works in a variety of manners. The pulses were applied in an increasing amplitude function. Each run consisted of a set pulse duration and a minimum pulse amplitude, program (2). As described earlier, because of the limitations of the DAQ devise, the exact duration of the pulse could not be guaranteed and the pulse durations come in minimum increments of approximately 3 ms. During each run, the amplitude would increase steadily by 0.25 V (the minimum increment without disrupting the duration) until the particle was fully dislodged from the bed. Figure IV.7 shows a typical run with 27 ms duration pulses; the final pulse shows when the particle was dislodged, with dislodgement defined as the particle completely rolled out of the pocket, not able to roll back in.

As the run progresses and the amplitude of the pulses increase, it is clearly visible that the duration of the pulse plays a roll in determining if the particle will be fully dislodged or not. Standard digital movies were taken showing entire runs until dislodgement. In most instances the particle is seen to “twitch” in the pocket when pulses that do not supply

enough amplitude and duration are applied. However, there is a certain force-time combination for each ball that will fully dislodge the particle. Each run was repeated until the same force-time combination was achieved three times. The same process was then repeated with another pulse duration. The process continued until every 3 ms interval was covered between the minimum pulse duration (dependant on available voltage) through to approximately the "steady state voltage." The steady state voltage is the voltage at which the particle will roll from its pocket if under a theoretical pulse of infinite duration; equating to the minimum voltage needed to remove the particle. These pulses were actually approximately 1.5 s in duration, however, the particles always moved prior to the completion of the pulse, and so served the purposed of being "infinite." Figure IV.8 shows all of the pulse values applied to an 8 mm ball on an 8 mm bed 6.31 mm from the face of the magnet. The graph shows a line through the pulses, labeled as "Movement" which caused the particle to be dislodged; all the other pulses below the line were insufficient. The steady state voltage is also shown in the graph. Also recall that earlier it was shown that force is proportional to $(\text{voltage})^2$; each of these graphs display $(\text{voltage})^2$ or force, versus the time duration causing dislodgement. This shows that it is not necessarily the amount of force applied alone, but the duration of the force as well, which together determine if the particle will be dislodged. Figures IV.9, IV.10, and IV.11 show how these force-time combinations for the 8 mm, 6 mm, and 4 mm ball respectively. Because the experiments are limited to a 0.25 V increment, it cannot be determined if the force-time combination that dislodged the ball was precisely the incipient motion point or slightly above that. For this reason, the graphs all show a possible 15% "error bar" on the lower side of the data point. This bar gives a visual

representation of where the true point of incipient motion could be. If for instance, the particle did not dislodge a 4 V but did dislodge at 4.25 V, the true point of incipient motion could be anywhere between these values, but no higher than 4.25 V and no lower than 4 V. The "error bars" try to show this visually, however the best-fit lines use only the actual data points in their regression. Each of the three experiments produces a similar incipient motion curve. Figure IV.12 shows the three curves together, depicting the difference in voltages needed for the different size and weight particles.

IV.5.2 Equal Distance Experiments

While the previous experiments showed that the same type of pattern regarding force-time combinations was needed to cause dislodgement in several different situations, it was difficult to relate the curves because of the varied air gap distances in each situation. The air gap distance between an electromagnet and its target has a significant impact on the amount of force felt by the object. For instance, while theoretically it should take less force to remove the 4 mm particle from its 4 mm bed because of its reduced weight, the 4 mm particle was also 1.58 mm closer to the magnet than the 8 mm particle and was thereby receiving higher forces at lower voltages. The next set of experiments tries to neutralize this effect by placing each moveable particle so that their centers are equally distant from the magnet face. The center of the particle was chosen because the magnet and its field are larger than the particles and acting over the entire particle rather than a point. In most electromagnet examples, the magnet is significantly smaller than the flat surfaced object it is attracting and then only the distance between the flat surfaces is used. All discussions with other researchers led to the belief that the center would be a

reasonable distance; however, it is possible that future studies should try to compare the differences between center locations and front face locations.

Each of these experiments was conducted with the center of the moveable particle 6.31 mm from the face of the electromagnet. This is the same distance as an 8 mm base particle touching the electromagnet. At this distance, all of the particles are able to make a full dislodgement; closer distances did not allow this. Larger distances required higher voltages to dislodge the particle than the circuit was capable of producing.

Four additional curves were developed to compare the 8 mm on 8 mm original curve. Different combinations of base size and moveable particle size were used including 8 mm on 6 mm, 6 mm on 8 mm, 6 mm on 6 mm and 4 mm on 6 mm. The 4 mm on 8 mm test was attempted; however, an entire curve could not be developed because high enough voltages could not be generated. Figure IV.13 shows the top and side views of these setups. Each of these curves was developed in the same manner as the original same geometry experiments. Similarly, each curve resembled the same exponential curve with a seemingly asymptotic lower end. Figures IV.14 to IV.17 show the individual curves for the different combinations while Figure IV.18 shows all five curves at the 6.31mm from the magnet face location for comparison.

Even with these new experiments, it is difficult to determine an exact relationship to the force required to remove the particle. The results tend to show that there is a difference in the amount of force for different geometries and pivot angles; when the moveable

particle is sitting in the pocket of a larger diameter bed, it requires more force to remove it and the opposite is true when the moveable particle has a larger diameter than its bed. These are intuitively true. It can also be seen that weight plays some roll, but it is difficult to tell from these plots. In order to exactly determine the force-voltage relationship, additional resources would be necessary.

IV.6 Force-Time Relationship

Although exact force-time relationships were not able to be determined, other patterns were able to be seen. Impulse is defined as the product of the average force by the time interval over which it was applied. In the studies conducted by Balakrishnan and Papanicolaou, the researcher's data showed high fluctuations in streamwise velocities where some rare events were several times the mean velocity. It would be assumed that these extreme events, well above the threshold level, would cause the particle to entrain, however this was not always the case. There were also events that were not as high, yet did entrain the particle. The difference in these events was their time duration. This led to the assumption that impulse may play a roll as to whether a particle will dislodge or not.

The electromagnetic experiments associated with this work were a method of testing for a relationship between impulse and particle dislodgement and how that impulse level would change over time duration or force level. Equation (IV.12) already showed that force varies with $(\text{voltage})^2$; and the graphs previously discussed for each experiment clearly show an exponential trend. Table IV.1 lists each experiment and its

corresponding best fit equation. In every instance, the curve best fitting the data determines an exponent near negative one (-1); for example, the 6 mm ball on 6 mm bed 4.73 mm from the magnet face shows

$$V^2 = 745.33\ T^{-1.0018} \qquad \textbf{(IV.13)}$$

where V is voltage and T is time duration of the pulse in milliseconds. Substituting equation (IV.12) leads to

$$F = 745.33\ T^{-1.0018} \qquad \textbf{(IV.14)}$$

and simply rearranging to put both variables on one side leaves

$$F \cdot T^{1.0018} = 745.33 \qquad \textbf{(IV.15)}$$

In this case, with the exponent nearly equal to 1 it shows that the product of the force and its applied duration are equal to a constant. In other words, the same amount of impulse was needed in every instance to dislodge the particle, whether the force was near threshold (similar to steady state voltage) or significantly above it.

Similar equations were derived for each separate case. There are variations in the exponents, but none deviates more than 12% from 1. Error in each curve can be attributed to the accuracy of the system as discussed previously. In addition, the case with the most errant exponent, the 4 mm on 6 mm bed 6.31 mm from the magnet, was not able to develop a full curve. The circuit was incapable of producing voltages high enough to dislodge the particle at low time durations and so the final curve does not contain as many data points or the range of the others. Figures IV.19 through IV.25 show the impulse required to fully dislodge each particle as the time duration of the pulse increases. These graphs show a good deal of scatter, the impulse is not as constant as the

best fit equations may project. Again there is an approximate 15% error in the force level due to the minimum size of the increment that the voltage can be increased by (3 ms). Table VI.2 shows the best fit equations. Another feature to note is that in almost every case, the linear slope of the necessary impulse increases slightly as the time duration of the pulse increases and as the force necessary becomes asymptotically close to the threshold value. This suggests that the time duration of the pulse might have an increased effect on the impulse needed.

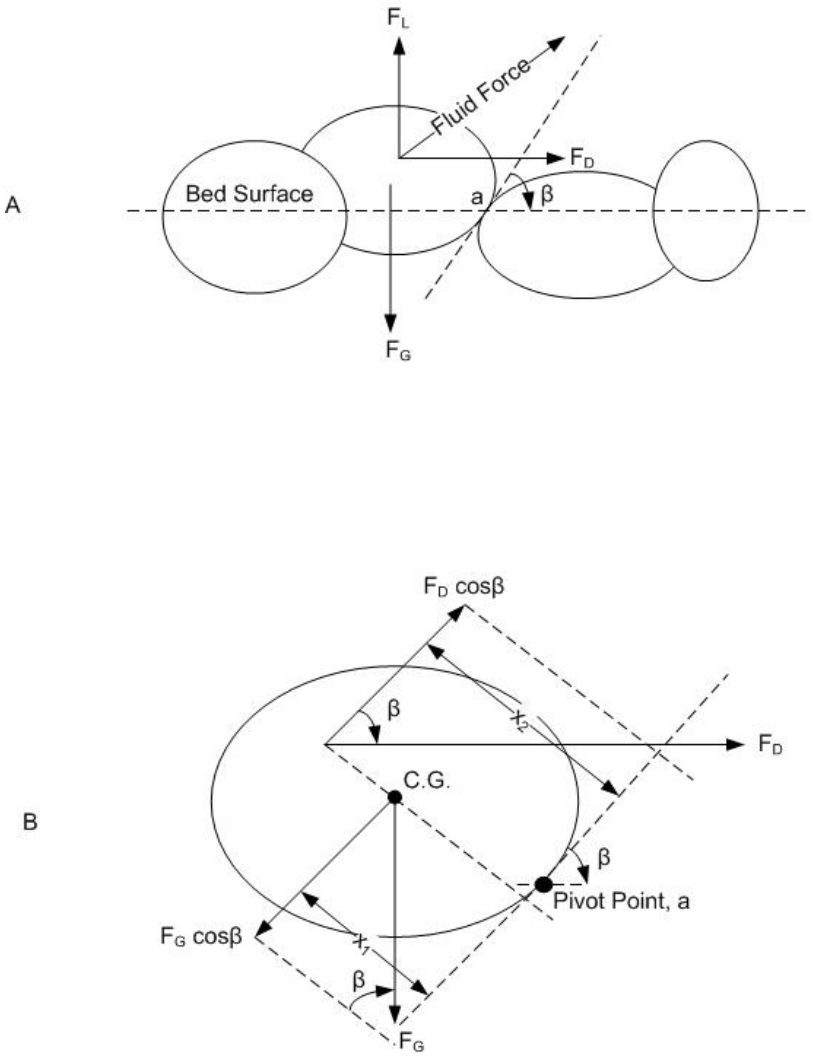

Figure IV.1: A) Typical sediment located in bed with dominant forces, B) Single particle with moments for gravitational and drag forces

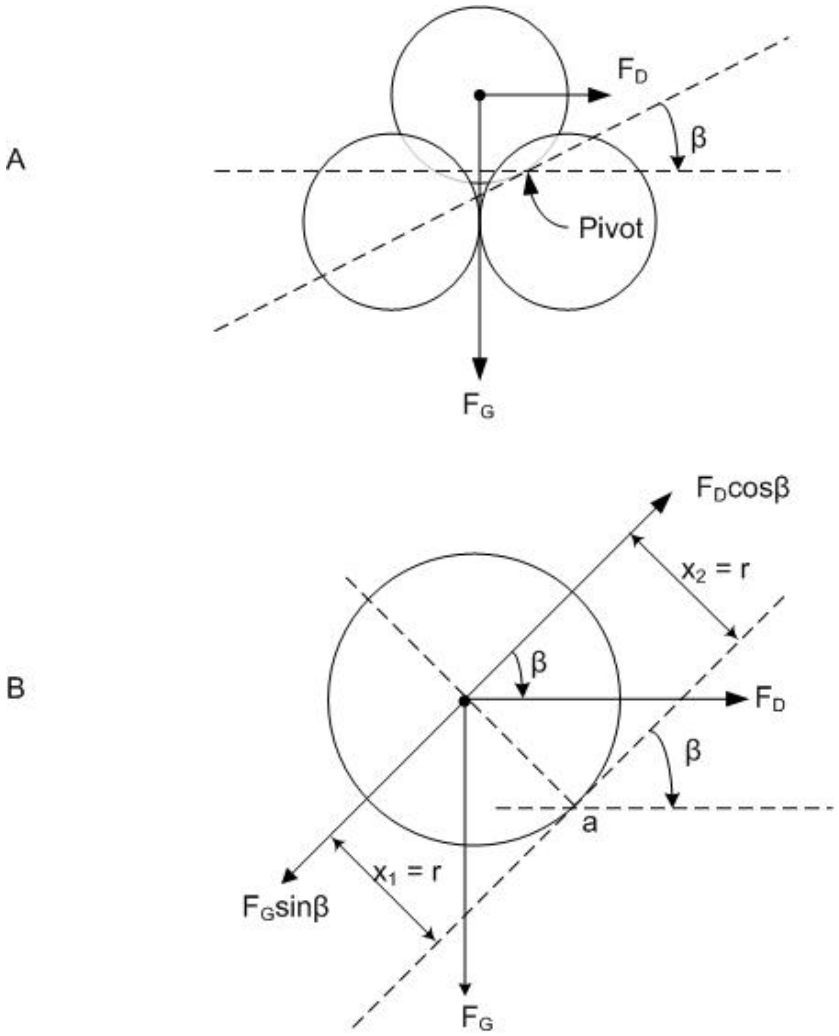

Figure IV.2: A) Simplified particle force diagram with spherical particles, B) Moments for spherical particle arrangement

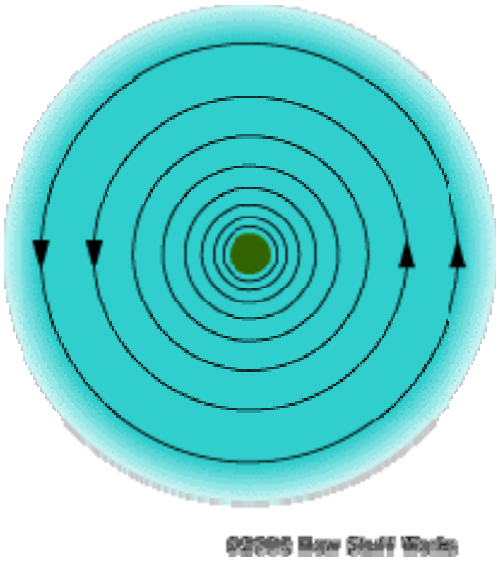

Figure IV.3: Magnetic field about a wire. (Brain 2000)

Figure IV.4: Magnetic field around one loop. The field has a high density inside the loop and the density decreases away from the loop. (Brain 2000)

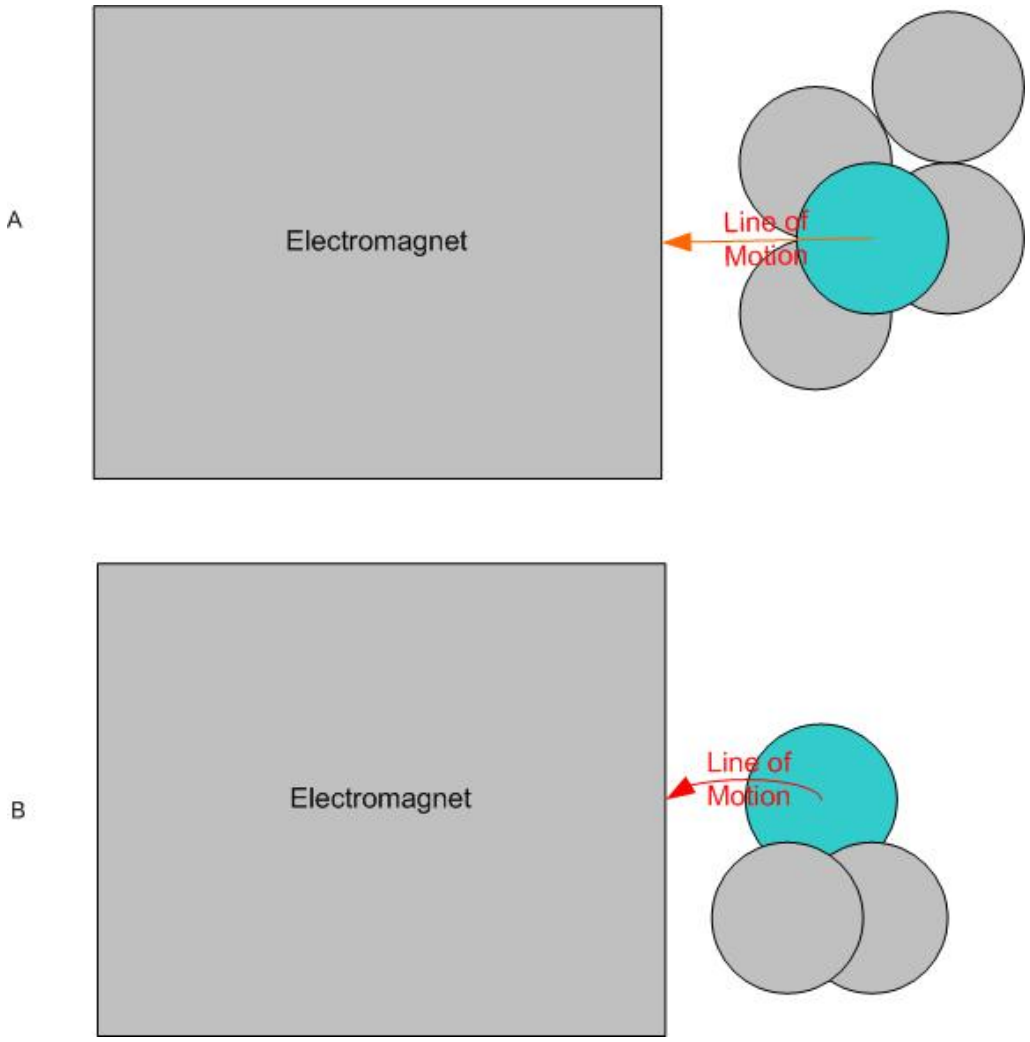

Figure IV.5: A) Top view of particle line of motion, B) Side view of particle line of motion.

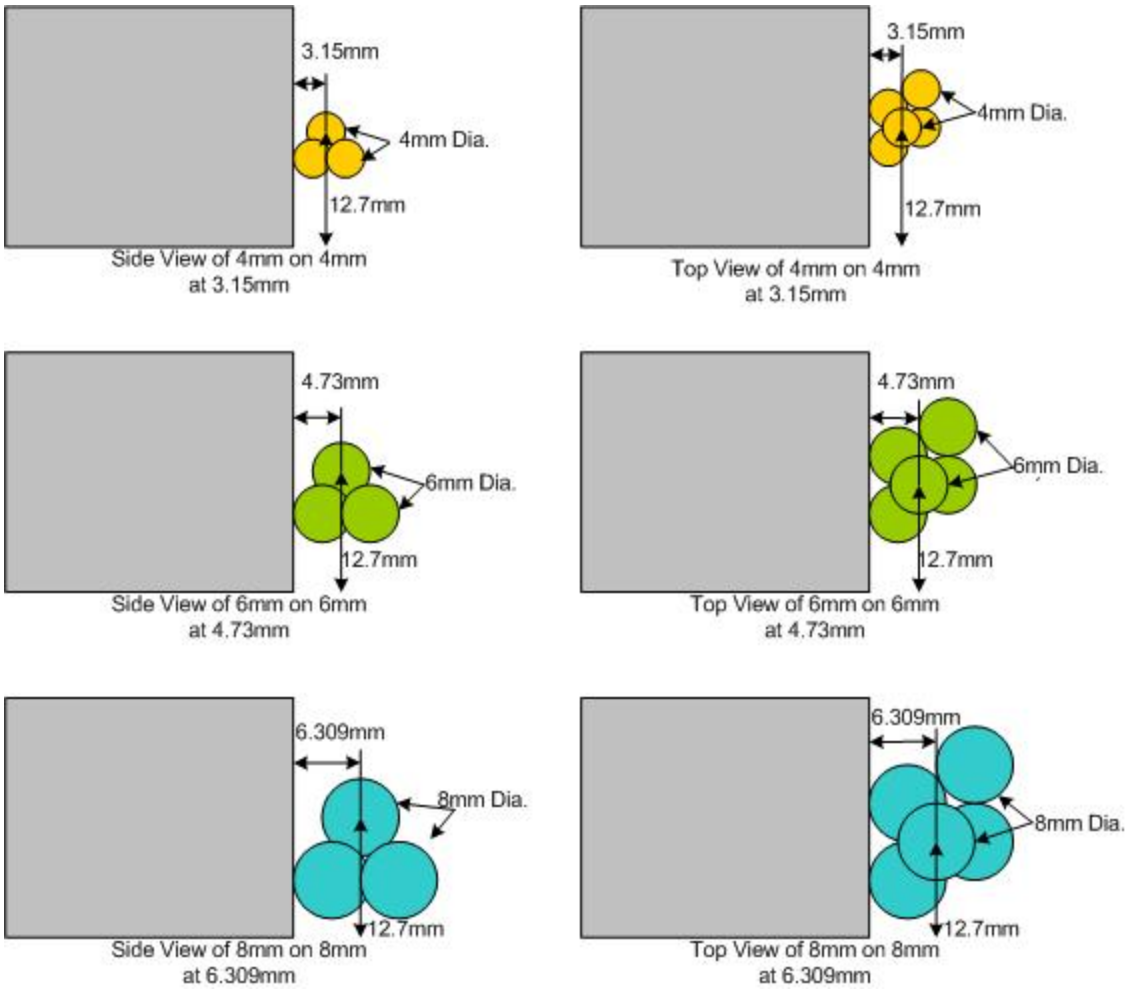

Figure IV.6: Side and top views for each of the set ups for the three same geometry experiments

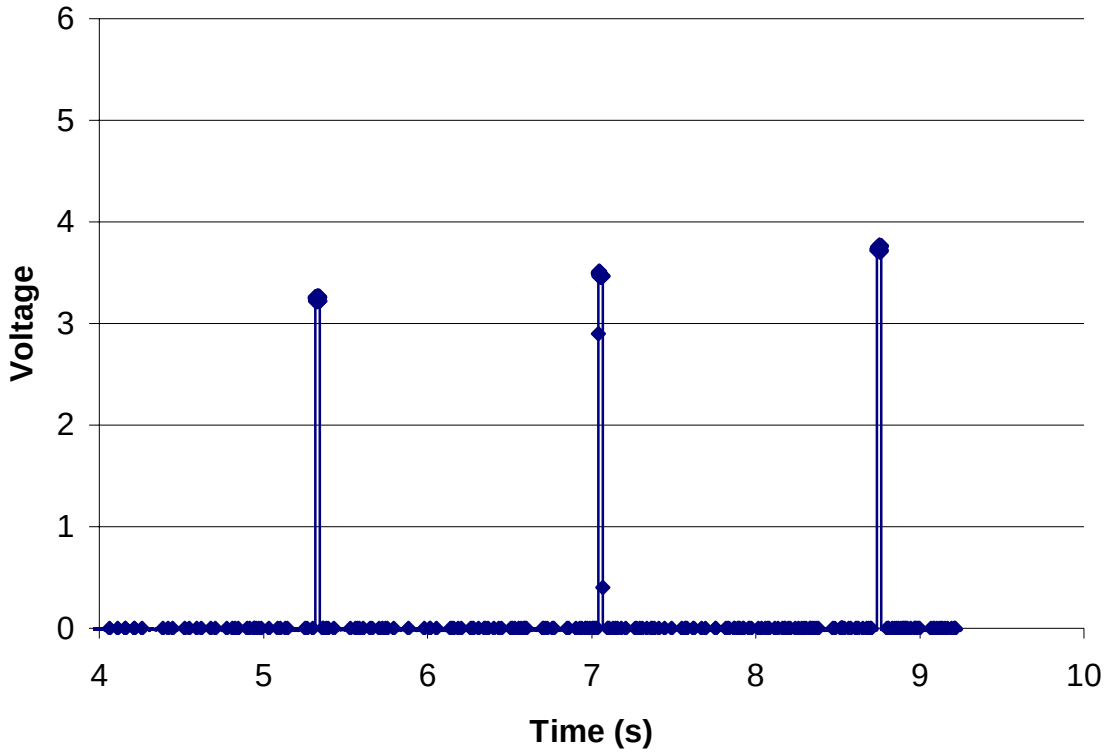

Figure IV.7: Typical increasing amplitude pulse generation run. Pulses of 27 ms duration at 0.25 V increments.

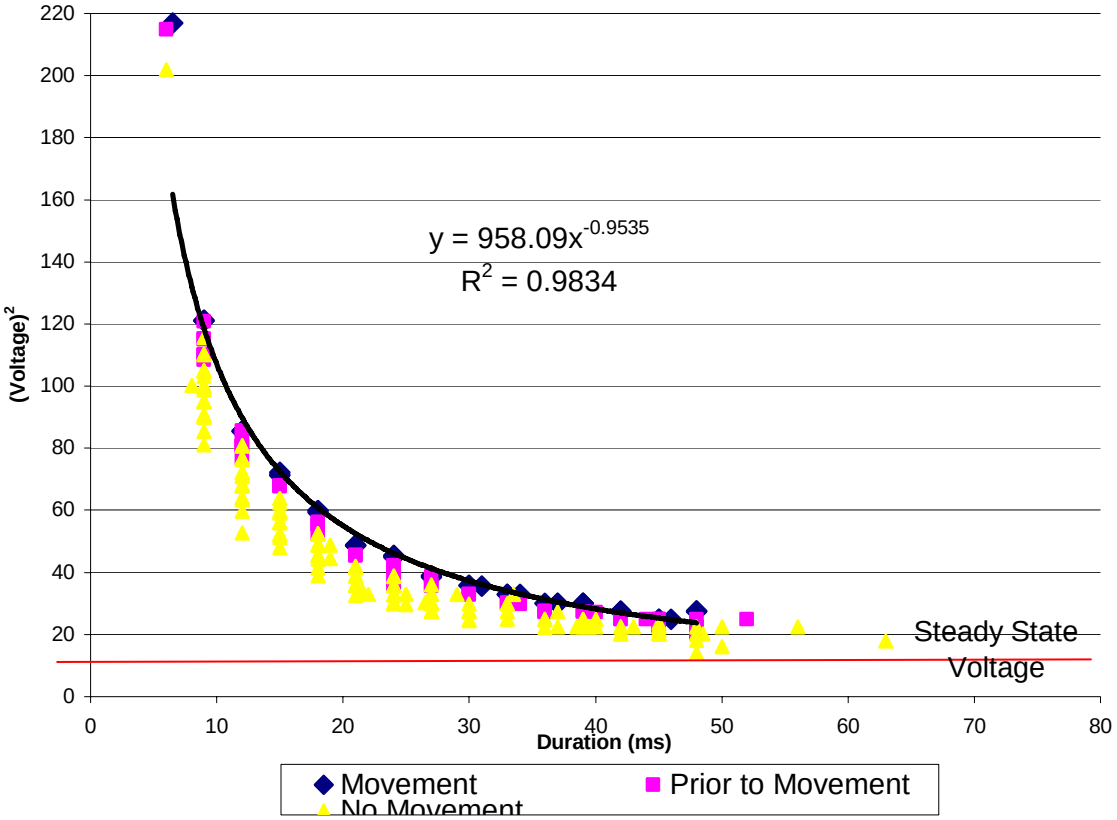

Figure IV.8: All pulses applied to 8 mm ball on 8 mm bed at 6.309 mm from face of magnet.

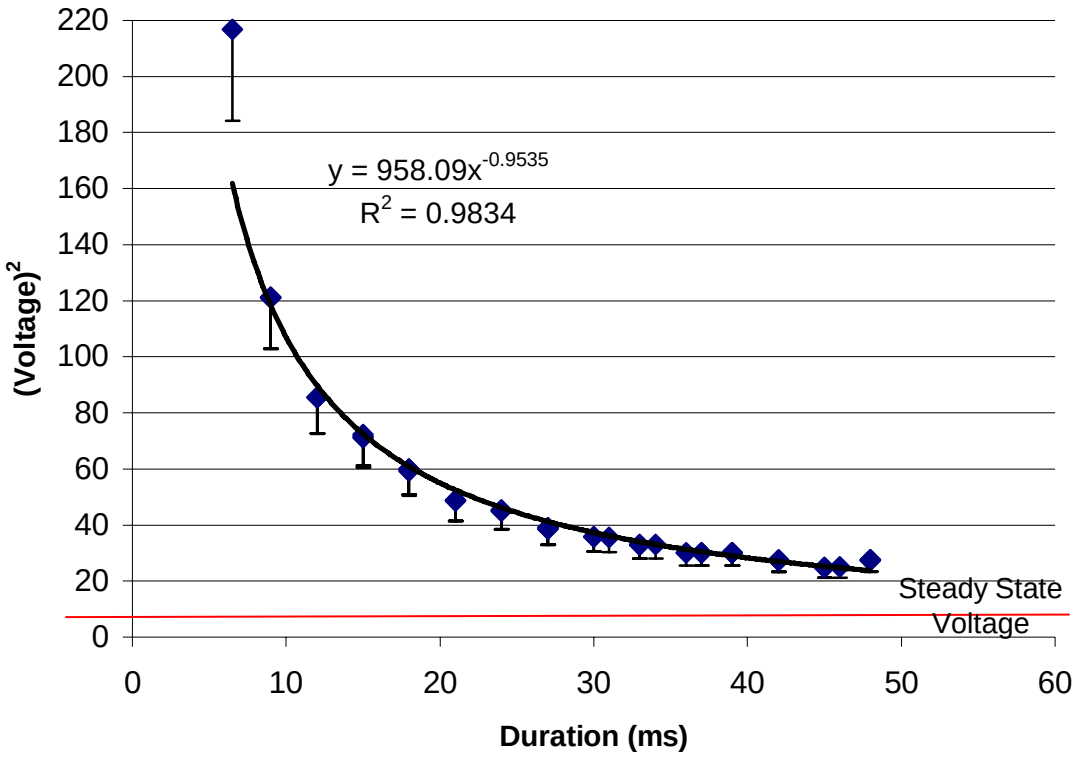

Figure IV.9: Force-time combinations required to dislodge 8 mm particle on 8 mm bed at 6.31 mm from magnet face.

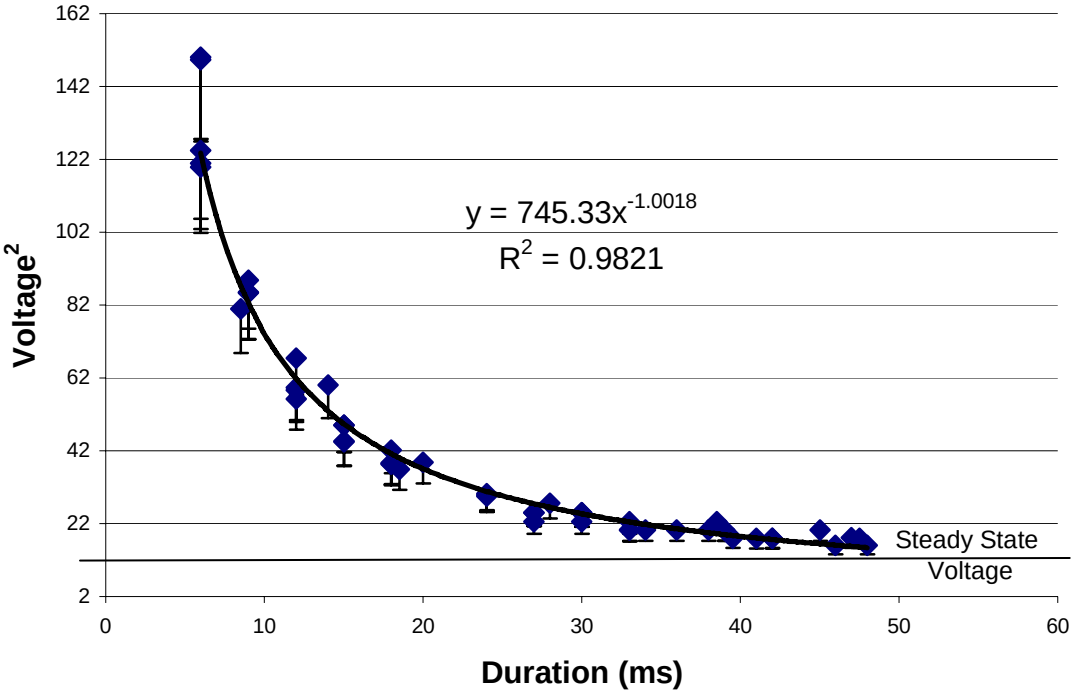

Figure IV.10: Force-time combinations required to dislodge 6 mm particle from 6 mm bed at 4.73 mm from magnet face.

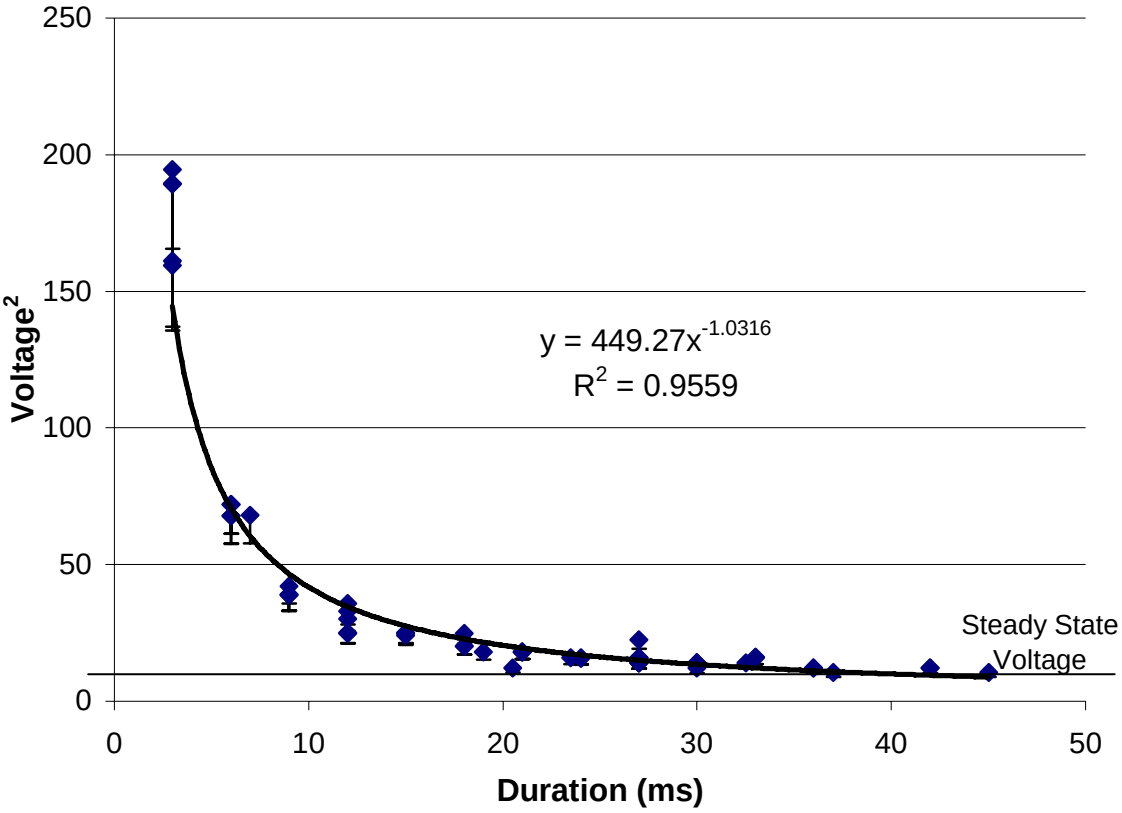

Figure IV.11: Force-time combinations required to dislodge a 4 mm particle from a 4 mm bed at 3.15 mm from magnet face.

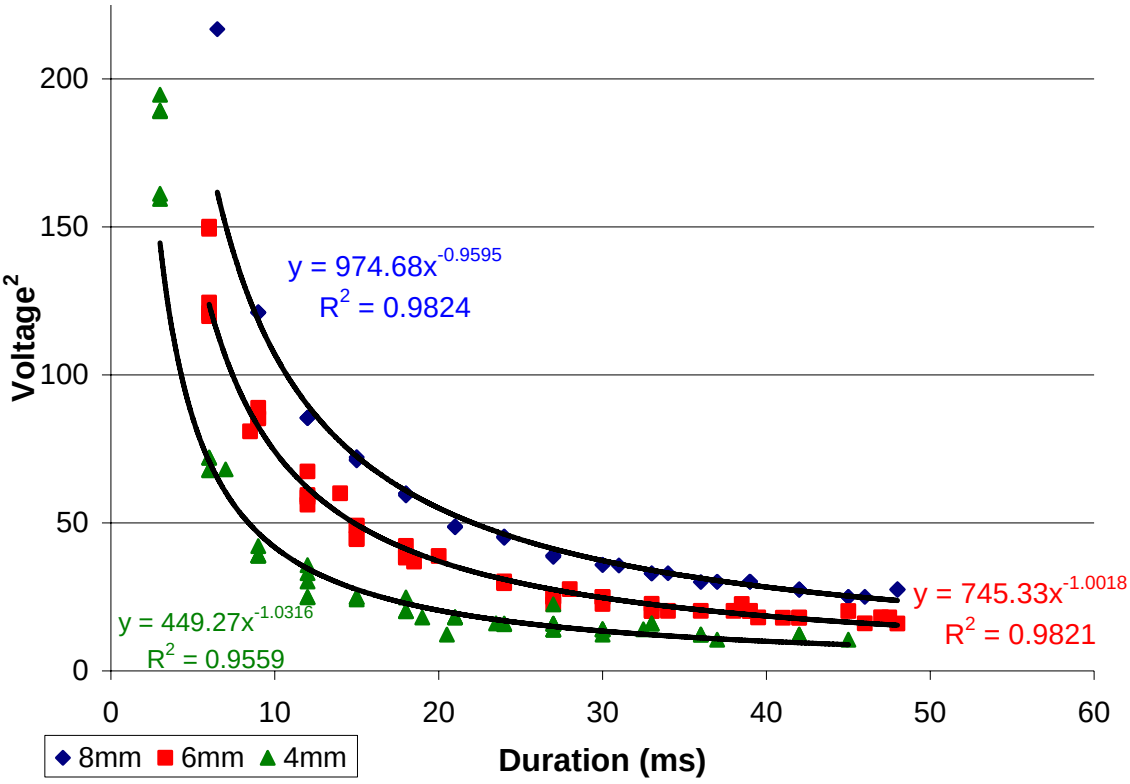

Figure IV.12: Same geometry force-duration curves resulting in dislodgement

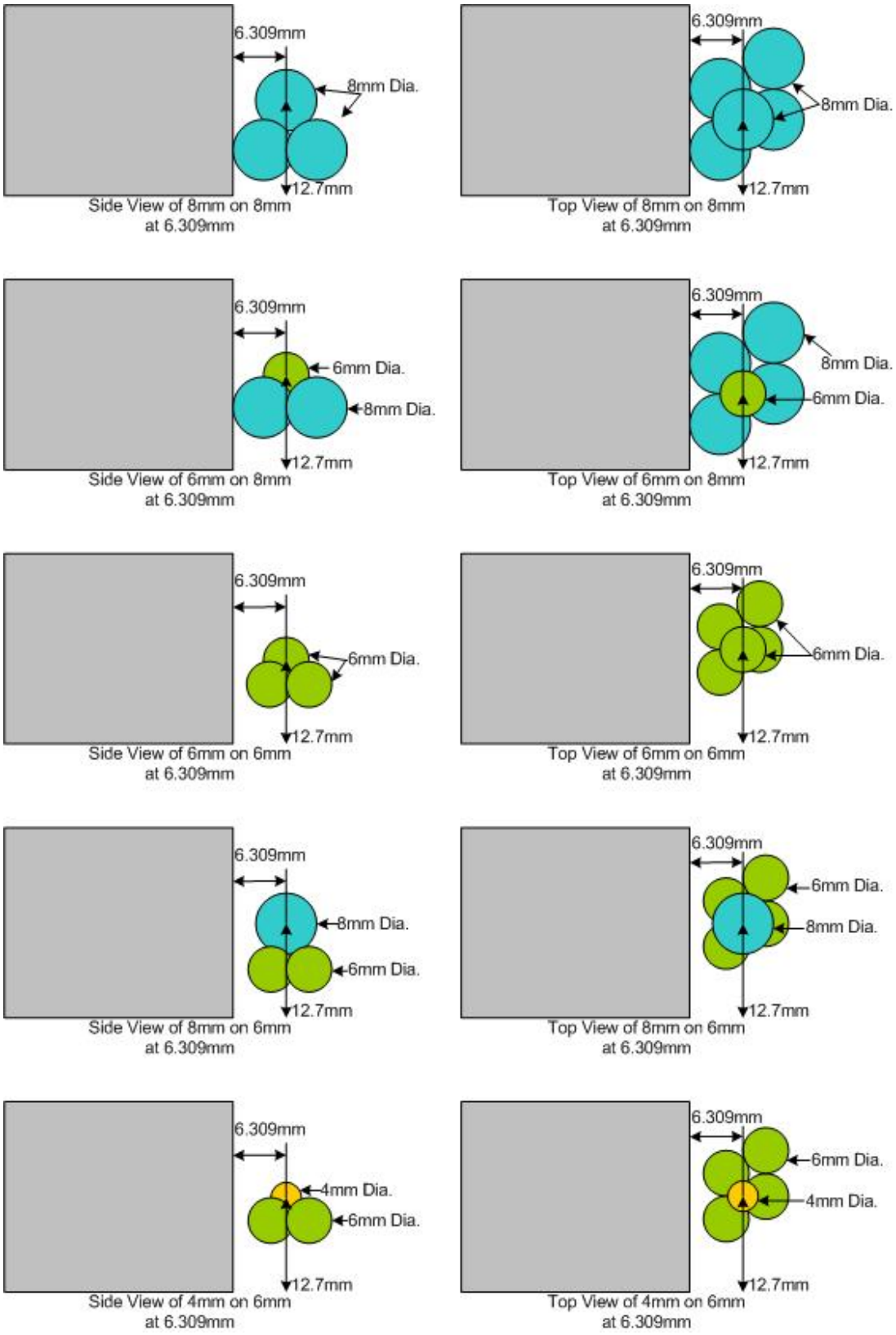

Figure IV.13: Top and side views for all 5 equal distance experiments.

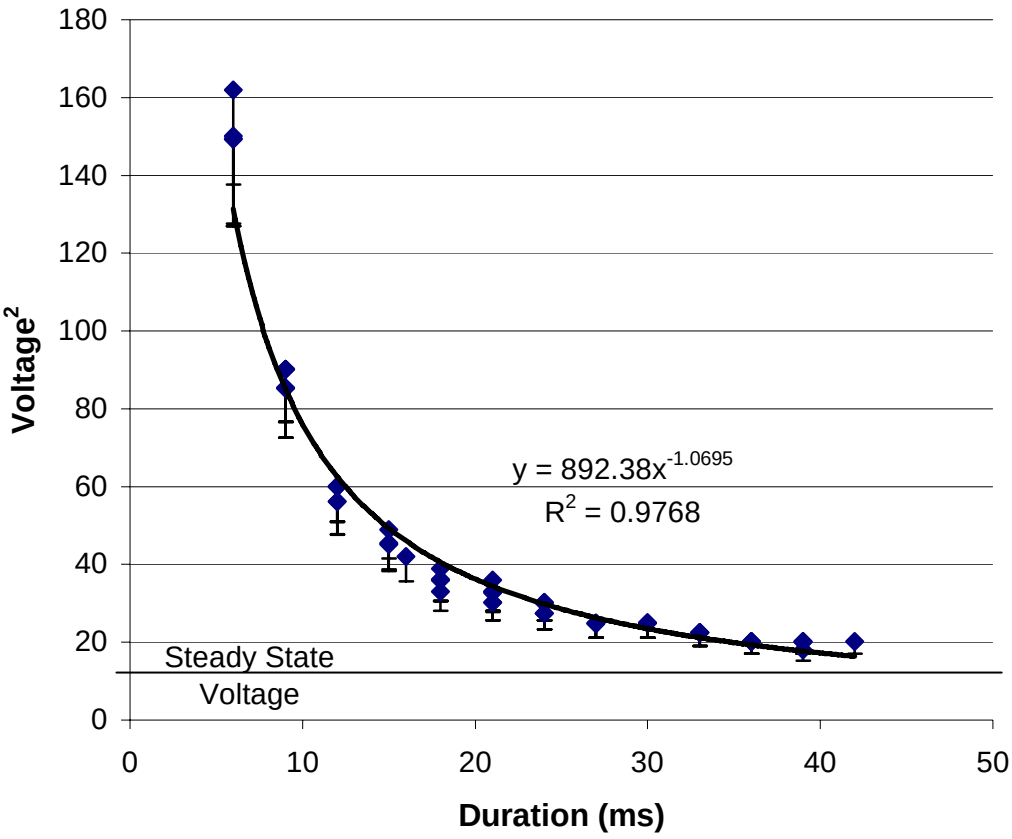

Figure IV.14: Force-time combinations required to dislodge 8 mm particle from 6 mm bed, 6.31 mm from magnet face.

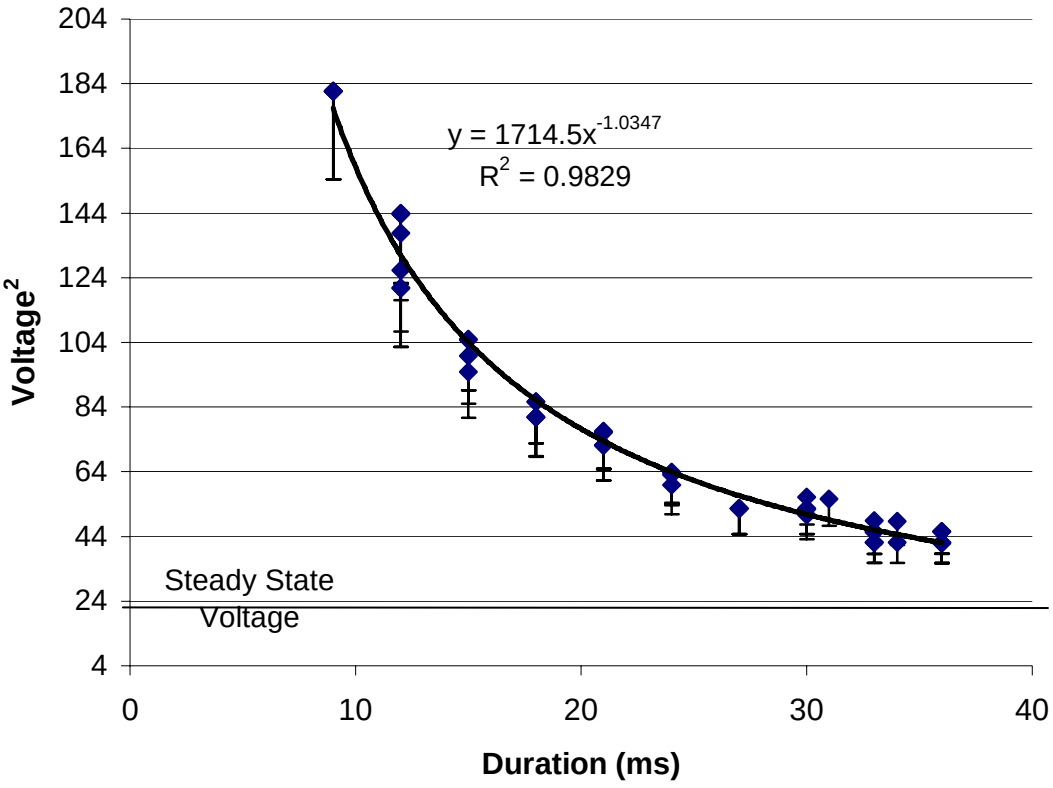

Figure IV.15: Force-time combinations required to dislodge a 6 mm particle on an 8 mm bed, 6.31 mm from magnet face.

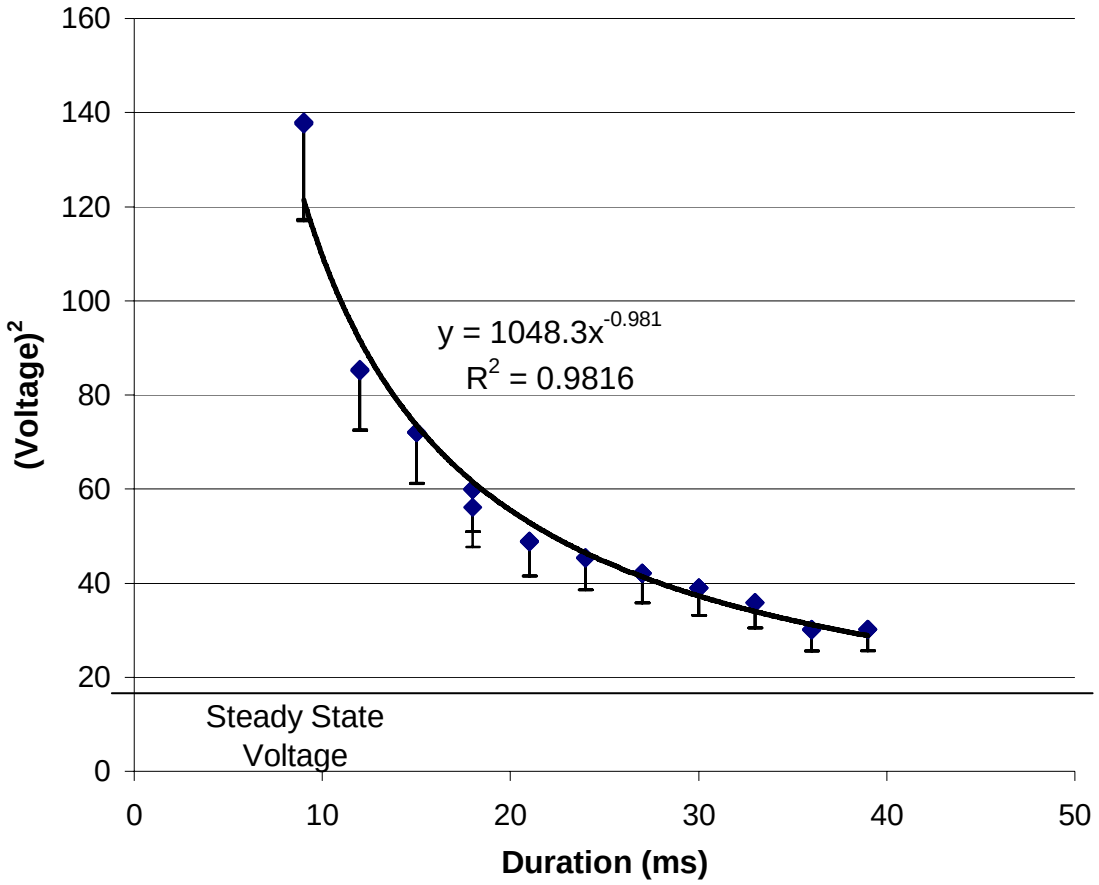

Figure IV.16: Force-time combinations required to dislodge 6 mm particle from 6 mm bed, 6.31 mm from magnet face.

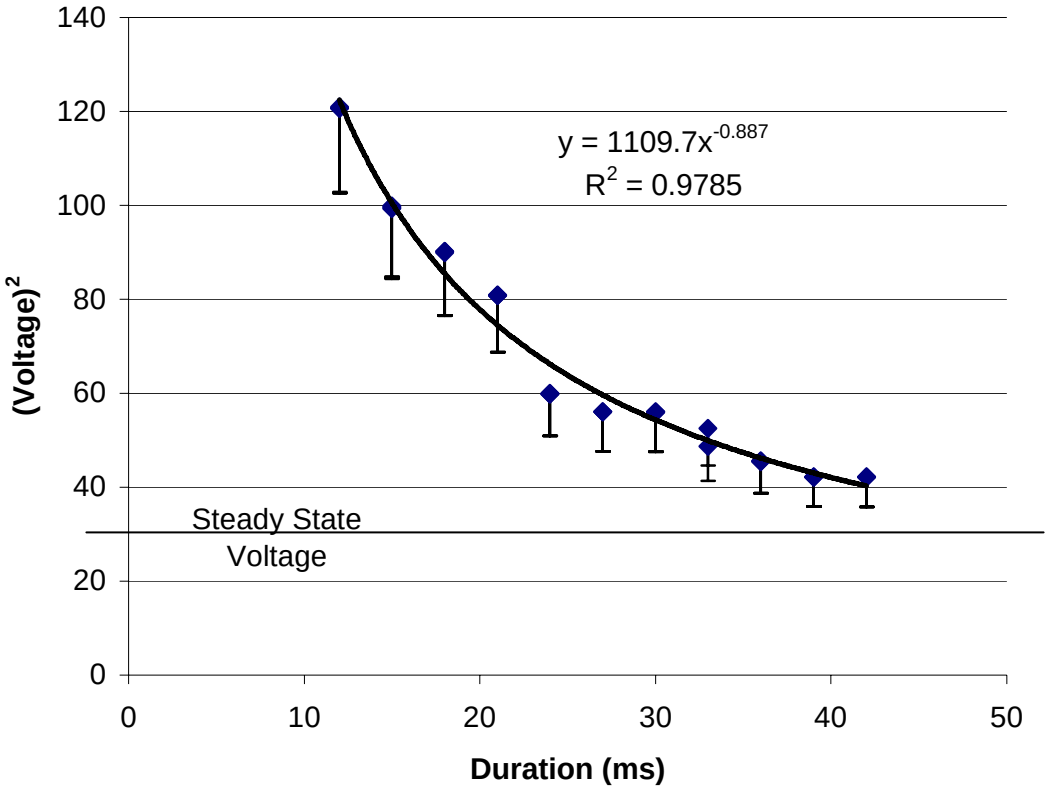

Figure IV.17: Force-time combinations required to dislodge 4 mm particle from 6 mm bed, 6.31 mm from magnet face.

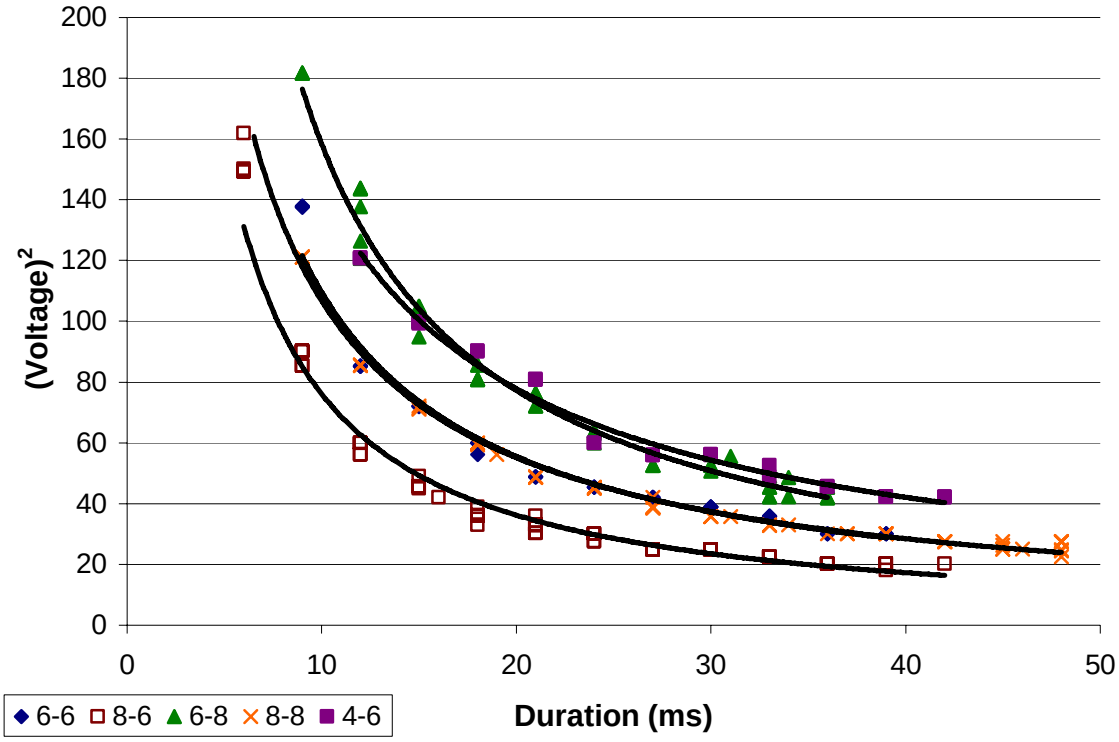

Figure IV.18: Force-time combination curves for all five equal distance experiments.

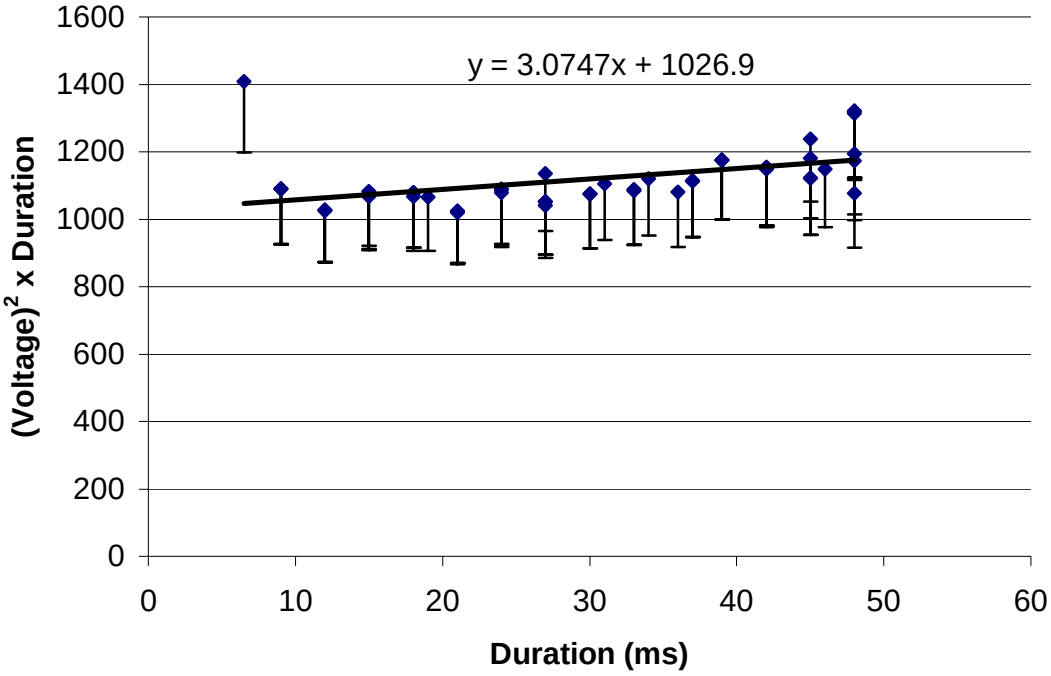

Figure IV.19: Impulses required to dislodge 8 mm particle from 8 mm bed 6.31 mm from magnet face.

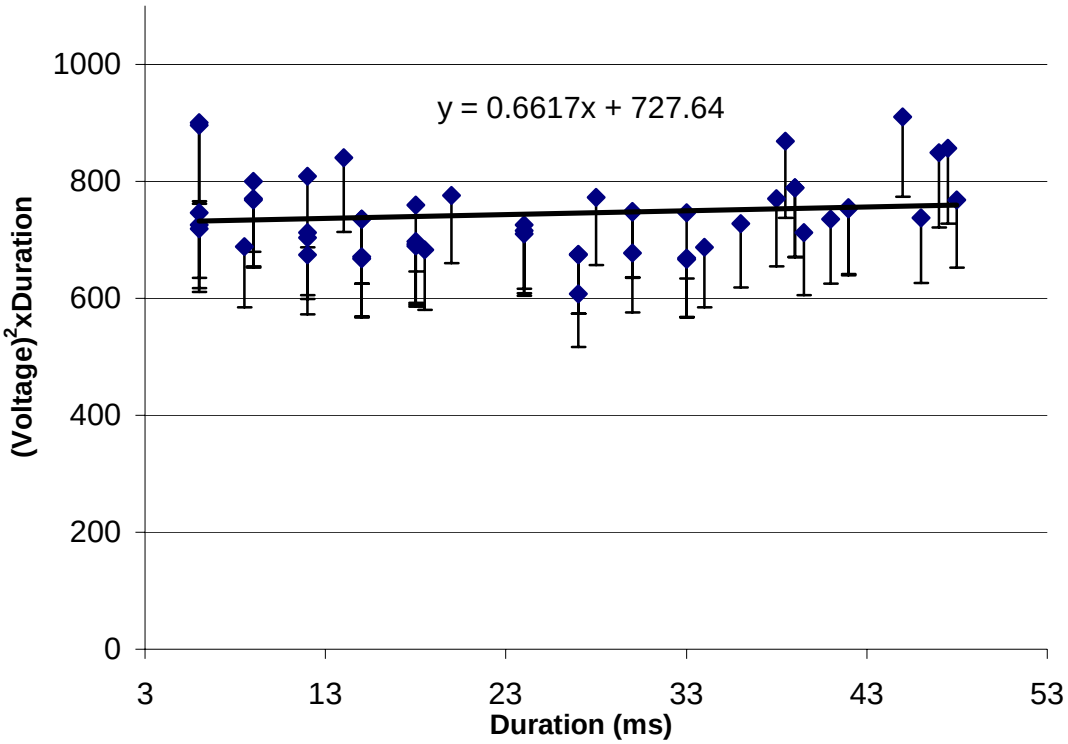

Figure IV.20: Impulses required to dislodge 6 mm particle from 6 mm bed 4.73 mm from magnet face.

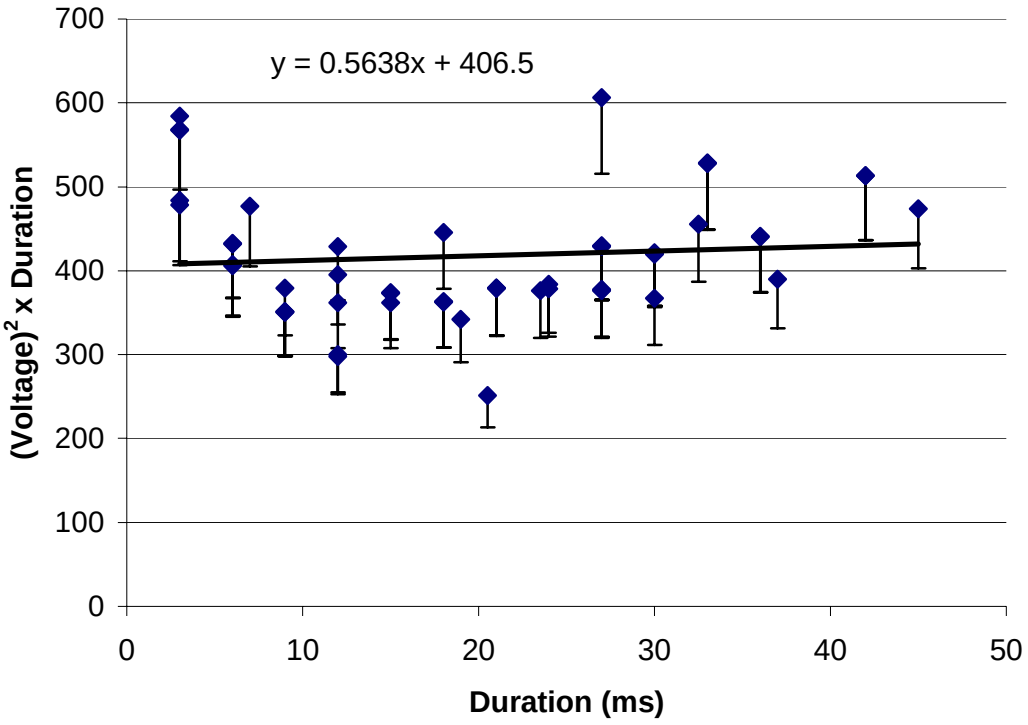

Figure IV.21: Impulses required to dislodge 4 mm particle from 4 mm bed 3.15 mm from magnet face.

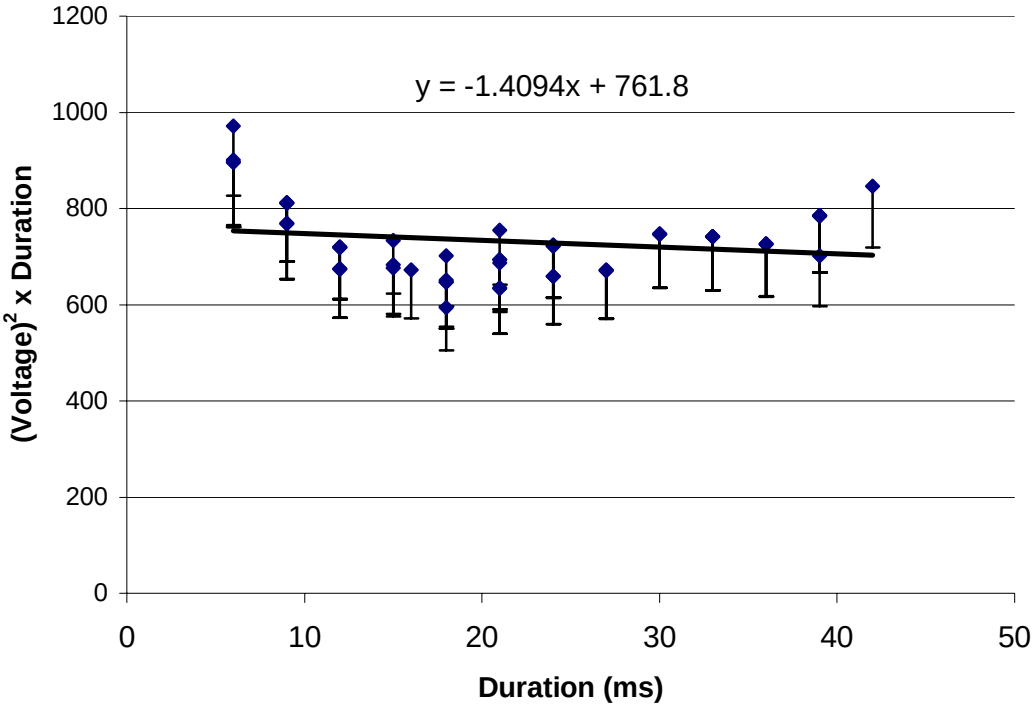

Figure IV.22: Impulses required to dislodge 8 mm particle from 6 mm bed 6.31 mm from magnet face.

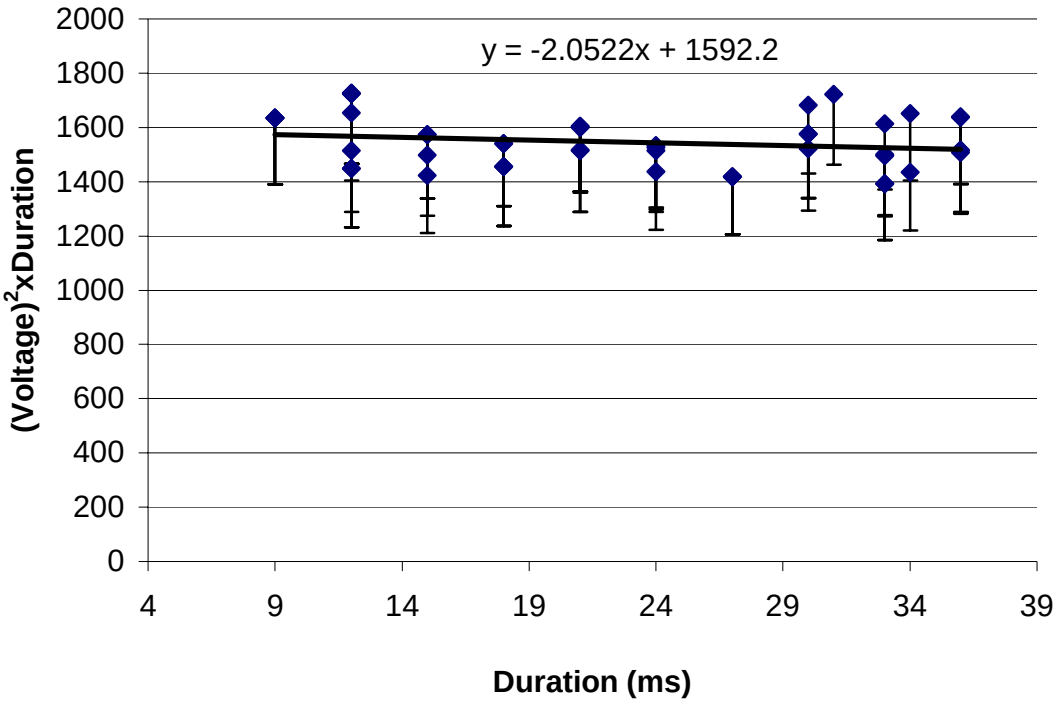

Figure IV.23: Impulses required to dislodge 6 mm particle from 8 mm bed 6.31 mm from magnet face.

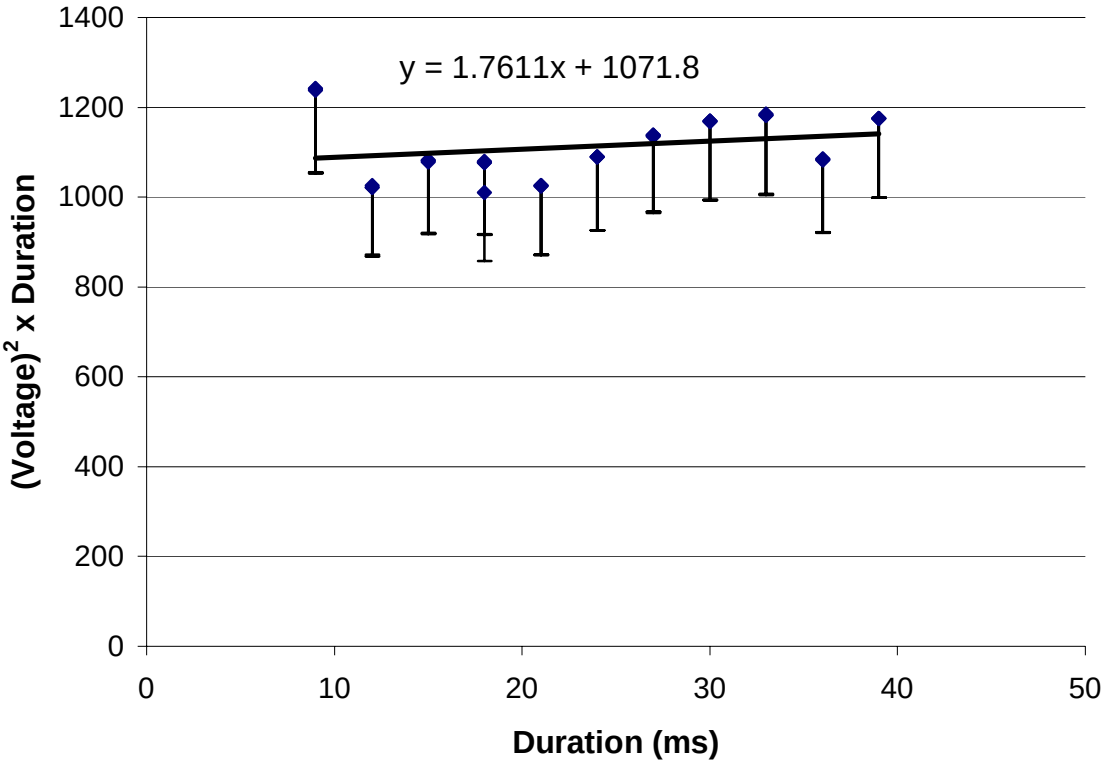

Figure IV.24: Impulses required to dislodge 6 mm particle from 6 mm bed 6.31 mm from magnet face.

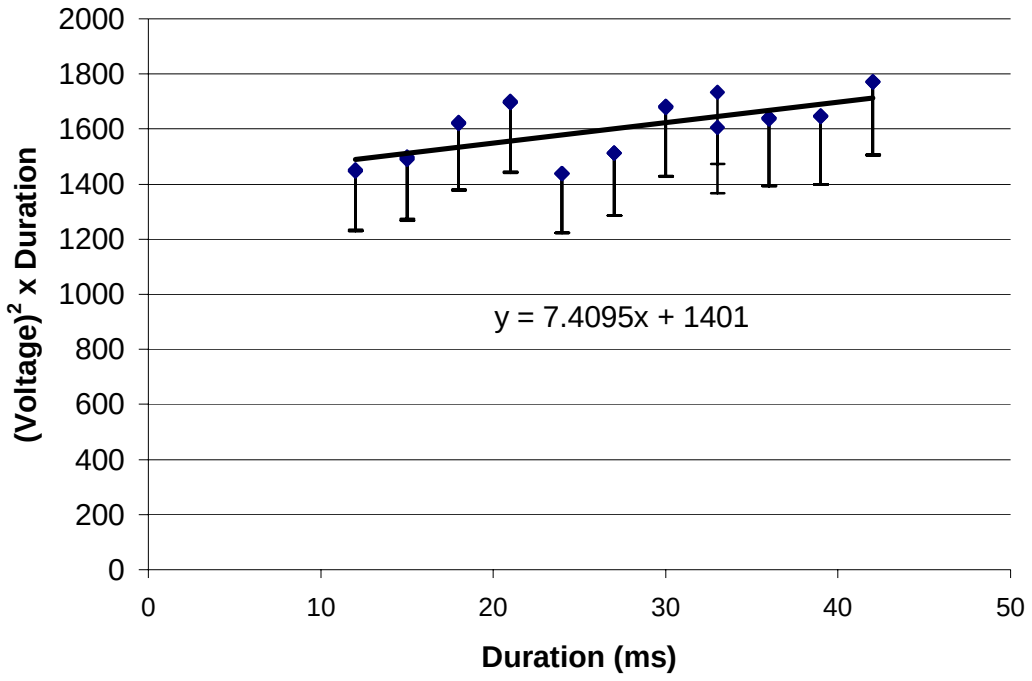

Figure IV.25: Impulses required to dislodge 4 mm particle from 6 mm bed 6.31 mm from magnet face.

Table IV.1: Best fit equations for all electromagnetic experiments where V is voltage and T is time duration of applied voltage in ms.

Ball Size	Bed Size	Distance from Magnet	Best-fit Equation	R^2
8 mm	8 mm	6.31 mm	$V^2 = 958.09\ T^{-0.9535}$	0.9834
6 mm	6 mm	4.73 mm	$V^2 = 745.33\ T^{-1.0018}$	0.9821
4 mm	4 mm	3.15 mm	$V^2 = 449.27\ T^{-1.0316}$	0.9559
8 mm	6 mm	6.31 mm	$V^2 = 892.38\ T^{-1.0695}$	0.9768
6 mm	8 mm	6.31 mm	$V^2 = 1714.5\ T^{-1.0347}$	0.9829
6 mm	6 mm	6.31 mm	$V^2 = 1048\ T^{-0.9810}$	0.9816
4 mm	6 mm	6.31 mm	$V^2 = 1109.7\ T^{-0.887}$	0.9785

Table IV.2: Linear best fit equations for all experiments where V is voltage and T is time duration of the pulse.

Ball Size	Bed Size	Distance from Magnet	Best-fit Equation	R^2
8 mm	8 mm	6.31 mm	$V^2 = 3.0747\ T + 1026.9$	0.2311
6 mm	6 mm	4.73 mm	$V^2 = 0.6617\ T + 727.64$	0.0174
4 mm	4 mm	3.15 mm	$V^2 = 0.5638\ T + 406.5$	0.0079
8 mm	6 mm	6.31 mm	$V^2 = -1.4094\ T + 761.8$	0.0374
6 mm	8 mm	6.31 mm	$V^2 = -2.0522\ T\ 1592.2$	0.0375
6 mm	6 mm	6.31 mm	$V^2 = 1.7611\ T + 1071.8$	0.0601
4 mm	6 mm	6.31 mm	$V^2 = 7.4075\ T + 1401$	0.4347

Chapter V
Preliminary Camera Work

V.1: Introduction

The electromagnetic experiments that have been the focus of this document, have shown that the force-time combination is important in determining if a particle will dislodge from its bed pocket, however it has not been able to show at what forces or impulses this may happen. As discussed earlier, several different methods of determining forces were examined in preparation for these experiments, however, were rejected because of their interference with either the shape of the particle or with its natural rolling movement. The most non-invasive method of determining force was concluded to be through the use of high speed imagery. These experiments were unable to completely implement the high speed digital cameras into the final testing, however some preliminary tests were done and their methods and results are discussed here.

V.2: Initial Digital Imagery

The first digital videos taken of the electromagnetic experiments were taken with a Kodak 3 Pixel digital camera. This camera was capable of taking short digital videos at a rate of 30 pps. These images were taken to show that the motion involved with the

particle dislodgement was indeed rolling. It was assumed that movement other than rolling, or pivoting about a point, would imply a point greater than incipient motion. The videos did depict the particles rolling out from their pockets.

In addition to the rolling, these videos were able to capture movement by the particle prior to dislodgement. At several points where there was insufficient impulse to dislodge the particle, the ball would "twitch" or vibrate slightly in its pocket. Several different times the impulses were strong enough to cause the particle to roll partially out of its pocket, however at these instances the particle did not reach the top of the pocket and when the pulse died, gravity overcame the momentum and the particle would roll back to its original position.

V.3: Methods and Procedures

Determining the magnetic force applied using high speed digital imagery is a relatively rudimentary way to calculate the force without interfering with the particle or the magnet. With the video, images of just the particle movement can be selected using an image processing program such as LabView or Phantom, it is possible to create a position track of the particle's center of mass as the particle rolls from its pocket. Using this position track, equations can be derived for velocity and acceleration in both the x (horizontal) and y (vertical) directions as depicted in Figure V.1. Once the acceleration is known, the force can be back calculated from Newton's Second Law of Motion where m is the mass of the object and dv/dt is its change in velocity over time, or acceleration

$$F = m\, dv/dt \qquad \textbf{(V.1)}$$

The camera used for these preliminary experiments was the Phantom V.4 from Vision Research, Inc. This camera is capable of taking images at up to 30,000 pps at low resolutions. For these purposes, the camera was set to take images at 256x256 resolution at 2000 pps. The DAQ system was sampling the voltages at 2000 S/s, so it was determined that a faster frame rate was unnecessary. The camera has a 2048 megabyte on board memory that saves all of the images before transferring them to a computer. This results in a limited space and so video length for each attempt. With the rate and resolution used in these experiments, the camera could only save 4072 pictures (approximately 2 seconds worth of images). To compensate for this limitation, the camera can be set to continuously take video after a trigger is applied, however still only the last 4072 pictures will be saved and available for analysis. Since for all of our experiments, the ball dislodging from the pocket is the last event, this method was acceptable for capturing the motion.

The Phantom V.4 camera records video in a post trigger fashion; meaning that the camera starts previewing images once a TTL signal is received by the camera and stops when a set number of frames have been received. This requires programming that would send a TTL to start both the camera and the pulse generation program which would make a direct correlation between the voltages sent and a frame in the video and thereby a location in the position track. This TTL trigger however, was not successfully implemented during these experiments and so the voltage to frame correlation could not be directly made. However, even though the correlation cannot be proved and plotted as

desired, the assumption can be made that the particle movement begins at the start of the pulse. Because the previous video shows that the particle does indeed move at lower impulses, just not enough to dislodge, and that physically, once an appropriate force threshold is met, the particle will at least move somewhat, one can say that the particle movement begins once that threshold value is met. As shown earlier, the time for the voltage to reach its peak is between 0.2 and 0.4 ms, which is less than the time between frames, one can assume that the start of particle movement corresponds to the start of the pulse. The graphs and figures shown later in this chapter use this assumption.

Another portion of the image analysis that was unable to be completed for these preliminary experiments was the LabView image programming. Instead, Vision Research, Inc. has its own image analysis program, Phantom 6.0.4 that was used for these videos. This program allows frame by frame play and selection of certain ranges of the entire video to analyze. This was used to isolate only those frames from the start of the particle movement to the point where the particle hits the face of the magnet. Additionally, the program allows the user to set a point of origin and scale the pixels to a known distance. For these experiments, the center of the particle prior to movement was set to be the origin and the scale was set to millimeters. There is human error involved with this as the program is completely dependent on the points the user hand picks, there is no computer automation available with this program. A collection of points can then be made which records the position and frame number as the user chooses points. With this, the user again hand picks the center of the ball as it rolls from the pocket. This method is not ideally accurate, but is considered acceptable for these experiments.

V.4: Analysis and Results

Using the Phantom V.4 high speed digital camera and the Phantom 6.0.4 image analysis program as described above, several sets of videos were taken of each set of particle and base combinations. Video was not taken for every point along the curve, in most cases four points were selected: a 150 ms pulse (the steady state condition), a 30 ms pulse, a 15 ms pulse, and a 9 ms pulse (often the shortest pulse available). Each of these videos was position tracked with the Phantom software and plotted using Excel, separating the vertical movement from the horizontal movement. Best fit curves were used to create equations to describe the movement of the particle. The derivatives of these equations were then taken to obtain the velocity and acceleration profiles with time. Figures V.2 through V.13 show the data obtained for the 8 mm ball on 8 mm bed at 6.31 mm from the magnet face experiment and their position, velocity, and acceleration profiles.

The graphs shown are those of the actual position track data taken from the Phantom software. The software collects the points based on the user's input and so can have significant error. In addition, the zoom for the camera lens in conjunction with the resolution of the images will cause the step like movements as seen in the data. The best fit lines were chosen as polynomials of either second or third order. It was difficult to capture the increased curvature that can be seen at the beginning of most of the curves (times corresponding to the actual pulse). In the case of the 9 ms pulse curve, the data was broken into two sections to show the change in curvature. The curvature is significant in that it shows a change in acceleration between times when the pulse is applied and times when the pulse is over. In the 9 ms pulse case, the sharp curvature lasts

approximately 11-12 ms, slightly longer than the pulse, and then drops off as the ball continues its roll.

The high speed digital imagery was very beneficial for viewing the movement as the ball rolled from its pocket. Marks were placed on the ball that their rotation could be watched as the particle rolled. It was interesting to see the ball pivot over its contact point and roll just as expected, but the real interest in the imagery was to determine forces. Although these experiments were preliminary and had many rough points with possible sources of error, the methods used still show interesting results. Using the position tracker, velocities and accelerations were able to be determined. Because best fit polynomials were used to represent the data, the accelerations were often shown to be constant throughout the entire roll, which is against the original thought. As mentioned previously, the increased curvature of the data earlier in the time sequence suggests a higher rate of constant acceleration during the pulse and a lower rate of constant acceleration once the pulse has ended and gravity takes over. However, the inaccuracies of these few experiments do not show this well. The data really needs to have a better method of determining the best fit equation, additionally the data should be broken into separate regions to better understand how the data moves. The accelerations are expected to be constant during the pulse of a constant force, but would ideally be greater than the acceleration without the pulse force. But still, accelerations were able to be found and forces determined, even though these values are not exactly accurate. Table V.1 contains the results for the 8 mm ball on 8 mm bed 6.31 mm from magnet face experiments.

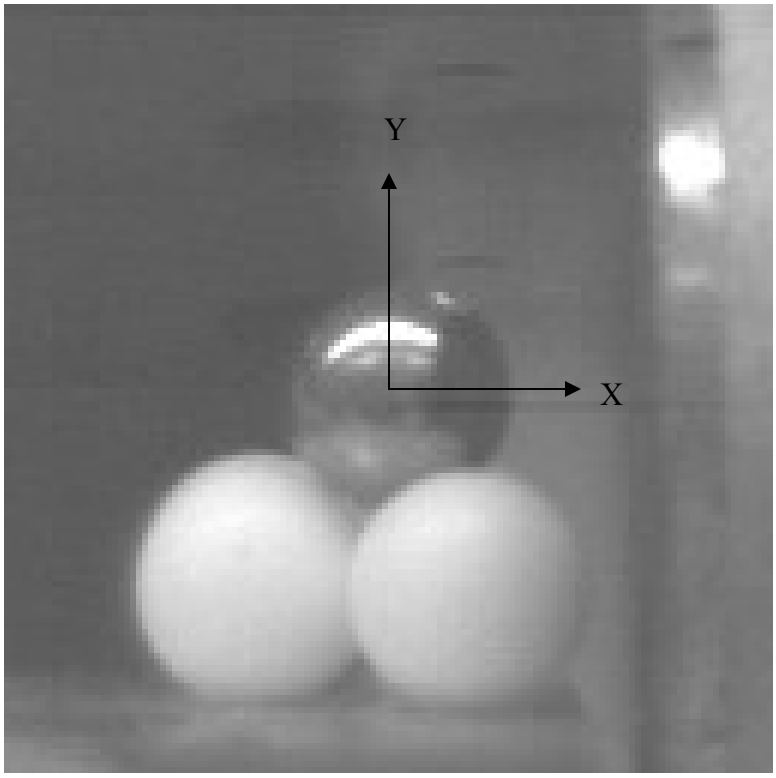

Figure V.1: Sample picture from high speed digital camera with coordinate axes shown. Origin defined as center of moveable particle prior to movement.

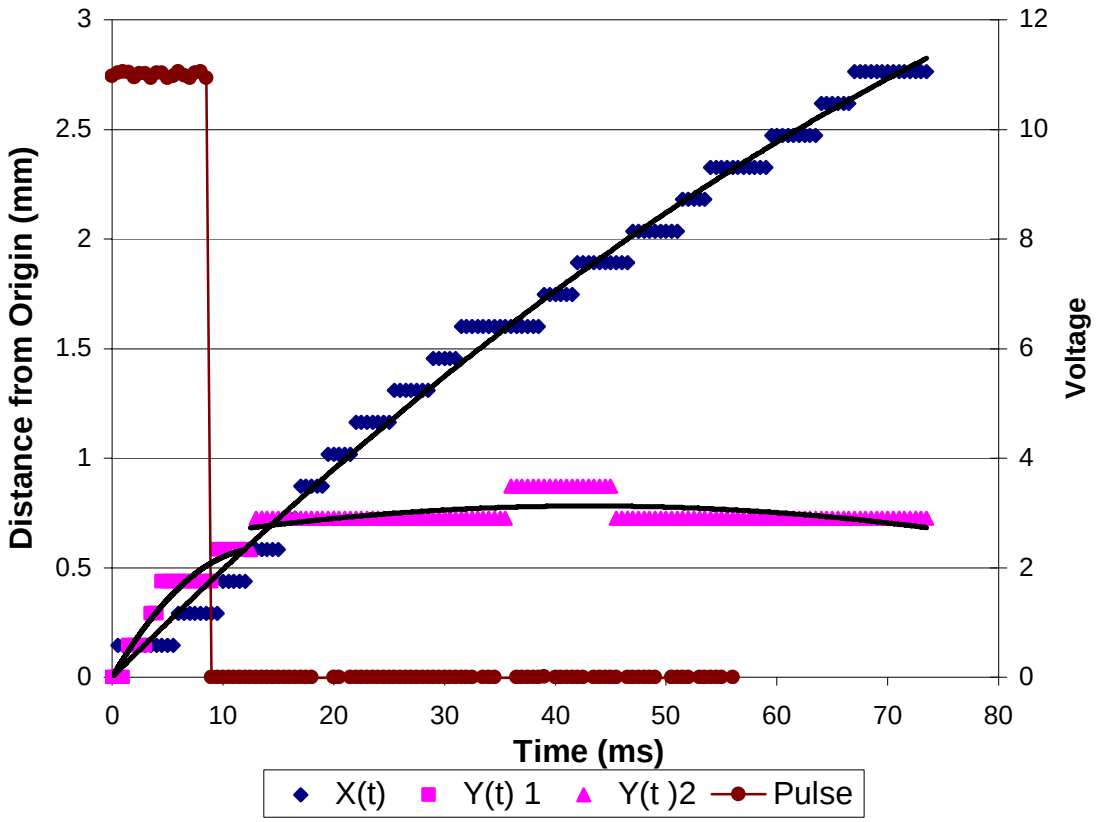

Figure V.2: Position track of an 8 mm particle on 8 mm bed 6.31 mm from magnet face. Particle dislodge with a 9 ms pulse of 11 V.

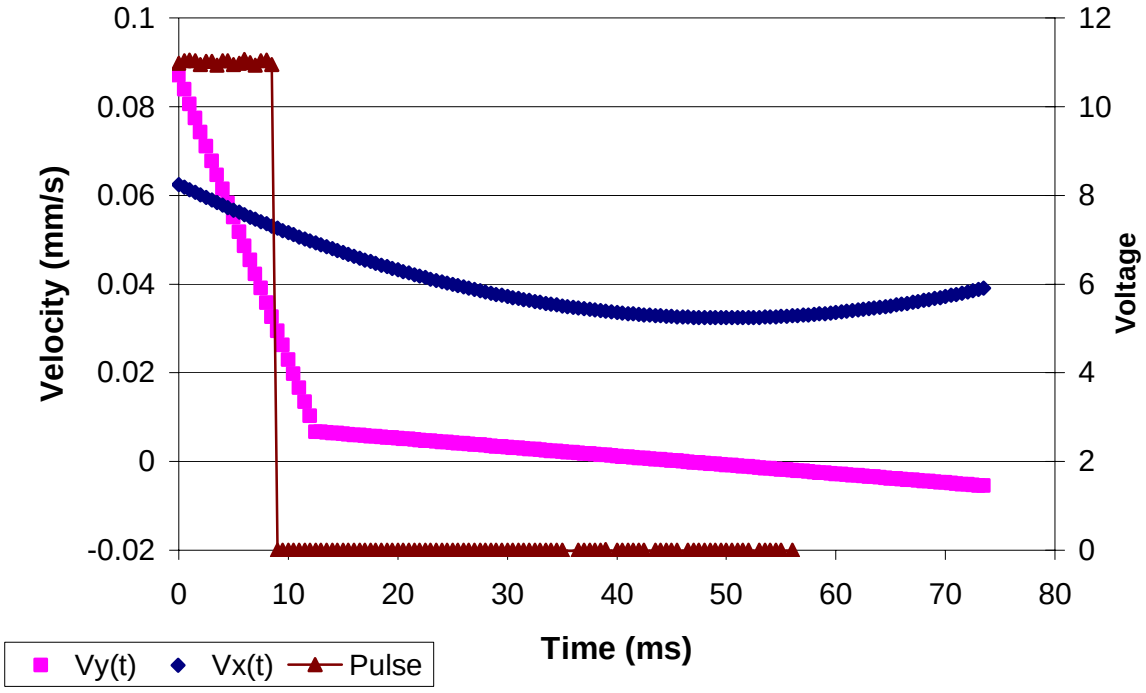

Figure V.3: Velocity profile for 8 mm ball on 8 mm bed 6.31 mm from magnet face, with 9 ms pulse of 11 V.

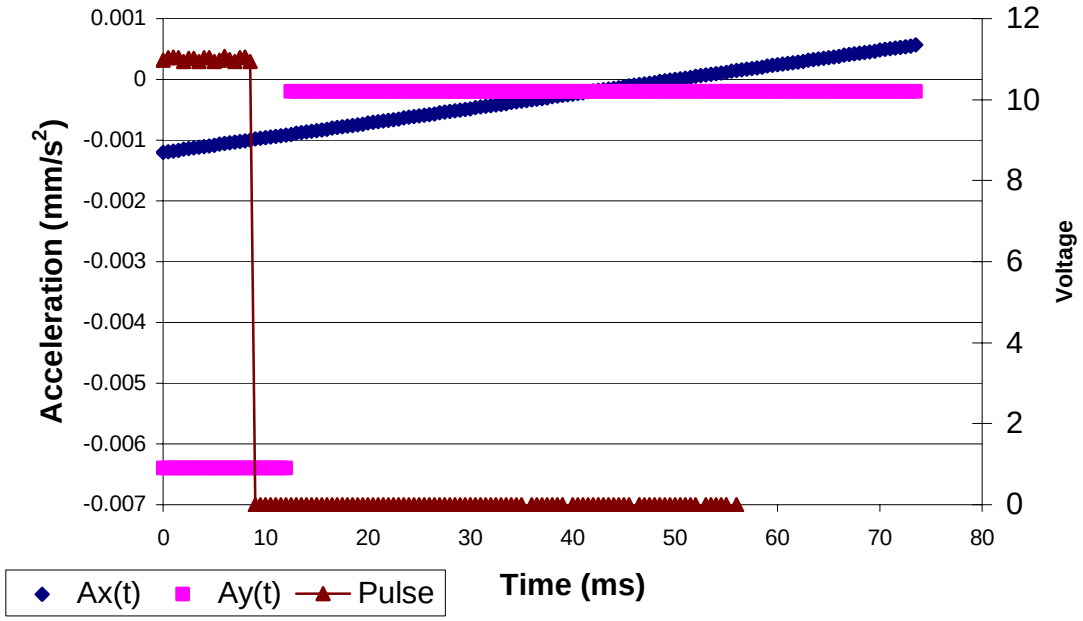

Figure V.4: Acceleration profile for 8 mm ball on 8 mm bed 6.31 mm from magnet face, with 9 ms pulse of 11 V.

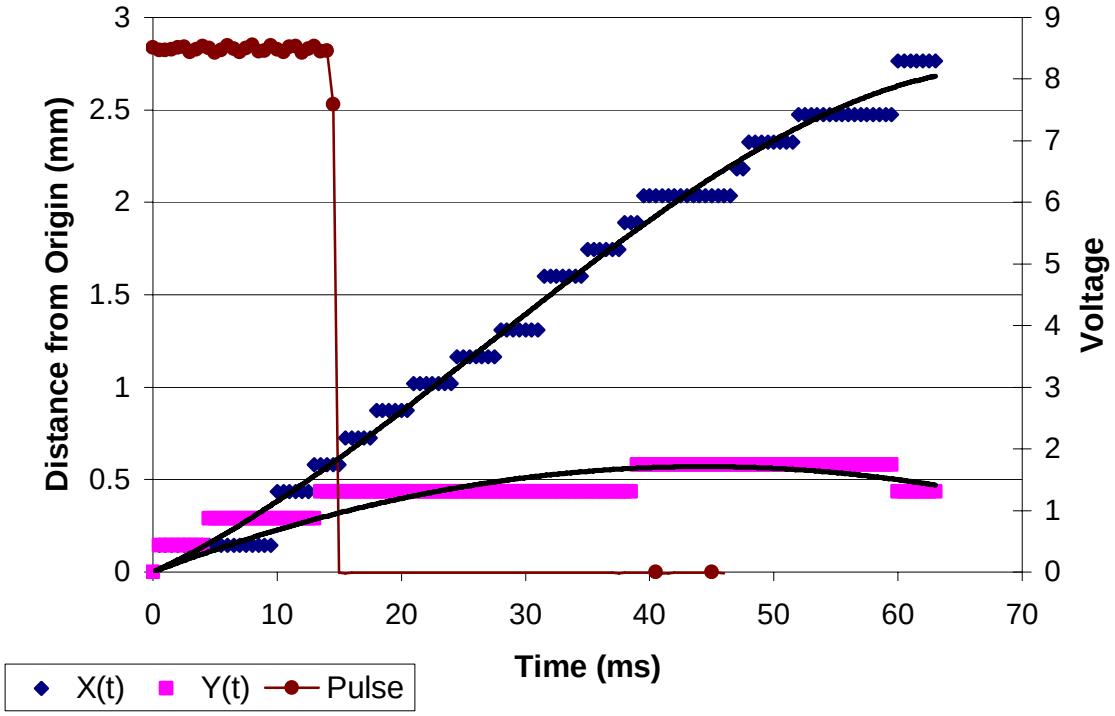

Figure V.5: Position track of an 8 mm ball on 8 mm bed 6.31 mm from magnet face. Particle dislodged with a 15 ms pulse of 8.5 V.

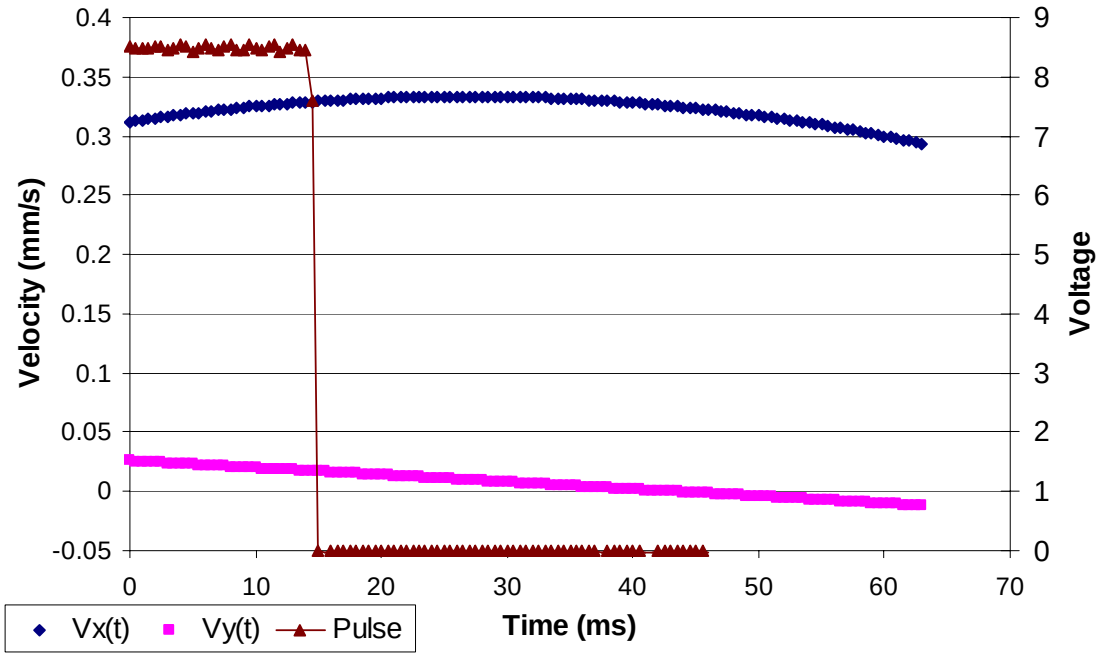

Figure V.6: Velocity profile for 8 mm ball on 8 mm bed 6.31 mm from magnet face, with 15 ms pulse of 8.5 V.

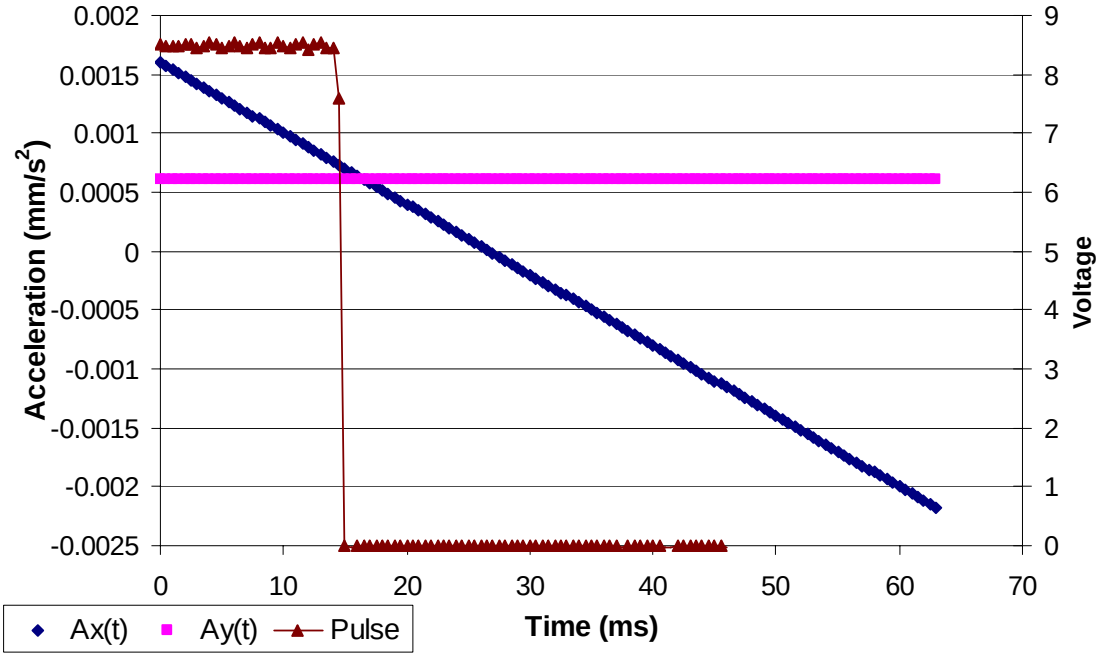

Figure V.7: Acceleration profile for 8 mm ball on 8 mm bed 6.31 mm from magnet face, with 15 ms pulse of 8.5 V.

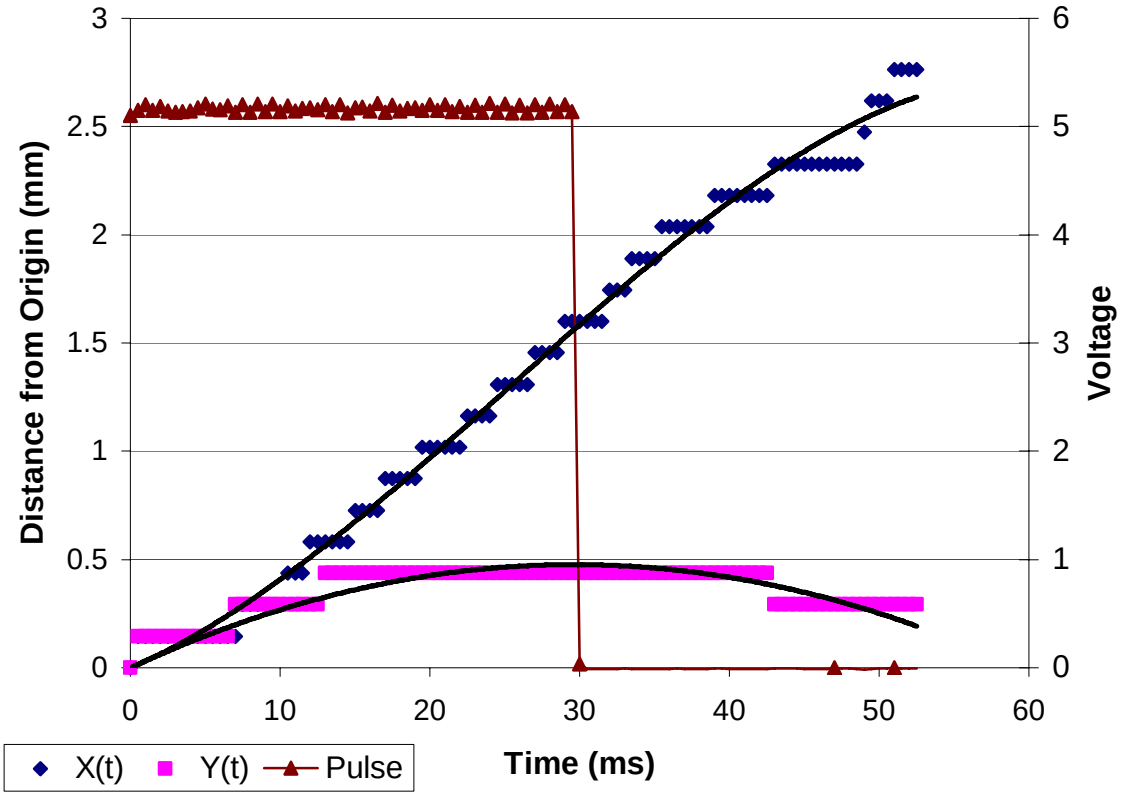

Figure V.8: Position track of an 8 mm particle on an 8 mm bed 6.31mm from magnet face. Particle dislodged with a 30 ms pulse of 5.25 V.

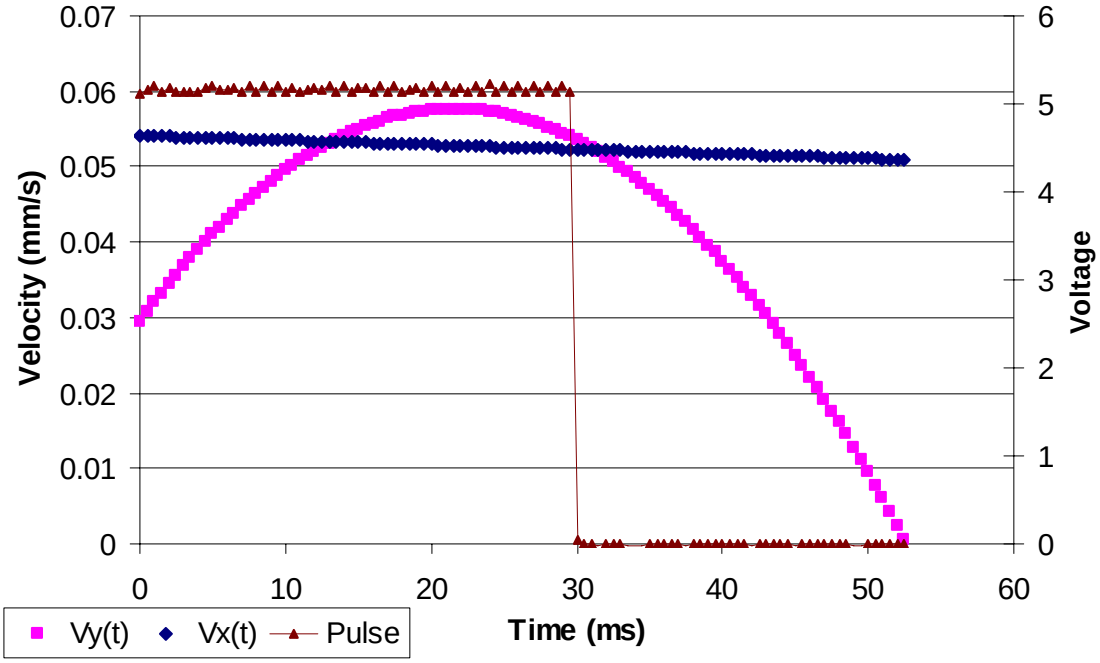

Figure V.9: Velocity profile for 8 mm ball on 8 mm bed 6.31 mm from magnet face, with 30 ms pulse of 5.25 V.

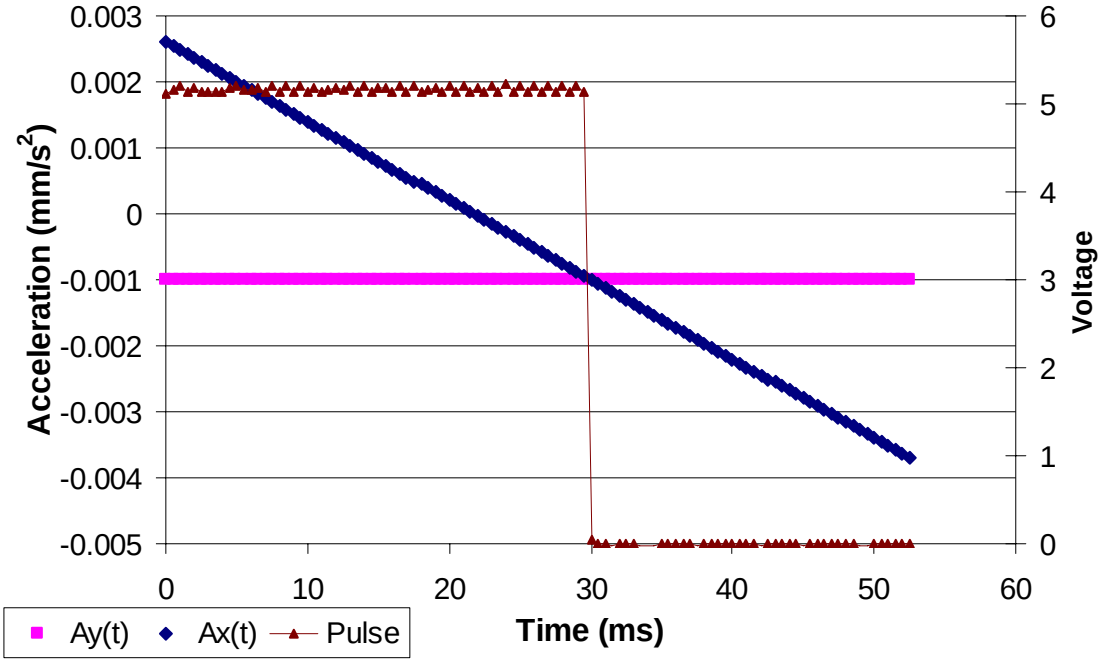

Figure V.10: Acceleration profile for 8 mm ball on 8 mm bed 6.31 mm from magnet face, with 30 ms pulse of 5.25 V.

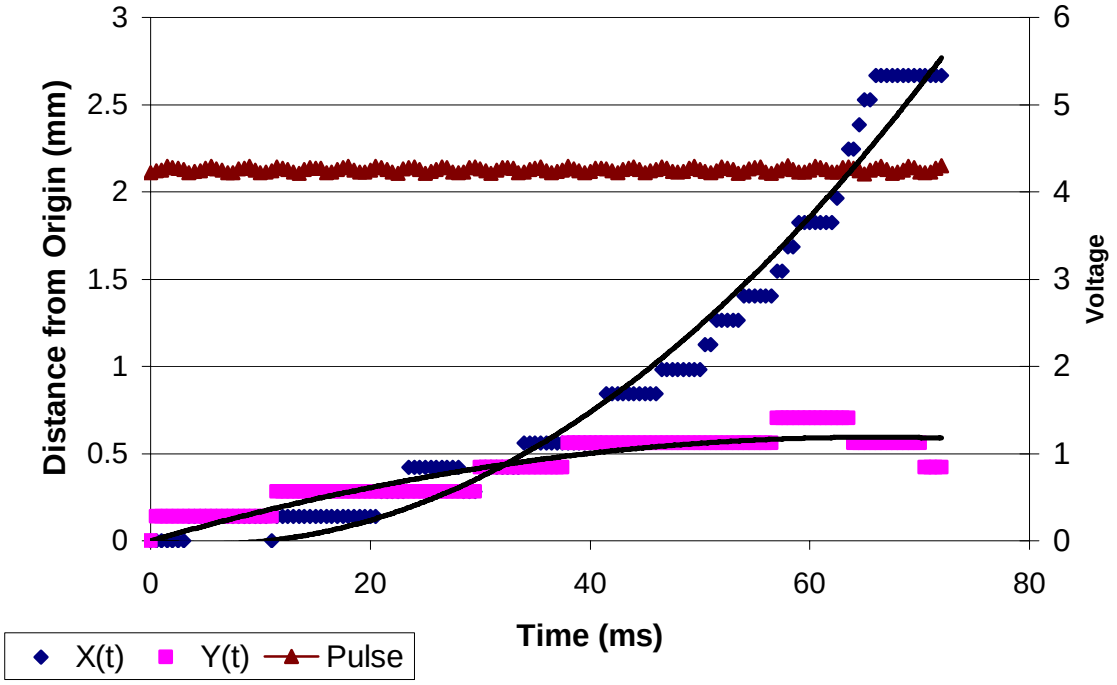

Figure V.11: Position track of an 8 mm particle leaving an 8 mm bed 6.31 mm from magnet face. Particle dislodged at the steady state condition with a 150 ms pulse of 4.25 V.

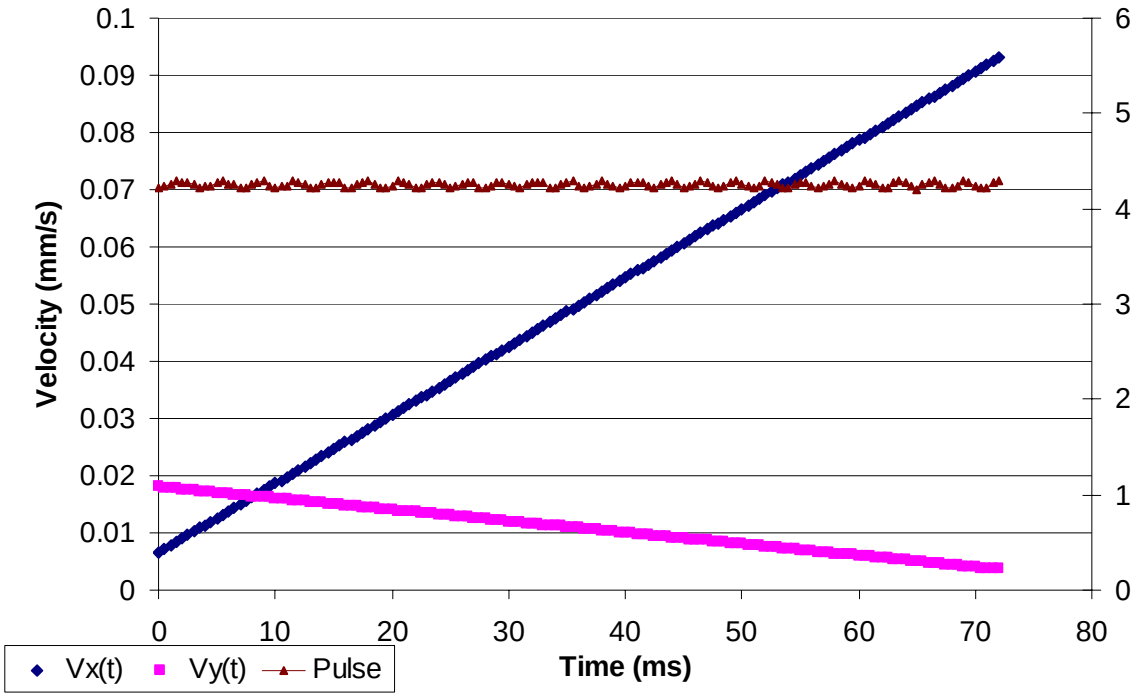

Figure V.12: Velocity profile for 8 mm ball on 8 mm bed 6.31 mm from magnet face, with 150 ms pulse of 4.25 V (steady state condition).

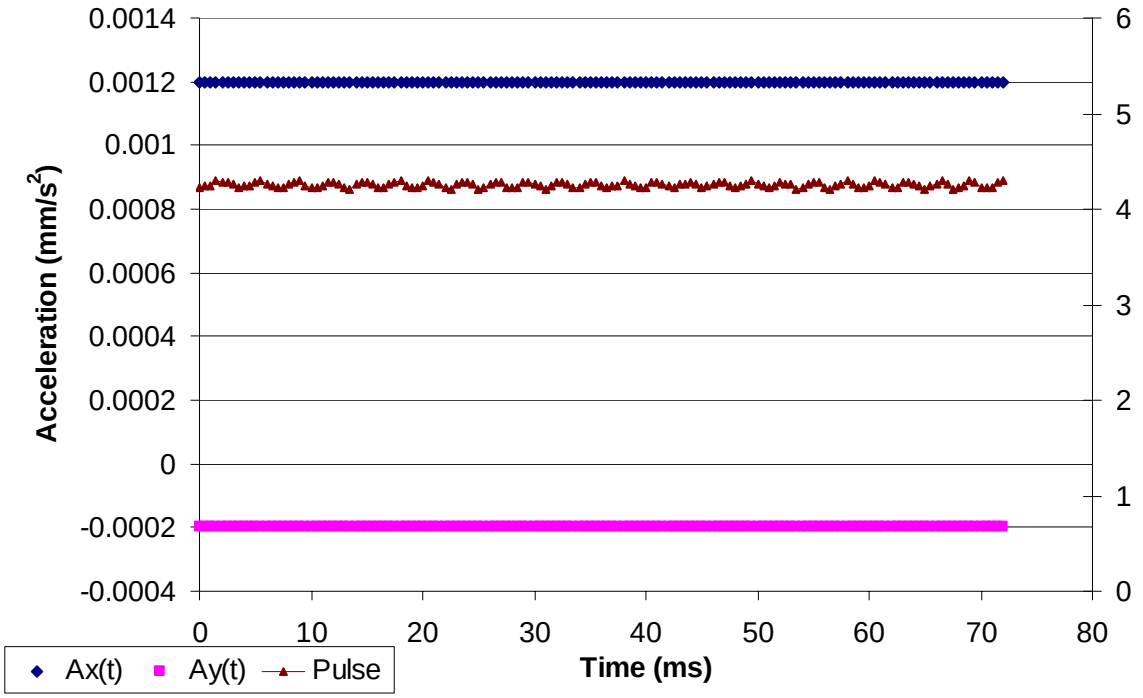

Figure V.13: Acceleration profile for 8 mm ball on 8 mm bed 6.31 mm from magnet face, with 150 ms pulse of 4.25 V (steady state condition).

Table V.1: Derived acceleration profiles for both X and Y directions along with corresponding force values in both X and Y directions calculated from F=ma.

	Pulse Durations			
	9ms	**15ms**	**30ms**	**150ms (SS)**
Voltage^2	121	72.3	27.6	18.1
Mass of Ball (g)	2.09	2.09	2.09	2.09
X(t) (mm)	$-2E-08t^3 - 0.0002t^2 + 0.0508t$ $R^2 = 0.933$	$-1E-05t^3 + 0.0008t^2 + 0.0312t$ $R^2 = 0.9916$	$-2E-05t^3 + 0.0013t^2 + 0.0295t$ $R^2 = 0.993$	$0.0006t^2 - 0.0066t$ $R^2 = 0.9739$
Y(t) (mm)	$(t<12) = -0.0032t^2 + 0.087t$ $R^2 = 0.9316$ $(t>12) = -0.0001t^2 + 0.0092t + 0.5832$ $R^2 = 0.2324$	$-0.0003t^2 + 0.0257t$ $R^2 = 0.6806$	$-0.0005t^2 + 0.0321t$ $R^2 = 0.7958$	$-0.0001t^2 + 0.018t$ $R^2 = 0.8605$
Vx(t) (mm/s)	$-6E-08t^2 - 0.0004t + 0.0508$	$-3E-05t^2 + 0.0016t + 0.0312$	$-6E-05t^2 + 0.0026t + 0.0295$	$0.0012t - 0.0066$
Vy(t) (mm/s)	$(t<12) = -0.0064t + 0.087$ $(t>12) = -0.0002t + 0.0092$	$-0.0006t + 0.0257$	$-0.001t + 0.0321$	$-0.0002t + 0.018$
Ax(t) (mm/s^2)	$-1.2E-07t - 0.0003$	$-6E-05t + 0.0016$	$-1.2E-04t + 0.0026$	0.0012
Ay(t) (mm/s^2)	$(t<12) = -0.0064$ $(t>12) = -0.0002$	-0.0006	-0.001	-0.0002
Force x(t) (gmm/s^2 = µN)	$-2.51-07t - 6.27E-04$	$-1.25E-04t + 0.00334$	$-2.51E-04t + 0.00543$	0.00251
Force y(t) (gmm/s^2 = µN)	-0.013	$-0.00124t + 0.0537$	-0.00209	-0.000418

Chapter VI
Conclusions and Recommendations

Two types of investigations were discussed during the course of this work. The first, the electromagnetic studies, hoped to see better what might be causing particle dislodgement in a simplistic manner. The second, the high speed video imagery hoped to capture this particle dislodgement and determine the forces that caused it. Both investigations were carried out to the best of abilities at the time and methods were developed that will be able to be used in later studies.

VI.1: Electromagnetic Experiments

The electromagnetic experiments were a new and interesting way of looking at forces causing particles to move. Most experiments, especially those for sediment transport, require some sort of uncontrollable force such as the water in a flume. These experiments are highly informative for natural situations; however, repeatability and controllability are not at their highest. Localized velocities change suddenly and frequently, causing many researchers to use averaged velocities to compensate; but what if the fluctuations and variations were exactly what were driving the particle entrainment in the first place. These electromagnetic experiments hoped to be able to isolate forces

and apply them in a controlled manner to see how these fluctuations in force affected a particle.

Electromagnetics is still an evolving field and so has its own innate areas of uncertainty. The use of these forces in these experiments is not perfect, the air gaps and the locations of the particles in relation to the magnet caused many difficulties, but the overall outcome was still achieved. Through electromagnetics, specified forces with specified durations were able to be applied; and through these specific forces and specific durations, patterns were able to be recognized.

All seven different electromagnetic experiments produced a similar dislodgement curve. These graphs show that as the time duration of the pulse increases, the force needed to dislodge that particle decreases exponentially. To be more specific, the force decreases in such a way that the product of the force and time combination required to dislodge the particle appears to remain constant. In other words, there appears to be a constant impulse level that if met, will cause particle dislodgement. There are several sources of error that provide scattered data for this conclusion, but the trend is still apparent. Another question is raised, as it also appears for values where the force is close to threshold, the impulse required to dislodge increases slightly. This raises the point that the time variable in the force-time combinations might play a more significant roll and that the impulse may be only nearly constant, with increased values near threshold. But in order to determine what the impulse values were, not in terms of voltage and air distance, other means were necessary.

VI.2: Preliminary High Speed Camera Work

As the electromagnetics were a new and different method of providing force, a different method for measuring that force was needed as well. Without accurate means of calculating the force once applied, it was determined a method of measurement was needed. However, to keep the entire experiment as simple as possible, a method that did not change the shape or path of the particle was necessary. Strain gauges tend to put limitations of the means of movement and physically attaching something to the particle was not desired. The best method was determined to be through high speed imagery.

The Phantom V.4 high speed digital camera was used to take 256x256 resolution images at 2,000 pps; the regular Kodak hand-held digital camera operates at 30 pps. These two cameras were able to show the movement of the ball prior to entrainment up to the frame by frame rolling of the ball from its pocket. The hand-held camera gave additional evidence to support the minimum impulse theory. The experiments were designed to apply increasing levels of impulse and stop once the ball was dislodged. As the impulses increase, the video recorded the ball "twitching" in its pocket and at some instances nearly rolling out.

The high speed digital camera was intended to capture the dislodgement of the particle and correlate the images to the voltage readings from the electromagnet. The camera is post-trigger operated, however the TTL signal was never able to be correctly programmed or received by the camera so the images were not able to be time matched

with the voltage readings. However, the assumption was made that as seen in the other videos, the particle does move at lower levels of voltage, the ball could be assumed to start its motion once the voltage is greater than the threshold level. The voltage rise time for the system is between 0.2 and 0.4 ms, which is less than one frame of the high speed imagery, therefore, the assumption can be made that the particle starts its movement at the same time as the start of the pulse.

The Phantom software also allows for position tracking as the particle rolls from its pocket. Although the points are user defined and the zoom and resolution for this application is not ideal, the program was able to create fairly decent curves monitoring movement in both the x and y directions. Using Excel, best fit curves were developed and from the position curves, particle acceleration was able to be determined. Using Newton's Second Law of Motion, F=ma, the forces applied during these events were able to be determined. Although this particular arrangement including camera, lens, and image software was not as accurate as hoped, and the relationship used to determine force is not the exact one needed to determine the force moving the particle, the method and procedure was still able to be proven usable and recommendations can be made to improve upon them.

VI.3: Recommendations

The experiments and the work related to this document were intended as a means of learning and understanding the basics behind these new methods and to develop procedures that could be used in later experiments in a more refined manner. As such,

there are several recommendations that can be made to increase the accuracy and expand the present work.

1. The most evident recommendations come in the form of available equipment. Many of the sources of error in these experiments came from having equipment that was not exactly suitable. A DAQ system that was capable of handling faster analog output signals with hardware timing would greatly increase the overall accuracy of the pulses generated. The switch to hardware timing would then increase the accuracy of the voltages and so smaller increments could be investigated leading more closely to the true incipient point and providing better data at lower voltages near the threshold level.
2. The amount of voltage needed to generate an electromagnetic force across a 0.5 cm -1 cm air gap is impressive. The electronic circuitry that was created for these experiments had maximum voltage output of approximately 11 V. This was often not capable of generating enough force to move the particle at low durations. It's an interesting point to see if this trend continues as the durations decrease. It is recommended that the circuitry be designed to create significantly higher voltages and that investigations be made into possibly developing a new electromagnet that will make better use of those voltages.
3. The high speed imagery is important to these experiments. Several things need to be adjusted however to make the most of the images. A lens with greater zoom should be used to make the most of the available resolution. Additionally, creating or finding a better image processing software would be very beneficial to creating more accurate position tracks.

4. Investigations were made into the ball location in the magnetic field laterally and vertically and no significance was really noticed, however, there is a great deal of variability with the air gap distance. Modeling magnetic forces around a sphere is very difficult and for the purposes of these experiments, the locations were determined by the center of the particle. This may not be the case. There was a great deal of variation for particles at the same location, so it may be that the front of the particle is a better constant, but this should be investigated.

5. All of these experiments were conducted with the increasing impulse program. It would be interesting to see if random impulses were sent, in a more realistic pattern such as those of fluid velocities in a river, if the same impulses seem to be causing the particle entrainment, using the determined impulses as a predictor for movement.

6. The determination of the actual forces and impulses causing the particle movement would be the culmination of these experiments. The final step, taking this generalized data into specifics for prediction in flume experiments similar to those of Balakrishnan and Papanicolaou.

References

(2003). Data Acquisition and Signal Conditioning Course Manual. Austin, TX, National Instruments Corporation.

Allaire, P. E., R.L. Fittro, E.H. Maslen, W.C. Wakefield (1995). Measured Force/Current Relations in Solid Magnetic Thrust Bearings. International Gas Turbine and Aeroengine Congress & Exposition, Houston, Texas, The American Society of Mechanical Engineers.

Balakrishnan, M. (1997). The Role of Turbulence on the Entrainment of a Single Sphere and the Effects of Roughness on Fluid-Solid Interaction. Mechanical Engineering. Blacksburg, VA, Virginia Polytechnic Institute and State University. Doctoral Dissertation: 214.

Beckwith, T. G., R. D. Marangoni, J. H. Lienhard V (1993). Mechanical Measurements. New York, Addison-Wesley Publishing Company.

Brain, M. (2000). How Electromagnets Work, www.howstuffworks.com.

Bridge, J. S., S.J. Bennett (1992). "A Model for the Entrainment and Transport of Sediment Grains of Mixed Sizes, Shapes, and Densities." Water Resources Research 28(2): 337-363.

Chang, H. H. (1988). Fluvial Processes in River Engineering. Malabar, FL, Krieger Pulbishing.

Chien, N., Wan, Z. (1999). Mechanics of Sediment Transport. Reston, VA, American Society of Civil Engineers.

Coleman, N. L. (1967). A theoretical and EXperimental Study of Drag and Lift Forces Acting on a Sphere REsting on Hypothetical Stream Bed. 12th Congress, International Association for Hydraulics Research. Fort Collins, Colorado.

Dancey, C. L., Diplas, P. (2002). "Probability of Individual Grain Movement and Threshold Condition." Journal of Hydraulic Engineering 128(12): 1069-1075.

Day, T. J. (1980). A Study of Initial Motion Characteristics of Particles in Graded Bed Material, Geological Survey of Canada. 80-1A: 281-286.

Dorf, R. C., J. A. Svoboda (2001). Introduction to Electric Circuits. New York, John Wiley & Sons, Inc.

Einstein, H. A. (1937). Bed Load Transport as a Probability Problem. Sedimentation. H. W. Shed. Zurich, Verlag Rascher & Co.

Einstein, H. A. (1950). The Bedload Function for Sediment Transportation in Open Channels. Tech. Bull, U.S. Dept. of Angriculture: 1026.

Kalinske, A. (1943). "The Role of Turbulence in River Hydraulics." Bull. Univ. Iowa Studies Eng. 27: 266-279.

Kleinhans, M., van Rijn, L. (2002). "Stochastic Prediction of Sediment Transport in Sand-Gravel Bed Rivers." Journal Of Hydraulic Engineering(April): 412-425.

Kline, S. J., W.C. Reynolds, F.A. Schraub, and P.W. Raunstadler (1967). "The Structure of Turbulent boundary Layers." Journal of Fluid Mechanics Vol. 30: 741-773.

Middleton, G. V., J.B. Southard (1984). Mechanics of Sediment Movement. Providence, RI, Easter Section of Society of Economic Paleontologists and Minerologists: 165 - 204.

Moore, M. C. (1994). Bedload Transport: The Effects of Particle Shape and an Investigation of a Wide Range of Transport Rates. Civil Engineering. Blacksburg, VA, Virginia Tech. Master of Science: 214.

Morris, A. S. (1993). Principles of Measurement and Instrumentation. New York, Prentice Hall.

Paintal, A. S. (1971). "A Stochastic Model of Bed Load Transport." Journal of Hydraulic Research Vol. 9(No. 4): 527-554.

Papanicolaou, A. (1997). The Role of Turbulence on the Initiation of Sediment Motion. Civil Engineering. Blacksburg, VA, Virginia Polytechnic Institute and State University. Doctoral Dissertation.

Papanicolaou, A. (1999). "Pickup Probability for Sediment Entrainment." Journal Of Hydraulic Engineering 125(7): 788.

Papanicolaou, A. N., P. Diplas, C. Dancey, M. Balakrishnan (2001). "Surface Roughness Effects on Near-Bed Turbulence: Implications to Sediment Entrainment." Journal of Engineering Mechanics Vol. 127(No. 3): 211-218.

Papanicolaou, A. N., P. Diplas, N. Evaggelopoulos, S. Fotopoulos (2002). "Stochastic Incipient Motion Criterion for Spheres under Various Packing Conditions." Journal of Hydraulic Engineering Vol. 128(No.4): 369-380.

Plonus, M. A. (1978). Applied Electromagnetics. New York, McGraw-Hill, Inc.

Sabersky, R. H. (1999). Fluid Flow. New Jersey, Prentice Hall.

Shen, H. W., Ed. (1972). Sedimentation. Fort Collins, CO, Colorado State University.

Shields, A. (1936). Anwendung der Aehnlichkeitsmechanik und der Turbulenzforschung auf die Geschiebe-bewegung. Mitteilungen der Preussischen Versuchsanstalt fur Wasserbau und Schiffbau. Berlin, Germany. No. 26.

Strum, T. W. (2001). Open Channel Hydraulics. New York, McGraw-Hill.

Willmarth, W. W., S.S. Lu (1972). "Structure of the Reynolds Stress Near the Wall." Journal of Fluid Mechanics Vol. 55, part I: 65-92.

Appendix A

This appendix contains tables of all the voltages and pulse durations applied during the course of the experiments. Each set of experiments is separated by its particle ball and base ball size. The tables include the sampled voltage, Vin, the amplified voltage, Vmag, the pulse duration, Dur, the square of the amplified voltage, Vmag^2, and the square of the amplified voltage multiplied by its duration, or the Impulse.

Table A.1: Movement pulses for 8 mm ball on 8 mm bed 6.31 mm from magnet face.

Movement Vin	Dur	Vmag	Impulse	Vmag^2
5.609694	6.5	14.72545	1409.452	216.8388
4.191115	9	11.00168	1089.332	121.0369
4.191183	9	11.00185	1089.367	121.0408
4.193658	9	11.00835	1090.654	121.1838
3.520635	12	9.241667	1024.901	85.4084
3.522453	12	9.24644	1025.96	85.49665
3.524323	12	9.251347	1027.049	85.58742
3.213277	15	8.434853	1067.201	71.14674
3.2223	15	8.458538	1073.203	71.54687
3.23759	15	8.498673	1083.412	72.22744
2.932358	18	7.697439	1066.51	59.25057
2.948252	18	7.739162	1078.103	59.89464
2.948363	18	7.739452	1078.184	59.89911
2.853562	19	7.490601	1066.073	56.1091
2.654041	21	6.966858	1019.279	48.53711
2.658641	21	6.978931	1022.815	48.70548
2.660748	21	6.984463	1024.437	48.78272
2.554398	24	6.705294	1079.063	44.96096
2.56244	24	6.726406	1085.869	45.24453
2.567342	24	6.739273	1090.027	45.4178
2.365045	27	6.208242	1040.641	38.54227
2.37789	27	6.241962	1051.976	38.96208
2.378727	27	6.244157	1052.716	38.9895
2.47137	27	6.487346	1136.313	42.08566
2.280548	30	5.986439	1075.124	35.83745
2.281113	30	5.987921	1075.656	35.8552
2.274515	31	5.970601	1105.09	35.64807
2.184684	33	5.734796	1085.3	32.88788
2.186978	33	5.740816	1087.58	32.95697
2.18706	34	5.741033	1120.622	32.95946
2.086953	36	5.478252	1080.405	30.01124
2.089002	37	5.483631	1112.598	30.07021
2.091737	37	5.490809	1115.512	30.14898
2.090881	39	5.488561	1174.848	30.12431
2.090927	39	5.488685	1174.901	30.12566
2.091495	39	5.490174	1175.538	30.14201
1.992587	42	5.230541	1149.06	27.35856
1.996351	42	5.240421	1153.405	27.46202
1.997474	42	5.243368	1154.702	27.49291
1.901835	45	4.992317	1121.545	24.92323
1.901964	45	4.992655	1121.697	24.92661
1.950935	45	5.121203	1180.202	26.22672
1.997474	45	5.243369	1237.181	27.49292
1.904307	46	4.998805	1149.451	24.98805
1.80412	48	4.735814	1076.541	22.42794

1.883611	48	4.944479	1173.498	24.44787
1.899993	48	4.987481	1193.998	24.87496
1.992989	48	5.231595	1313.74	27.36959
1.997754	48	5.244104	1320.03	27.50062
1.998927	48	5.247183	1321.58	27.53293

Table A.2: Movement pulses for 6 mm particle on 6 mm bed 4.73 mm from magnet face.

Movement VIN	Dur	Vmag	Impulse	Vmag^2
4.169998	6	10.94624	718.9217	119.8203
4.24909	6	11.15386	746.4516	124.4086
4.655864	6	12.22164	896.2112	149.3685
4.666723	6	12.25015	900.3966	150.0661
4.189555	6	10.99758	725.6808	120.9468
3.52378	9	9.249922	770.0495	85.56106
3.426855	8.5	8.995494	687.8107	80.91891
3.517812	9	9.234257	767.4435	85.2715
3.591258	9	9.427052	799.8237	88.8693
3.126399	12	8.206797	808.2181	67.35151
2.95044	14	7.744904	839.7695	59.98353
2.855072	12	7.494564	674.0219	56.16849
2.917226	12	7.657718	703.6878	58.64065
2.935206	12	7.704916	712.3887	59.36573
2.546336	15	6.684131	670.1642	44.67761
2.666992	15	7.000854	735.1794	49.01196
2.541423	15	6.671234	667.5805	44.50536
2.666595	15	6.999813	734.9607	48.99738
2.372848	20	6.228727	775.9409	38.79704
2.314041	18.5	6.074357	682.6095	36.89781
2.357398	18	6.18817	689.2821	38.29345
2.474848	18	6.496477	759.6758	42.20421
2.36952	18	6.219991	696.3892	38.68829
2.362942	18	6.202723	692.5279	38.47377
2.094021	24	5.496805	725.1567	30.21486
2.072589	24	5.440545	710.3887	29.59953
2.080072	24	5.460189	715.5278	29.81366
1.807421	27	4.744479	607.7722	22.51008
2.00101	28	5.252652	772.5299	27.59035
1.904772	27	5.000025	675.0068	25.00025
1.903771	27	4.9974	674.2981	24.974
1.901932	30	4.992571	747.7729	24.92576
1.90126	30	4.990808	747.245	24.90817
1.80957	30	4.750122	676.9098	22.56366
1.811047	33	4.753999	745.8167	22.6005
1.71438	33	4.500249	668.3238	20.25224
1.711888	33	4.493706	666.3821	20.1934
1.713091	34	4.496863	687.5405	20.22178
1.713083	36	4.496843	727.9775	20.2216
1.714365	38	4.500209	769.5713	20.25188
1.617625	39.5	4.246265	712.2153	18.03077
1.808927	38.5	4.748435	868.0838	22.54763
1.712662	39	4.495738	788.2548	20.21166
1.712909	39	4.496385	788.4817	20.21748
1.612422	42	4.232607	752.4284	17.91496

1.614394	42	4.237785	754.2706	17.95882
1.612858	41	4.233751	734.9107	17.92465
1.523218	48	3.998448	767.404	15.98758
1.524652	46	4.00221	736.8136	16.01769
1.618896	47	4.249602	848.7783	18.05911
1.61766	47.5	4.246357	856.4984	18.03155
1.712748	45	4.495964	909.6162	20.21369

Table A.3: Movement pulses for 4 mm particle on 4 mm bed 3.15 mm from magnet face.

Movement Vin	Dur	Vmag	Impulse	Vmag^2
4.81074	3	12.62819	478.4138	159.4713
5.31545	3	13.95306	584.0633	194.6878
5.238892	3	13.75209	567.36	189.12
4.836985	3	12.69709	483.648	161.216
5.242055	3	13.76039	568.0454	189.3485
3.23232	6	8.48484	431.9551	71.99252
3.143049	7	8.250503	476.4956	68.07081
3.235728	6	8.493786	432.8664	72.1444
3.1397	6	8.241711	407.5548	67.9258
3.135045	6	8.229494	406.3474	67.72457
2.380727	9	6.249408	351.4959	39.05511
2.47406	9	6.494408	379.596	42.17733
2.379998	9	6.247495	351.2808	39.0312
2.376133	9	6.237348	350.1406	38.90451
2.091955	12	5.491381	361.8631	30.15526
1.904945	12	5.000482	300.0578	25.00482
1.898232	12	4.982858	297.9464	24.82887
1.427419	30	3.746975	421.1946	14.03982
1.332174	30	3.496956	366.861	12.2287
1.426921	30	3.745666	420.9005	14.03002
1.42509	30	3.74086	419.821	13.99403
1.426321	32.5	3.744093	455.5926	14.01823
1.523105	33	3.998149	527.5116	15.9852
1.524792	33	4.00258	528.6813	16.02064
2.186979	12	5.740819	395.484	32.957
2.278061	12	5.97991	429.1119	35.75933
1.871623	15	4.91301	362.0649	24.13766
1.90038	15	4.988498	373.2767	24.88512
1.902608	15	4.994346	374.1524	24.9435
1.616629	19	4.24365	342.1628	18.00857
1.709764	18	4.488131	362.5798	20.14332
1.89537	18	4.975347	445.5735	24.75408
1.710654	18	4.490468	362.9574	20.1643
1.805335	27	4.739005	606.3705	22.45817
1.520041	27	3.990108	429.8659	15.92096
1.42191	27	3.732514	376.1548	13.93166
1.425482	27	3.74189	378.0469	14.00174
1.518142	27	3.985123	428.7926	15.88121
1.519374	27	3.988357	429.4888	15.90699
1.424007	27	3.738018	377.2649	13.97278
1.333238	20.5	3.499751	251.0893	12.24826
1.619517	21	4.251232	379.5325	18.07297
1.619481	21	4.251137	379.5154	18.07216
1.61895	21	4.249744	379.2669	18.06033

1.512394	24	3.970034	378.2681	15.76117
1.524269	23.5	4.001205	376.2265	16.00964
1.522973	24	3.997805	383.5787	15.98245
1.23656	37	3.24597	389.8438	10.53632
1.332855	36	3.498745	440.6838	12.24122
1.332372	36	3.497477	440.3643	12.23234
1.236294	45	3.245272	473.9307	10.53179
1.33231	42	3.497315	513.7108	12.23121
1.331518	42	3.495236	513.1002	12.21667

Table A.4: Movement pulses for 8 mm particle on 6 mm bed 6.31 mm from magnet face.

Movement Vin	Dur	Vmag	Impulse	Vmag^2
4.654363	6	12.2177	895.6336	149.2723
4.656652	6	12.22371	896.5147	149.4191
4.668401	6	12.25455	901.0444	150.1741
4.84843	6	12.72713	971.8786	161.9798
3.518745	9	9.236704	767.8504	85.31671
3.521237	9	9.243247	768.9385	85.43761
3.616113	9	9.492296	810.9331	90.10368
3.618418	9	9.498348	811.9676	90.21862
3.618741	9	9.499194	812.1122	90.23469
2.853648	12	7.490826	673.3496	56.11247
2.856153	12	7.497401	674.5323	56.21103
2.94927	12	7.741833	719.2317	59.93597
2.949397	12	7.742166	719.2937	59.94114
2.951775	12	7.748408	720.4539	60.03783
2.558167	15	6.715187	676.4061	45.09374
2.570557	15	6.747711	682.9741	45.53161
2.664225	15	6.993591	733.6548	48.91032
2.469273	16	6.481841	672.2281	42.01426
2.189221	18	5.746705	594.4431	33.02462
2.284003	18	5.995509	647.0303	35.94613
2.284893	18	5.997845	647.5347	35.97415
2.292141	18	6.016871	651.6493	36.20274
2.377896	18	6.241976	701.3208	38.96227
2.093397	21	5.495167	634.134	30.19686
2.094516	21	5.498104	634.8121	30.22915
2.179159	21	5.720291	687.1563	32.72173
2.1892	21	5.746651	693.5039	33.024
2.190276	21	5.749474	694.1854	33.05645
2.283303	21	5.993671	754.406	35.9241
1.995869	24	5.239155	658.77	27.44875
1.996053	24	5.239639	658.8917	27.45382
2.089074	24	5.48382	721.7349	30.07229
2.091586	24	5.490413	723.4712	30.14463
2.092584	24	5.493033	724.1619	30.17341
1.899787	27	4.986941	671.4787	24.86958
1.900154	27	4.987905	671.7384	24.8792
1.901347	27	4.991035	672.5818	24.91044
1.901382	30	4.991129	747.341	24.91137
1.901469	30	4.991356	747.409	24.91363
1.901555	30	4.991583	747.477	24.9159
1.805272	33	4.738839	741.0676	22.4566
1.805577	33	4.73964	741.3182	22.46419
1.805919	33	4.740538	741.5991	22.4727
1.710048	36	4.488877	725.4005	20.15001

1.710786	36	4.490813	726.0263	20.1674
1.711354	36	4.492304	726.5085	20.18079
1.615874	39	4.24167	701.679	17.99177
1.708538	39	4.484913	784.4634	20.11445
1.709094	39	4.486371	784.9736	20.12753
1.709419	39	4.487224	785.272	20.13518
1.709627	42	4.487772	845.8841	20.1401

Table A.5: Movement pulses for 6 mm particle on 8 mm bed 6.31 mm from magnet face.

Movement Vin	Dur	Vmag	Impulse	Vmag^2
5.134922	9	13.47917	1635.192	181.688
5.135515	9	13.48073	1635.57	181.73
5.135905	9	13.48175	1635.818	181.7576
4.18677	12	10.99027	1449.433	120.7861
4.187355	12	10.99181	1449.838	120.8198
4.281133	12	11.23797	1515.505	126.2921
4.471054	12	11.73652	1652.95	137.7458
4.565659	12	11.98485	1723.641	143.6367
4.567083	12	11.98859	1724.716	143.7263
4.570516	12	11.9976	1727.31	143.9425
3.710714	15	9.740624	1423.196	94.87975
3.808207	15	9.996544	1498.963	99.93089
3.901276	15	10.24085	1573.125	104.875
3.902771	15	10.24477	1574.331	104.9554
3.425352	18	8.99155	1455.263	80.84797
3.425937	18	8.993085	1455.76	80.87558
3.426132	18	8.993597	1455.926	80.88479
3.523543	18	9.249299	1539.892	85.54953
3.524857	18	9.252749	1541.04	85.61336
3.23604	21	8.494606	1515.325	72.15833
3.236796	21	8.49659	1516.033	72.19204
3.324556	21	8.726959	1599.356	76.15982
3.329737	21	8.740559	1604.345	76.39737
3.330696	21	8.743077	1605.269	76.44139
2.94796	24	7.738395	1437.186	59.88275
3.026841	24	7.945459	1515.128	63.13032
3.038718	24	7.976635	1527.041	63.6267
3.045845	24	7.995343	1534.212	63.92551
2.761004	27	7.247637	1418.262	52.52824
2.761705	27	7.249476	1418.982	52.5549
2.761739	27	7.249565	1419.017	52.55619
2.713543	30	7.12305	1522.135	50.73785
2.760427	30	7.24612	1575.188	52.50626
2.761134	30	7.247976	1575.995	52.53316
2.853007	30	7.489143	1682.618	56.08727
2.83938	31	7.453373	1722.136	55.55277
2.47492	33	6.496665	1392.82	42.20666
2.475091	33	6.497114	1393.012	42.21249
2.56547	33	6.734357	1496.602	45.35157
2.569862	33	6.745888	1501.731	45.50701
2.663861	33	6.992635	1613.599	48.89694
2.474863	34	6.496516	1434.961	42.20472
2.65555	34	6.970819	1652.139	48.59231
2.465935	36	6.473079	1508.427	41.90075

2.470127	36	6.484082	1513.56	42.04333
2.472721	36	6.490892	1516.74	42.13167
2.568135	36	6.741354	1636.051	45.44585
2.570106	36	6.746527	1638.563	45.51563

Table A.6: Movement pulses for 6 mm particle on 6 mm bed 6.31 mm from magnet face.

Movement Vin	Dur	Vmag	Impulse	Vmag^2
4.468231	9	11.72911	1238.148	137.5719
4.472538	9	11.74041	1240.535	137.8373
4.47564	9	11.74856	1242.257	138.0286
3.514926	12	9.22668	1021.58	85.13163
3.515638	12	9.228549	1021.993	85.16612
3.521258	12	9.243303	1025.264	85.43864
3.230703	15	8.480595	1078.807	71.92048
3.23347	15	8.487858	1080.656	72.04373
3.235697	15	8.493706	1082.146	72.14304
2.853546	18	7.490559	1009.952	56.10847
2.946981	18	7.735824	1077.174	59.84298
2.94732	18	7.736715	1077.422	59.85675
2.950261	18	7.744436	1079.573	59.97629
2.66146	21	6.986332	1024.986	48.80884
2.662128	21	6.988087	1025.5	48.83335
2.662295	21	6.988525	1025.629	48.83949
2.566306	24	6.736553	1089.147	45.38114
2.567565	24	6.739857	1090.216	45.42567
2.567705	24	6.740224	1090.335	45.43062
2.470392	27	6.48478	1135.414	42.05237
2.47293	27	6.491441	1137.748	42.1388
2.473054	27	6.491767	1137.862	42.14304
2.377747	30	6.241585	1168.721	38.95738
2.378052	30	6.242386	1169.021	38.96738
2.378871	30	6.244535	1169.827	38.99422
2.279871	33	5.984662	1181.934	35.81618
2.280509	33	5.986337	1182.595	35.83623
2.283219	33	5.993449	1185.407	35.92144
2.088742	36	5.482947	1082.258	30.06271
2.090577	36	5.487765	1084.16	30.11556
2.091259	36	5.489556	1084.868	30.13522
2.090705	39	5.488099	1174.65	30.11923
2.090967	39	5.488787	1174.945	30.12679
2.091319	39	5.489712	1175.34	30.13694

Table A.7: Movement pulses for 4 mm particle on 6 mm bed 6.31 mm from magnet face.

Movement Vin	Dur	Vmag	Impulse	Vmag^2
4.184074	12	10.9832	1447.567	120.6306
4.184354	12	10.98393	1447.761	120.6467
4.189682	12	10.99792	1451.45	120.9541
3.795705	15	9.963726	1489.138	99.27584
3.802338	15	9.981136	1494.346	99.62308
3.806803	15	9.992859	1497.858	99.85723
3.613196	18	9.484641	1619.251	89.95841
3.616893	18	9.494343	1622.566	90.14255
3.617766	18	9.496635	1623.349	90.18607
3.423803	21	8.987484	1696.272	80.77487
3.424639	21	8.989677	1697.1	80.8143
3.427197	21	8.996391	1699.636	80.93505
2.948252	24	7.739162	1437.471	59.89463
2.948818	24	7.740648	1438.023	59.91763
2.95037	24	7.74472	1439.537	59.98069
2.850766	27	7.48326	1511.978	55.99918
2.85093	27	7.48369	1512.152	56.00562
2.851099	27	7.484135	1512.332	56.01228
2.848943	30	7.478476	1677.828	55.9276
2.852132	30	7.486847	1681.586	56.05288
2.853068	30	7.489304	1682.69	56.08967
2.658174	33	6.977706	1606.716	48.68837
2.76074	33	7.246943	1733.1	52.51819
2.571869	36	6.751156	1640.812	45.57811
2.571271	36	6.749587	1640.049	45.55693
2.568491	36	6.742288	1636.504	45.45845
2.475703	39	6.498721	1647.102	42.23338
2.475206	39	6.497417	1646.441	42.21642
2.474631	39	6.495907	1645.676	42.19681
2.475219	42	6.49745	1773.108	42.21685
2.473526	42	6.493006	1770.683	42.15912
2.473112	42	6.491918	1770.09	42.145

Appendix B

The following tables of data show the position tracking for the 8mm ball on 8mm bed 6.31mm from magnet face experiments. There are four (4) runs, 9ms, 15ms, 30ms and 150ms pulse durations. The data shows the frame number, x and y coordinates (where the center of the ball at the start position is 0,0) and added to the data is time. The images were taken at 2000pps, so every frame advances by 0.5ms.

Table B.1: Position tracking data for 8mm ball on 8mm bed 6.31mm from magnet face, 9ms pulse.

POSITION	1	mm	mm	
		x	y	ms
13579	-5.22E+06	0	0	0
13580	-5.22E+06	0.1455	0	0.5
13581	-5.22E+06	0.1455	0	1
13582	-5.22E+06	0.1455	0.1455	1.5
13583	-5.22E+06	0.1455	0.1455	2
13584	-5.22E+06	0.1455	0.1455	2.5
13585	-5.22E+06	0.1455	0.1455	3
13586	-5.22E+06	0.1455	0.2909	3.5
13587	-5.22E+06	0.1455	0.2909	4
13588	-5.22E+06	0.1455	0.4364	4.5
13589	-5.22E+06	0.1455	0.4364	5
13590	-5.22E+06	0.1455	0.4364	5.5
13591	-5.22E+06	0.2909	0.4364	6
13592	-5.22E+06	0.2909	0.4364	6.5
13593	-5.22E+06	0.2909	0.4364	7
13594	-5.22E+06	0.2909	0.4364	7.5
13595	-5.22E+06	0.2909	0.4364	8
13596	-5.22E+06	0.2909	0.4364	8.5
13597	-5.22E+06	0.2909	0.4364	9
13598	-5.22E+06	0.2909	0.5818	9.5
13599	-5.22E+06	0.4364	0.5818	10
13600	-5.22E+06	0.4364	0.5818	10.5
13601	-5.22E+06	0.4364	0.5818	11
13602	-5.22E+06	0.4364	0.5818	11.5
13603	-5.22E+06	0.4364	0.5818	12
13604	-5.22E+06	0.5818	0.5818	12.5
13605	-5.22E+06	0.5818	0.7273	13
13606	-5.22E+06	0.5818	0.7273	13.5
13607	-5.22E+06	0.5818	0.7273	14
13608	-5.22E+06	0.5818	0.7273	14.5
13609	-5.22E+06	0.5818	0.7273	15
13610	-5.22E+06	0.7273	0.7273	15.5
13611	-5.22E+06	0.7273	0.7273	16
13612	-5.22E+06	0.7273	0.7273	16.5
13613	-5.22E+06	0.8727	0.7273	17
13614	-5.22E+06	0.8727	0.7273	17.5
13615	-5.22E+06	0.8727	0.7273	18
13616	-5.22E+06	0.8727	0.7273	18.5
13617	-5.22E+06	0.8727	0.7273	19
13618	-5.22E+06	1.018	0.7273	19.5
13619	-5.22E+06	1.018	0.7273	20
13620	-5.22E+06	1.018	0.7273	20.5
13621	-5.22E+06	1.018	0.7273	21
13622	-5.22E+06	1.018	0.7273	21.5

13623	-5.22E+06	1.164	0.7273	22
13624	-5.22E+06	1.164	0.7273	22.5
13625	-5.22E+06	1.164	0.7273	23
13626	-5.22E+06	1.164	0.7273	23.5
13627	-5.22E+06	1.164	0.7273	24
13628	-5.22E+06	1.164	0.7273	24.5
13629	-5.22E+06	1.164	0.7273	25
13630	-5.22E+06	1.309	0.7273	25.5
13631	-5.22E+06	1.309	0.7273	26
13632	-5.22E+06	1.309	0.7273	26.5
13633	-5.22E+06	1.309	0.7273	27
13634	-5.22E+06	1.309	0.7273	27.5
13635	-5.22E+06	1.309	0.7273	28
13636	-5.22E+06	1.309	0.7273	28.5
13637	-5.22E+06	1.455	0.7273	29
13638	-5.22E+06	1.455	0.7273	29.5
13639	-5.22E+06	1.455	0.7273	30
13640	-5.22E+06	1.455	0.7273	30.5
13641	-5.22E+06	1.455	0.7273	31
13642	-5.22E+06	1.6	0.7273	31.5
13643	-5.22E+06	1.6	0.7273	32
13644	-5.22E+06	1.6	0.7273	32.5
13645	-5.22E+06	1.6	0.7273	33
13646	-5.22E+06	1.6	0.7273	33.5
13647	-5.22E+06	1.6	0.7273	34
13648	-5.22E+06	1.6	0.7273	34.5
13649	-5.22E+06	1.6	0.7273	35
13650	-5.22E+06	1.6	0.7273	35.5
13651	-5.22E+06	1.6	0.8727	36
13652	-5.22E+06	1.6	0.8727	36.5
13653	-5.22E+06	1.6	0.8727	37
13654	-5.22E+06	1.6	0.8727	37.5
13655	-5.22E+06	1.6	0.8727	38
13656	-5.22E+06	1.6	0.8727	38.5
13657	-5.22E+06	1.745	0.8727	39
13658	-5.22E+06	1.745	0.8727	39.5
13659	-5.22E+06	1.745	0.8727	40
13660	-5.22E+06	1.745	0.8727	40.5
13661	-5.22E+06	1.745	0.8727	41
13662	-5.22E+06	1.745	0.8727	41.5
13663	-5.22E+06	1.891	0.8727	42
13664	-5.22E+06	1.891	0.8727	42.5
13665	-5.22E+06	1.891	0.8727	43
13666	-5.22E+06	1.891	0.8727	43.5
13667	-5.22E+06	1.891	0.8727	44
13668	-5.22E+06	1.891	0.8727	44.5
13669	-5.22E+06	1.891	0.8727	45
13670	-5.22E+06	1.891	0.7273	45.5
13671	-5.22E+06	1.891	0.7273	46
13672	-5.22E+06	1.891	0.7273	46.5

13673	-5.22E+06	2.036	0.7273	47
13674	-5.22E+06	2.036	0.7273	47.5
13675	-5.22E+06	2.036	0.7273	48
13676	-5.22E+06	2.036	0.7273	48.5
13677	-5.22E+06	2.036	0.7273	49
13678	-5.22E+06	2.036	0.7273	49.5
13679	-5.22E+06	2.036	0.7273	50
13680	-5.22E+06	2.036	0.7273	50.5
13681	-5.22E+06	2.036	0.7273	51
13682	-5.22E+06	2.182	0.7273	51.5
13683	-5.22E+06	2.182	0.7273	52
13684	-5.22E+06	2.182	0.7273	52.5
13685	-5.22E+06	2.182	0.7273	53
13686	-5.22E+06	2.182	0.7273	53.5
13687	-5.22E+06	2.327	0.7273	54
13688	-5.22E+06	2.327	0.7273	54.5
13689	-5.22E+06	2.327	0.7273	55
13690	-5.22E+06	2.327	0.7273	55.5
13691	-5.22E+06	2.327	0.7273	56
13692	-5.22E+06	2.327	0.7273	56.5
13693	-5.22E+06	2.327	0.7273	57
13694	-5.22E+06	2.327	0.7273	57.5
13695	-5.22E+06	2.327	0.7273	58
13696	-5.22E+06	2.327	0.7273	58.5
13697	-5.22E+06	2.327	0.7273	59
13698	-5.22E+06	2.473	0.7273	59.5
13699	-5.22E+06	2.473	0.7273	60
13700	-5.22E+06	2.473	0.7273	60.5
13701	-5.22E+06	2.473	0.7273	61
13702	-5.22E+06	2.473	0.7273	61.5
13703	-5.22E+06	2.473	0.7273	62
13704	-5.22E+06	2.473	0.7273	62.5
13705	-5.22E+06	2.473	0.7273	63
13706	-5.22E+06	2.473	0.7273	63.5
13707	-5.22E+06	2.618	0.7273	64
13708	-5.22E+06	2.618	0.7273	64.5
13709	-5.22E+06	2.618	0.7273	65
13710	-5.22E+06	2.618	0.7273	65.5
13711	-5.22E+06	2.618	0.7273	66
13712	-5.22E+06	2.618	0.7273	66.5
13713	-5.22E+06	2.764	0.7273	67
13714	-5.22E+06	2.764	0.7273	67.5
13715	-5.22E+06	2.764	0.7273	68
13716	-5.22E+06	2.764	0.7273	68.5
13717	-5.22E+06	2.764	0.7273	69
13718	-5.22E+06	2.764	0.7273	69.5
13719	-5.22E+06	2.764	0.7273	70
13720	-5.22E+06	2.764	0.7273	70.5
13721	-5.22E+06	2.764	0.7273	71
13722	-5.22E+06	2.764	0.7273	71.5

13723	-5.22E+06	2.764	0.7273	72
13724	-5.22E+06	2.764	0.7273	72.5
13725	-5.22E+06	2.764	0.7273	73
13726	-5.22E+06	2.764	0.7273	73.5

Table B.2: Position tracking data for 8mm ball on 8mm bed 6.31mm from magnet face, 15ms pulse.

POSITION	1	mm x	mm y	ms
11003	-1.85E+07	0	0	0
11004	-1.85E+07	0.1455	0.1455	0.5
11005	-1.85E+07	0.1455	0.1455	1
11006	-1.85E+07	0.1455	0.1455	1.5
11007	-1.85E+07	0.1455	0.1455	2
11008	-1.85E+07	0.1455	0.1455	2.5
11009	-1.85E+07	0.1455	0.1455	3
11010	-1.85E+07	0.1455	0.1455	3.5
11011	-1.85E+07	0.1455	0.1455	4
11012	-1.85E+07	0.1455	0.2909	4.5
11013	-1.85E+07	0.1455	0.2909	5
11014	-1.85E+07	0.1455	0.2909	5.5
11015	-1.85E+07	0.1455	0.2909	6
11016	-1.85E+07	0.1455	0.2909	6.5
11017	-1.85E+07	0.1455	0.2909	7
11018	-1.85E+07	0.1455	0.2909	7.5
11019	-1.85E+07	0.1455	0.2909	8
11020	-1.85E+07	0.1455	0.2909	8.5
11021	-1.85E+07	0.1455	0.2909	9
11022	-1.85E+07	0.1455	0.2909	9.5
11023	-1.85E+07	0.4364	0.2909	10
11024	-1.85E+07	0.4364	0.2909	10.5
11025	-1.85E+07	0.4364	0.2909	11
11026	-1.85E+07	0.4364	0.2909	11.5
11027	-1.85E+07	0.4364	0.2909	12
11028	-1.85E+07	0.4364	0.2909	12.5
11029	-1.85E+07	0.5818	0.2909	13
11030	-1.85E+07	0.5818	0.4364	13.5
11031	-1.85E+07	0.5818	0.4364	14
11032	-1.85E+07	0.5818	0.4364	14.5
11033	-1.85E+07	0.5818	0.4364	15
11034	-1.85E+07	0.7273	0.4364	15.5
11035	-1.85E+07	0.7273	0.4364	16
11036	-1.85E+07	0.7273	0.4364	16.5
11037	-1.85E+07	0.7273	0.4364	17
11038	-1.85E+07	0.7273	0.4364	17.5
11039	-1.85E+07	0.8727	0.4364	18
11040	-1.85E+07	0.8727	0.4364	18.5
11041	-1.85E+07	0.8727	0.4364	19
11042	-1.85E+07	0.8727	0.4364	19.5
11043	-1.85E+07	0.8727	0.4364	20
11044	-1.85E+07	0.8727	0.4364	20.5
11045	-1.85E+07	1.018	0.4364	21
11046	-1.85E+07	1.018	0.4364	21.5

11047	-1.85E+07	1.018	0.4364	22
11048	-1.85E+07	1.018	0.4364	22.5
11049	-1.85E+07	1.018	0.4364	23
11050	-1.85E+07	1.018	0.4364	23.5
11051	-1.85E+07	1.018	0.4364	24
11052	-1.85E+07	1.164	0.4364	24.5
11053	-1.85E+07	1.164	0.4364	25
11054	-1.85E+07	1.164	0.4364	25.5
11055	-1.85E+07	1.164	0.4364	26
11056	-1.85E+07	1.164	0.4364	26.5
11057	-1.85E+07	1.164	0.4364	27
11058	-1.85E+07	1.164	0.4364	27.5
11059	-1.85E+07	1.309	0.4364	28
11060	-1.85E+07	1.309	0.4364	28.5
11061	-1.85E+07	1.309	0.4364	29
11062	-1.85E+07	1.309	0.4364	29.5
11063	-1.85E+07	1.309	0.4364	30
11064	-1.85E+07	1.309	0.4364	30.5
11065	-1.85E+07	1.309	0.4364	31
11066	-1.85E+07	1.6	0.4364	31.5
11067	-1.85E+07	1.6	0.4364	32
11068	-1.85E+07	1.6	0.4364	32.5
11069	-1.85E+07	1.6	0.4364	33
11070	-1.85E+07	1.6	0.4364	33.5
11071	-1.85E+07	1.6	0.4364	34
11072	-1.85E+07	1.6	0.4364	34.5
11073	-1.85E+07	1.745	0.4364	35
11074	-1.85E+07	1.745	0.4364	35.5
11075	-1.85E+07	1.745	0.4364	36
11076	-1.85E+07	1.745	0.4364	36.5
11077	-1.85E+07	1.745	0.4364	37
11078	-1.85E+07	1.745	0.4364	37.5
11079	-1.85E+07	1.891	0.4364	38
11080	-1.85E+07	1.891	0.4364	38.5
11081	-1.85E+07	1.891	0.5818	39
11082	-1.85E+07	2.036	0.5818	39.5
11083	-1.85E+07	2.036	0.5818	40
11084	-1.85E+07	2.036	0.5818	40.5
11085	-1.85E+07	2.036	0.5818	41
11086	-1.85E+07	2.036	0.5818	41.5
11087	-1.85E+07	2.036	0.5818	42
11088	-1.85E+07	2.036	0.5818	42.5
11089	-1.85E+07	2.036	0.5818	43
11090	-1.85E+07	2.036	0.5818	43.5
11091	-1.85E+07	2.036	0.5818	44
11092	-1.85E+07	2.036	0.5818	44.5
11093	-1.85E+07	2.036	0.5818	45
11094	-1.85E+07	2.036	0.5818	45.5
11095	-1.85E+07	2.036	0.5818	46
11096	-1.85E+07	2.036	0.5818	46.5

11097	-1.85E+07	2.182	0.5818	47
11098	-1.85E+07	2.182	0.5818	47.5
11099	-1.85E+07	2.327	0.5818	48
11100	-1.85E+07	2.327	0.5818	48.5
11101	-1.85E+07	2.327	0.5818	49
11102	-1.85E+07	2.327	0.5818	49.5
11103	-1.85E+07	2.327	0.5818	50
11104	-1.85E+07	2.327	0.5818	50.5
11105	-1.85E+07	2.327	0.5818	51
11106	-1.85E+07	2.327	0.5818	51.5
11107	-1.85E+07	2.473	0.5818	52
11108	-1.85E+07	2.473	0.5818	52.5
11109	-1.85E+07	2.473	0.5818	53
11110	-1.85E+07	2.473	0.5818	53.5
11111	-1.85E+07	2.473	0.5818	54
11112	-1.85E+07	2.473	0.5818	54.5
11113	-1.85E+07	2.473	0.5818	55
11114	-1.85E+07	2.473	0.5818	55.5
11115	-1.85E+07	2.473	0.5818	56
11116	-1.85E+07	2.473	0.5818	56.5
11117	-1.85E+07	2.473	0.5818	57
11118	-1.85E+07	2.473	0.5818	57.5
11119	-1.85E+07	2.473	0.5818	58
11120	-1.85E+07	2.473	0.5818	58.5
11121	-1.85E+07	2.473	0.5818	59
11122	-1.85E+07	2.473	0.5818	59.5
11123	-1.85E+07	2.764	0.4364	60
11124	-1.85E+07	2.764	0.4364	60.5
11125	-1.85E+07	2.764	0.4364	61
11126	-1.85E+07	2.764	0.4364	61.5
11127	-1.85E+07	2.764	0.4364	62
11128	-1.85E+07	2.764	0.4364	62.5
11128	-1.85E+07	2.764	0.4364	63

Table B.3: Position tracking data for 8mm ball on 8mm bed 6.31mm from magnet face, 30ms pulse.

POSITION	1	mm	mm	
		x	y	ms
13419	8.53E+06	0	0	0
13420	8.53E+06	0.1455	0.1455	0.5
13421	8.53E+06	0.1455	0.1455	1
13422	8.53E+06	0.1455	0.1455	1.5
13423	8.53E+06	0.1455	0.1455	2
13424	8.53E+06	0.1455	0.1455	2.5
13425	8.53E+06	0.1455	0.1455	3
13426	8.53E+06	0.1455	0.1455	3.5
13427	8.53E+06	0.1455	0.1455	4
13428	8.53E+06	0.1455	0.1455	4.5
13429	8.53E+06	0.1455	0.1455	5
13430	8.53E+06	0.1455	0.1455	5.5
13431	8.53E+06	0.1455	0.1455	6
13432	8.53E+06	0.1455	0.1455	6.5
13433	8.53E+06	0.1455	0.2909	7
13434	8.53E+06	0.2909	0.2909	7.5
13435	8.53E+06	0.2909	0.2909	8
13436	8.53E+06	0.2909	0.2909	8.5
13437	8.53E+06	0.2909	0.2909	9
13438	8.53E+06	0.2909	0.2909	9.5
13439	8.53E+06	0.2909	0.2909	10
13440	8.53E+06	0.4364	0.2909	10.5
13441	8.53E+06	0.4364	0.2909	11
13442	8.53E+06	0.4364	0.2909	11.5
13443	8.53E+06	0.5818	0.2909	12
13444	8.53E+06	0.5818	0.2909	12.5
13445	8.53E+06	0.5818	0.4364	13
13446	8.53E+06	0.5818	0.4364	13.5
13447	8.53E+06	0.5818	0.4364	14
13448	8.53E+06	0.5818	0.4364	14.5
13449	8.53E+06	0.7273	0.4364	15
13450	8.53E+06	0.7273	0.4364	15.5
13451	8.53E+06	0.7273	0.4364	16
13452	8.53E+06	0.7273	0.4364	16.5
13453	8.53E+06	0.8727	0.4364	17
13454	8.53E+06	0.8727	0.4364	17.5
13455	8.53E+06	0.8727	0.4364	18
13456	8.53E+06	0.8727	0.4364	18.5
13457	8.53E+06	0.8727	0.4364	19
13458	8.53E+06	1.018	0.4364	19.5
13459	8.53E+06	1.018	0.4364	20
13460	8.53E+06	1.018	0.4364	20.5
13461	8.53E+06	1.018	0.4364	21
13462	8.53E+06	1.018	0.4364	21.5

13463	8.53E+06	1.018	0.4364	22
13464	8.53E+06	1.164	0.4364	22.5
13465	8.53E+06	1.164	0.4364	23
13466	8.53E+06	1.164	0.4364	23.5
13467	8.53E+06	1.164	0.4364	24
13468	8.53E+06	1.309	0.4364	24.5
13469	8.53E+06	1.309	0.4364	25
13470	8.53E+06	1.309	0.4364	25.5
13471	8.53E+06	1.309	0.4364	26
13472	8.53E+06	1.309	0.4364	26.5
13473	8.53E+06	1.455	0.4364	27
13474	8.53E+06	1.455	0.4364	27.5
13475	8.53E+06	1.455	0.4364	28
13476	8.53E+06	1.455	0.4364	28.5
13477	8.53E+06	1.6	0.4364	29
13478	8.53E+06	1.6	0.4364	29.5
13479	8.53E+06	1.6	0.4364	30
13480	8.53E+06	1.6	0.4364	30.5
13481	8.53E+06	1.6	0.4364	31
13482	8.53E+06	1.6	0.4364	31.5
13483	8.53E+06	1.745	0.4364	32
13484	8.53E+06	1.745	0.4364	32.5
13485	8.53E+06	1.745	0.4364	33
13486	8.53E+06	1.891	0.4364	33.5
13487	8.53E+06	1.891	0.4364	34
13488	8.53E+06	1.891	0.4364	34.5
13489	8.53E+06	1.891	0.4364	35
13490	8.53E+06	2.036	0.4364	35.5
13491	8.53E+06	2.036	0.4364	36
13492	8.53E+06	2.036	0.4364	36.5
13493	8.53E+06	2.036	0.4364	37
13494	8.53E+06	2.036	0.4364	37.5
13495	8.53E+06	2.036	0.4364	38
13496	8.53E+06	2.036	0.4364	38.5
13497	8.53E+06	2.182	0.4364	39
13498	8.53E+06	2.182	0.4364	39.5
13499	8.53E+06	2.182	0.4364	40
13500	8.53E+06	2.182	0.4364	40.5
13501	8.53E+06	2.182	0.4364	41
13502	8.53E+06	2.182	0.4364	41.5
13503	8.53E+06	2.182	0.4364	42
13504	8.53E+06	2.182	0.4364	42.5
13505	8.53E+06	2.327	0.2909	43
13506	8.53E+06	2.327	0.2909	43.5
13507	8.53E+06	2.327	0.2909	44
13508	8.53E+06	2.327	0.2909	44.5
13509	8.53E+06	2.327	0.2909	45
13510	8.53E+06	2.327	0.2909	45.5
13511	8.53E+06	2.327	0.2909	46
13512	8.53E+06	2.327	0.2909	46.5

13513	8.53E+06	2.327	0.2909	47
13514	8.53E+06	2.327	0.2909	47.5
13515	8.53E+06	2.327	0.2909	48
13516	8.53E+06	2.327	0.2909	48.5
13517	8.53E+06	2.473	0.2909	49
13518	8.53E+06	2.618	0.2909	49.5
13519	8.53E+06	2.618	0.2909	50
13520	8.53E+06	2.618	0.2909	50.5
13521	8.53E+06	2.764	0.2909	51
13522	8.53E+06	2.764	0.2909	51.5
13523	8.53E+06	2.764	0.2909	52
13523	8.53E+06	2.764	0.2909	52.5

Table B.4: Position tracking data for 8mm ball on 8mm bed 6.31mm from magnet face, 150ms steady state pulse.

POSITION	1	mm	mm	
		x	y	ms
11816	1.69E+07	0	0	0
11817	1.69E+07	0	0.1403	0.5
11818	1.69E+07	0	0.1403	1
11819	1.69E+07	0	0.1403	1.5
11820	1.69E+07	0	0.1403	2
11821	1.69E+07	0	0.1403	2.5
11822	1.69E+07	0	0.1403	3
11823	1.69E+07	0.1403	0.1403	3.5
11824	1.69E+07	0.1403	0.1403	4
11825	1.69E+07	0.1403	0.1403	4.5
11826	1.69E+07	0.1403	0.1403	5
11827	1.69E+07	0.1403	0.1403	5.5
11828	1.69E+07	0.1403	0.1403	6
11829	1.69E+07	0.1403	0.1403	6.5
11830	1.69E+07	0.1403	0.1403	7
11831	1.69E+07	0.1403	0.1403	7.5
11832	1.69E+07	0.1403	0.1403	8
11833	1.69E+07	0.1403	0.1403	8.5
11834	1.69E+07	0.1403	0.1403	9
11835	1.69E+07	0.1403	0.1403	9.5
11836	1.69E+07	0.1403	0.1403	10
11837	1.69E+07	0.1403	0.1403	10.5
11838	1.69E+07	0	0.1403	11
11839	1.69E+07	0.1403	0.2807	11.5
11840	1.69E+07	0.1403	0.2807	12
11841	1.69E+07	0.1403	0.2807	12.5
11842	1.69E+07	0.1403	0.2807	13
11843	1.69E+07	0.1403	0.2807	13.5
11844	1.69E+07	0.1403	0.2807	14
11845	1.69E+07	0.1403	0.2807	14.5
11846	1.69E+07	0.1403	0.2807	15
11847	1.69E+07	0.1403	0.2807	15.5
11848	1.69E+07	0.1403	0.2807	16
11849	1.69E+07	0.1403	0.2807	16.5
11850	1.69E+07	0.1403	0.2807	17
11851	1.69E+07	0.1403	0.2807	17.5
11852	1.69E+07	0.1403	0.2807	18
11853	1.69E+07	0.1403	0.2807	18.5
11854	1.69E+07	0.1403	0.2807	19
11855	1.69E+07	0.1403	0.2807	19.5
11856	1.69E+07	0.1403	0.2807	20
11857	1.69E+07	0.1403	0.2807	20.5
11858	1.69E+07	0.2807	0.2807	21

11859	1.69E+07	0.2807	0.2807	21.5
11860	1.69E+07	0.2807	0.2807	22
11861	1.69E+07	0.2807	0.2807	22.5
11862	1.69E+07	0.2807	0.2807	23
11863	1.69E+07	0.421	0.2807	23.5
11864	1.69E+07	0.421	0.2807	24
11865	1.69E+07	0.421	0.2807	24.5
11866	1.69E+07	0.421	0.2807	25
11867	1.69E+07	0.421	0.2807	25.5
11868	1.69E+07	0.421	0.2807	26
11869	1.69E+07	0.421	0.2807	26.5
11870	1.69E+07	0.421	0.2807	27
11871	1.69E+07	0.421	0.2807	27.5
11872	1.69E+07	0.421	0.2807	28
11873	1.69E+07	0.2807	0.2807	28.5
11874	1.69E+07	0.2807	0.2807	29
11875	1.69E+07	0.2807	0.2807	29.5
11876	1.69E+07	0.421	0.421	30
11877	1.69E+07	0.421	0.421	30.5
11878	1.69E+07	0.421	0.421	31
11879	1.69E+07	0.421	0.421	31.5
11880	1.69E+07	0.421	0.421	32
11881	1.69E+07	0.421	0.421	32.5
11882	1.69E+07	0.421	0.421	33
11883	1.69E+07	0.421	0.421	33.5
11884	1.69E+07	0.5613	0.421	34
11885	1.69E+07	0.5613	0.421	34.5
11886	1.69E+07	0.5613	0.421	35
11887	1.69E+07	0.5613	0.421	35.5
11888	1.69E+07	0.5613	0.421	36
11889	1.69E+07	0.5613	0.421	36.5
11890	1.69E+07	0.5613	0.421	37
11891	1.69E+07	0.5613	0.421	37.5
11892	1.69E+07	0.5613	0.5613	38
11893	1.69E+07	0.5613	0.5613	38.5
11894	1.69E+07	0.5613	0.5613	39
11895	1.69E+07	0.5613	0.5613	39.5
11896	1.69E+07	0.5613	0.5613	40
11897	1.69E+07	0.5613	0.5613	40.5
11898	1.69E+07	0.5613	0.5613	41
11899	1.69E+07	0.842	0.5613	41.5
11900	1.69E+07	0.842	0.5613	42
11901	1.69E+07	0.842	0.5613	42.5
11902	1.69E+07	0.842	0.5613	43
11903	1.69E+07	0.842	0.5613	43.5
11904	1.69E+07	0.842	0.5613	44
11905	1.69E+07	0.842	0.5613	44.5
11906	1.69E+07	0.842	0.5613	45
11907	1.69E+07	0.842	0.5613	45.5
11908	1.69E+07	0.842	0.5613	46

11909	1.69E+07	0.9823	0.5613	46.5
11910	1.69E+07	0.9823	0.5613	47
11911	1.69E+07	0.9823	0.5613	47.5
11912	1.69E+07	0.9823	0.5613	48
11913	1.69E+07	0.9823	0.5613	48.5
11914	1.69E+07	0.9823	0.5613	49
11915	1.69E+07	0.9823	0.5613	49.5
11916	1.69E+07	0.9823	0.5613	50
11917	1.69E+07	1.123	0.5613	50.5
11918	1.69E+07	1.123	0.5613	51
11919	1.69E+07	1.263	0.5613	51.5
11920	1.69E+07	1.263	0.5613	52
11921	1.69E+07	1.263	0.5613	52.5
11922	1.69E+07	1.263	0.5613	53
11923	1.69E+07	1.263	0.5613	53.5
11924	1.69E+07	1.403	0.5613	54
11925	1.69E+07	1.403	0.5613	54.5
11926	1.69E+07	1.403	0.5613	55
11927	1.69E+07	1.403	0.5613	55.5
11928	1.69E+07	1.403	0.5613	56
11929	1.69E+07	1.403	0.5613	56.5
11930	1.69E+07	1.544	0.7016	57
11931	1.69E+07	1.544	0.7016	57.5
11932	1.69E+07	1.684	0.7016	58
11933	1.69E+07	1.684	0.7016	58.5
11934	1.69E+07	1.824	0.7016	59
11935	1.69E+07	1.824	0.7016	59.5
11936	1.69E+07	1.824	0.7016	60
11937	1.69E+07	1.824	0.7016	60.5
11938	1.69E+07	1.824	0.7016	61
11939	1.69E+07	1.824	0.7016	61.5
11940	1.69E+07	1.824	0.7016	62
11941	1.69E+07	1.965	0.7016	62.5
11942	1.69E+07	2.105	0.7016	63
11943	1.69E+07	2.245	0.7016	63.5
11944	1.69E+07	2.245	0.5613	64
11945	1.69E+07	2.386	0.5613	64.5
11946	1.69E+07	2.526	0.5613	65
11947	1.69E+07	2.526	0.5613	65.5
11948	1.69E+07	2.666	0.5613	66
11949	1.69E+07	2.666	0.5613	66.5
11950	1.69E+07	2.666	0.5613	67
11951	1.69E+07	2.666	0.5613	67.5
11952	1.69E+07	2.666	0.5613	68
11953	1.69E+07	2.666	0.5613	68.5
11954	1.69E+07	2.666	0.5613	69
11955	1.69E+07	2.666	0.5613	69.5
11956	1.69E+07	2.666	0.5613	70
11957	1.69E+07	2.666	0.421	70.5
11958	1.69E+07	2.666	0.421	71

11959	1.69E+07	2.666	0.421	71.5
11960	1.69E+07	2.666	0.421	72